Applications of the Droop Cell Quota Model to Data Based Cancer Growth and Treatment Models

by

Rebecca Anne Everett

A Dissertation Presented in Partial Fulfillment
of the Requirements for the Degree
Doctor of Philosophy

Approved April 2015 by the
Graduate Supervisory Committee:

Yang Kuang, Chair
John Nagy
Fabio Milner
Sharon Crook
Zdzislaw Jackiewicz

ARIZONA STATE UNIVERSITY

May 2015

ABSTRACT

The phycologist, M. R. Droop, studied vitamin B_{12} limitation in the flagellate *Monochrysis lutheri* and concluded that its specific growth rate depended on the concentration of the vitamin within the cell; i.e. the cell quota of the vitamin B_{12}. The Droop model provides a mathematical expression to link growth rate to the intracellular concentration of a limiting nutrient. Although the Droop model has been an important modeling tool in ecology, it has only recently been applied to study cancer biology. Cancer cells live in an ecological setting, interacting and competing with normal and other cancerous cells for nutrients and space, and evolving and adapting to their environment. Here, the Droop equation is used to model three cancers.

First, prostate cancer is modeled, where androgen is considered the limiting nutrient since most tumors depend on androgen for proliferation and survival. The model's accuracy for predicting the biomarker for patients on intermittent androgen deprivation therapy is tested by comparing the simulation results to clinical data as well as to an existing simpler model. The results suggest that a simpler model may be more beneficial for a predictive use, although further research is needed in this field prior to implementing mathematical models as a predictive method in a clinical setting.

Next, two chronic myeloid leukemia models are compared that consider Imatinib treatment, a drug that inhibits the constitutively active tyrosine kinase BCR-ABL. Both models describe the competition of leukemic and normal cells, however the first model also describes intracellular dynamics by considering BCR-ABL as the limiting nutrient. Using clinical data, the differences in estimated parameters between the models and the capacity for each model to predict drug resistance are analyzed.

Last, a simple model is presented that considers ovarian tumor growth and tumor induced angiogenesis, subject to on and off anti-angiogenesis treatment. In this

environment, the cell quota represents the intracellular concentration of necessary nutrients provided through blood supply. Mathematical analysis of the model is presented and model simulation results are compared to pre-clinical data. This simple model is able to fit both on- and off-treatment data using the same biologically relevant parameters.

To my parents and my husband, Charlie

ACKNOWLEDGEMENTS

First, I would like to sincerely thank my advisor, Dr. Yang Kuang, for his incredible mentorship and continuous support. Dr. Kuang goes above and beyond an advisor's duties, providing guidance not only in research, but in principles and character. Working with him has been extremely rewarding and enjoyable. I am deeply grateful.

I would also like to thank my committee members, Dr. John Nagy, Dr. Fabio Milner, Dr. Sharon Crook, and Dr. Zdzislaw Jackiewicz, for their encouragement, advice, and thoughtful insights. I would like to recognize my collaborators, Dr. Kevin Flores, Dr. Yuqin Zhao, and Dr. Aaron Packer. I thoroughly enjoyed working with and learning from them. A special thank you to Debbie Olson, the Graduate Program Coordinator of the School of Mathematical and Statistical Sciences, for all that she does for the graduate students.

I am extremely grateful to my Arizona State University friends, including Angie Peace, Michael Tallman, and Chester Ismay, for their support, optimism, and help throughout graduate school, and to Courtney Tallman for being my Arizona family.

I would like to express enormous appreciation and gratitude to my parents for their love and support and for inspiring me to do my best, and especially to my dad for instilling in me a love of mathematics. I also would like to thank my sister and in-laws for their constant love and encouragement.

Lastly, but certainly not least, I would wholeheartedly like to thank my husband, Charlie, for his unconditional love and for always believing in me.

I gratefully acknowledge the Achievement Rewards for College Students (ARCS) foundation for their financial support.

TABLE OF CONTENTS

CHAPTER Page

CHAPTER Page

LIST OF TABLES

LIST OF FIGURES

Figure Page

Figure Page

Figure Page

Chapter 1

INTRODUCTION

1.1 Investigating Tumor Dynamics with Mathematical Ecology

It is well-known that cancer is a major public health problem world-wide. Although cancer mortality rates are declining and survival rates improving, one in three women and one in two men will develop cancer in his or her lifetime in the United States (Siegel *et al.*, 2012). Cancer is still the cause of approximately a quarter of deaths in the United States, a statistic that was also true about 40 years ago (Howlander *et al.*, 2011; Korolev *et al.*, 2014). Thus, there is a need for new approaches and interdisciplinary research in order to better understand cancer and improve treatment.

One recent interdisciplinary approach consists of applying a combination of mathematics and ecology to cancer biology. Cancerous cells live in an ecological setting, interacting with each other, healthy cells, as well as their environment, and evolving and adapting to changes in their environment (Nagy, 2004, 2005; Merlo *et al.*, 2006; Pienta *et al.*, 2008; Nagy and Armbruster, 2012; Basanta and Anderson, 2013; Bickel *et al.*, 2014; Korolev *et al.*, 2014). Studying tumor cells in this framework can provide important insights. Merlo *et al.* (2006) discuss several types of ecological interactions observed in cancer: competition exists between non-cancerous cells as well as other cancerous cells for resources, nutrients, and space; the immune system acts as a predator to cancerous cells; and parasitism, the benefit of one species at the expense of another, can be seen in "free riders" in the example of angiogenesis, the development of new blood vessels from pre-existing blood vessels. Here, the "free riders" are the clones that do not produce the pro-angiogenic signals, saving metabolic energy, while

still benefiting from their neighbor's investments (Merlo *et al.*, 2006; Bickel *et al.*, 2014).

Cancer treatment in an ecological setting would aim to ensure that the host, or patient, out-competes the tumor, or at least establishes a stable coexistence that does not harm the patient (Elser *et al.*, 2003). A species can become extinct by being directly killed. In terms of cancer therapy, this is represented through cytotoxic chemotherapy and targeted drugs, although this rarely cures cancer. Alternative extinction strategies are to alter the environment or to kill other species that support the tumor cells (Pienta *et al.*, 2008). Tumors are heterogeneous, consisting of several genetically different subpopulations, with some clones being selected due to natural selection (Kareva, 2011). One of the main problems with cancer therapy is that it often selects for resistance (Merlo *et al.*, 2006). Using evolutionary game theory, Basanta and Anderson (2013) hypothesize that treatment results will improve by embracing tumor evolution instead of ignoring it; instead of killing as many tumor cells as possible, it might be more beneficial to find the correct sequence of treatments that selects for tumors that are easier to treat. Merlo *et al.* (2006) state that the timing of therapy can affect evolutionary dynamics; selective pressures in intermittent compared to continuous treatment can produce different outcomes.

Ecological mathematical models have provided beneficial insights into tumor biology (Kuang *et al.*, 2004b; Nagy, 2004, 2005; Nagy and Armbruster, 2012; Basanta and Anderson, 2013; Bickel *et al.*, 2014; Korolev *et al.*, 2014). Nagy (2005) presents a review of mathematical models that investigate the causes of necrosis and tumor cell diversity. Bickel *et al.* (2014) and Nagy and Armbruster (2012) use mathematical models to understand why angiogenesis, a hallmark of cancer (Hanahan and Weinberg, 2000), occurs from an evolutionary standpoint, which is not a straightforward question due to the "free riders" described above. Kuang *et al.* (2004b) use an ecological

mathematical model to propose reducing tumor cell phosphorus uptake as a potential treatment for cancer.

Since ecological dynamics in tumors are not well understood, there are a few common growth models that are often used, such as logistic growth. Korolev *et al.* (2014) discuss treatment in the presence of Allee effects; with a strong Allee effect, a population size greater than the Allee threshold will grow towards the carrying capacity whereas a population size below the threshold will decrease to extinction. The authors state that if this threshold exists in a tumor ecosystem, then treatment would not need to kill all the tumor cells, but simply reduce the population size to below the threshold. A new approach to therapy could focus on the size of the threshold and increasing the Allee effect. Similarly, treatment could consider evolutionary thresholds; "small tumors accumulate more damaging mutations, lose fitness and get smaller, whereas large tumors accumulate more drivers, gain fitness and get bigger" (Korolev *et al.*, 2014).

The Droop model (Droop, 1968) is another growth model and was developed based on laboratory data. This model links growth rate to an intracellular limiting nutrient concentration. Since tumor growth is often dependent upon intracellular nutrients, we propose using this ecological model to provide insights into cancer biology. Section 1.2 presents this Droop model and analysis of the model. Section 1.3 discusses the motivations and goals of this research.

1.2 The Droop Model

The phycologist Droop studied the behavior of *Monochrysis lutheri*, a flagellate later re-allocated to *Pavlova*, in limiting concentrations of vitamin B_{12}, with a goal of relating specific growth rate to the substrate vitamin B_{12} concentrations (Droop, 1968; Leadbeater, 2006). Droop concluded that the specific growth rate μ did not depend

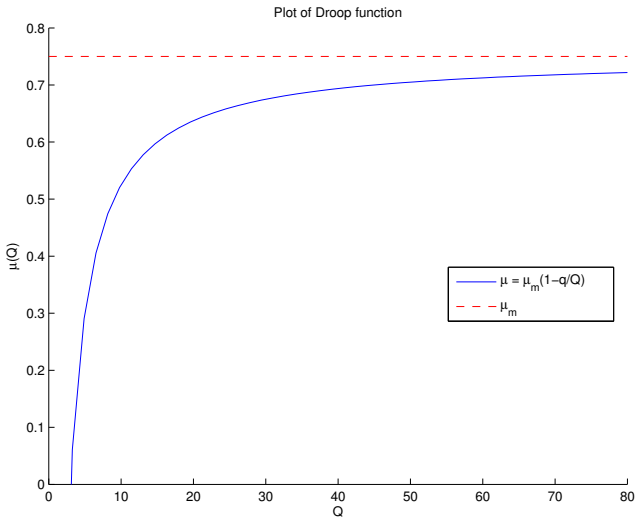

Figure 1.1: Plot of Droop Function with $q = 3, \mu_m = 0.75$

directly on the concentration of vitamin in the media, but rather on the concentration of the vitamin within the cell, or the cell quota Q:

$$\mu = \mu_m \left(1 - \frac{q}{Q}\right). \tag{1.1}$$

The quota Q is defined as the quantity of nutrients in a cell. The parameter q represents the minimum quota of nutrient needed for life (the Q value for which $\mu = 0$). The parameter μ_m is the value of the horizontal asymptote and represents the growth rate for an infinite amount of intracellular nutrient. Figure 1.1 presents a plot of the Droop function and Table 1.1 lists the symbols, their meanings, and their units from Droop's publications (Droop, 1968, 1973).

1.2.1 Population Model Formulation

Using Droop's equation, we now build a population model to serve as the basis of the tumor model. Let $x(t)$ represent a population density. We assume the population

Symbol	Explanation	Units
μ	Specific growth rate	day^{-1}
	(increase in biomass per unit biomass per unit time)	
μ_m	Maximum specific growth rate	day^{-1}
	(at infinite internal substrate concentration)	
q	Subsistence quota of a limiting nutrient	$\mu\mu g/10^6$ cells
Q	Cell Quota (mass per unit biomass)	$\mu\mu g/10^6$ cells
	(internal substrate concentration), C/x	
C	Concentration of substrate within cells	$\mu\mu$g/ml
x	Cell mass (biomass, mass per unit volume)	10^6 cells/ml

Table 1.1: Droop Model Symbols, Meanings, and Units (Droop, 1968, 1973)

growth is governed by the cell quota model in equation (1.1) and assume a constant per capita death rate D:

$$\frac{dx}{dt} = \mu_m \left(1 - \frac{q}{Q}\right) x - Dx. \tag{1.2}$$

We now need to consider how the cell quota Q changes over time. Let N_t represent the total limiting nutrient concentration in the system, N_f represent the free nutrient concentration in the environment, and N_x represent the nutrient concentration in the cells. Then

$$N_t = N_f + N_x = N_f + Qx.$$

Solving for Q, we see

$$Q = \frac{N_t - N_f}{x},$$

where N_t is a constant, and N_f and x change over time. Then

$$\frac{dQ}{dt} = \frac{-xN_f' - (N_t - N_f)x'}{x^2},$$

where x' is given by equation (1.2) and $N_f' = -\alpha x N_f + DQx$. The parameter α represents the uptake rate of the nutrient and xN_f represents the interaction between the population and free nutrient. The term DQx represents the amount of nutrient that returns to the environment as cells die. Then

$$\begin{aligned}\frac{dQ}{dt} &= \frac{x(\alpha x N_f - DQx) - (N_t - N_f)\left[\mu_m x\left(1 - \frac{q}{Q}\right) - Dx\right]}{x^2} \\ &= \alpha N_f - \mu_m(Q - q) \\ &= \alpha(N_t - Qx) - \mu_m(Q - q).\end{aligned}$$

Thus we have the following system

$$\frac{dx}{dt} = \mu_m\left(1 - \frac{q}{Q}\right)x - Dx \tag{1.3a}$$

$$\frac{dQ}{dt} = \alpha(N_t - Qx) - \mu_m(Q - q). \tag{1.3b}$$

We assume that the parameters are all non-negative so that the model is biologically meaningful.

1.2.2 Model Analysis

Boundedness and Positive Invariance

The following lemma provides a basic analysis of the model verifying the boundedness and positive invariance of solutions.

Lemma 1.2.1. *Solutions with initial conditions in the region* $\Omega = \{(x, Q) : 0 < x, q < Q < \frac{\alpha N_t + \mu_m q}{\mu_m} + c, N_t > xQ\}$*, where* $c > 0$*, remain there for all future time.*

Proof. Assume, by contradiction, there exists a time t_1 such that a trajectory with initial conditions $\{(x_0, Q_0) : 0 < x_0, q < Q_0 < \frac{\alpha N_t + \mu_m q}{\mu_m} + c, N_t > x_0 Q_0\}$, where $c > 0$, crosses a boundary of Ω for the first time.

Case 1. $Q(t_1) = q$: For $t \in [0, t_1]$,

$$\begin{aligned} Q' &= \alpha(N_t - Qx) - \mu_m(Q - q) \\ &\geq -\mu_m(Q - q). \end{aligned}$$

Then

$$Q' + \mu_m Q \geq \mu_m q$$

and so

$$Q(t) \geq q + (Q_0 - q)e^{-\mu_m t}.$$

This implies that $Q(t_1) \geq q + (Q_0 - q)e^{-\mu_m t_1} > q$. This contradicts $Q(t_1) = q$ and proves that a trajectory cannot cross this boundary.

Case 2. $x(t_1) = 0$: Let $\bar{f} = \min\left\{\mu_m\left(1 - \frac{q}{Q(t)}\right) - D : t \in [0, t_1]\right\}$, which does not equal $-\infty$ by Case 1. Then for $t \in [0, t_1]$,

$$x' = \mu_m\left(1 - \frac{q}{Q}\right)x - Dx \geq \bar{f}x.$$

Then $x(t) \geq x_0 e^{\bar{f}t}$ and so $x(t_1) \geq x_0 e^{\bar{f}t_1} > 0$. This contradicts $x(t_1) = 0$ and proves that a trajectory cannot cross this boundary.

Case 3. $N_t = Q(t_1)x(t_1)$: First we will show that x is bounded above by showing $x \leq N_t/q$. Then for $t \in [0, t_1]$,

$$\begin{aligned} x' &= \mu_m\left(1 - \frac{q}{Q}\right)x - Dx \\ &\leq \mu_m\left(1 - \frac{q}{Q}\right)x \\ &= \mu_m x\left(1 - \frac{x}{(Qx)/q}\right) \\ &\leq \mu_m x\left(1 - \frac{x}{N_t/q}\right), \end{aligned}$$

which is comparable to the logistic equation. Then $x \leq N_t/q$ by a standard comparison argument.

Now we will show that $N_t > xQ$. Let $z = N_t - xQ$ with $z_0 > 0$ and $\bar{x} = \max\{x(t) : t \in [0, t_1]\}$, since x is bounded above by N_t/q.

Then for $t \in [0, t_1]$,

$$\begin{aligned} z'(t) &= -x\Big(\alpha(N_t - Qx) - \mu_m(Q - q)\Big) - Q\left(\mu_m\left(1 - \frac{q}{Q}\right)x - Dx\right) \\ &= -x\Big(\alpha(N_t - Qx) - DQ\Big) \\ &= -\alpha xz + DQx \\ &\geq -\alpha\bar{x}z. \end{aligned}$$

Then $z(t) \geq z_0 e^{-\alpha\bar{x}t}$ and so $z(t_1) \geq z_0 e^{-\alpha\bar{x}t_1} > 0$. Thus $N_t - x(t_1)Q(t_1) > 0$ and so $N_t > x(t_1)Q(t_1)$. This contradicts $N_t = x(t_1)Q(t_1)$ and so the trajectory cannot cross this boundary.

Case 4. $Q(t_1) = \dfrac{\alpha N_t + \mu_m q}{\mu_m} + c$: Consider the vertical line $Q = \dfrac{\alpha N_t + \mu_m q}{\mu_m} + c$ for some $c > 0$. The Q nullcline, $x^* = \dfrac{\alpha N_t - \mu_m(Q^* - q)}{\alpha Q^*}$, is a monotone decreasing function of Q and intersects the Q axis at $Q = \dfrac{\alpha N_t + \mu_m q}{\mu_m}$. Since $\dfrac{\alpha N_t + \mu_m q}{\mu_m} < \dfrac{\alpha N_t + \mu_m q}{\mu_m} + c$, the vertical line boundary is greater than the Q nullcline. To the right of the Q nullcline, $Q' < 0$ and so no trajectory can cross this vertical line boundary. □

See Figure 1.2 for a sketch of the phase plane and region Ω.

Equilibria and Global Stability

For the system (1.3), we have the following equilibrium points (x^*, Q^*): $E_1 = \left(\dfrac{N_t}{q} - D\left(\dfrac{N_t}{q\mu_m} + \alpha^{-1}\right), \dfrac{q\mu_m}{\mu_m - D}\right)$ and $E_2 = \left(0, \dfrac{\alpha N_t + \mu_m q}{\mu_m}\right)$. In order for E_1 to be positive, we assume $\mu_m > D$ and

$$\frac{N_t}{q} > D\left(\frac{N_t}{q\mu_m} + \alpha^{-1}\right), \text{ or equivalently, } N_t > \frac{q\mu_m D\alpha^{-1}}{\mu_m - D}. \tag{1.4}$$

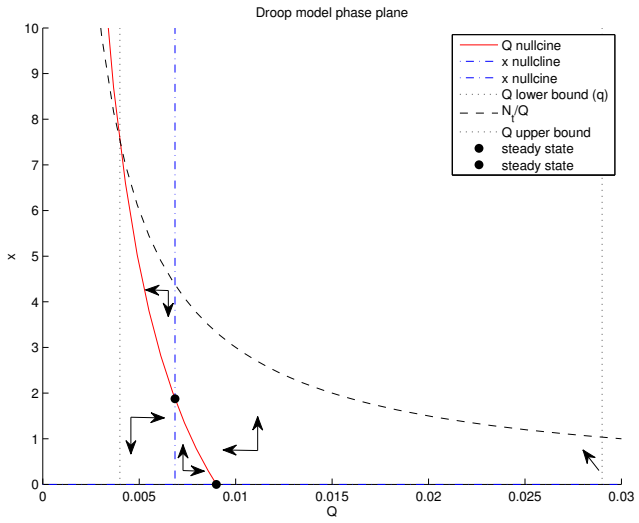

Figure 1.2: (Q, x) Phase Plane with the Q Nullcline (solid red) and x Nullclines (dot-dash blue). The curved black dotted black line represents $xQ = N_t$. The left vertical black dotted black line represents $Q = q$ and the right vertical black dotted black line represents $Q = \frac{\alpha N_t + \mu_m q}{\mu_m} + c$. $N_t = 0.03, \mu_m = 1.2, q = .004, \alpha = .2, D = .5, c = .02$.

Biologically we are assuming the maximum growth rate is greater than the death rate, and relation (1.4) specifies the minimum environmental nutrient concentration to make the population viable. Note that E_2 represents the case for population extinction. The following theorems give results on the stability of these equilibria. The Jacobian of the system (1.3) is

$$J = \begin{bmatrix} \mu_m \left(1 - \frac{q}{Q^*}\right) - D & \mu_m x^* \frac{q}{(Q^*)^2} \\ -\alpha Q^* & -\alpha x^* - \mu_m \end{bmatrix}.$$

Theorem 1.2.1. *(i) If (1.4) has the reverse inequality and $\mu_m > D$, then E_1 is a saddle point.*

(ii) If (1.4) has the reverse inequality and $\mu_m < D$, then E_1 is unstable.

(iii) If (1.4) holds, then the equilibrium E_1 is locally asymptotically stable.

Proof. The Jacobian takes the following form:

$$J(E_1) = \begin{bmatrix} 0 & \mu_m \left[\frac{N_t}{q} - D\left(\frac{N_t}{q\mu_m} + \alpha^{-1}\right)\right] \frac{q}{\left(\frac{q\mu_m}{\mu_m - D}\right)^2} \\ -\alpha\frac{q\mu_m}{\mu_m - D} & -\left[\alpha\left(\frac{N_t}{q} - D(\frac{N_t}{q\mu_m} + \alpha^{-1})\right) + \mu_m\right] \end{bmatrix}$$

with

$$\begin{aligned} \mathrm{Tr}(J_{E_1}) &= -\left[\alpha\left(\frac{N_t}{q} - D(\frac{N_t}{q\mu_m} + \alpha^{-1})\right) + \mu_m\right], \\ \mathrm{Det}(J_{E_1}) &= -\frac{(\mu_m - D)^2}{q\mu_m}\left(\frac{N_t}{q} - D(\frac{N_t}{q\mu_m} + \alpha^{-1})\right)\left(\frac{-\alpha q\mu_m}{\mu_m - D}\right). \end{aligned}$$

If (1.4) has the reverse inequality and $\mu_m > D$, then $\mathrm{Tr}(J_{E_1}) > 0$ and $\mathrm{Det}(J_{E_1}) < 0$ and so E_1 is a saddle point. If (1.4) has the reverse inequality and $\mu_m < D$, then $\mathrm{Tr}(J_{E_1}) > 0$ and $\mathrm{Det}(J_{E_1}) > 0$ and so E_1 is unstable. If (1.4) holds, then $\mathrm{Tr}(J_{E_1}) < 0$ and $\mathrm{Det}(J_{E_1}) > 0$ and so E_1 is a stable equilibrium point.

□

Theorem 1.2.2. *(i) If (1.4) has the reverse inequality, then E_2 is locally asymptotically stable.*

(ii) If (1.4) holds, then E_2 is a saddle point.

Proof. The Jacobian takes the following form:

$$J(E_2) = \begin{bmatrix} \frac{\mu_m \alpha N_t}{\alpha N_t + \mu_m q} - D & 0 \\ -\alpha\left(\frac{\alpha N_t + \mu_m q}{\mu_m}\right) & -\mu_m \end{bmatrix}.$$

Since J_{E_2} is lower triangular, $\lambda_1 = \dfrac{\mu_m \alpha N_t}{\alpha N_t + \mu_m q} - D = \dfrac{\alpha N_t(\mu_m - D) - D\mu_m q}{\alpha N_t + \mu_m q}$ and $\lambda_2 = -\mu_m < 0$. If (1.4) has the reverse inequality then $\lambda_1 < 0$ and so E_2 is locally asymptotically stable. If (1.4) holds, then $\lambda_1 > 0$ and so E_2 is a saddle point. □

Theorem 1.2.3. *Assuming (1.4) holds, the equilibrium point E_1 is globally asymptotically stable.*

Proof. First we must show there are no periodic orbits. Consider the system

$$x' = \mu_m \left(1 - \frac{q}{Q}\right) x - Dx = F(x, Q)$$

$$Q' = \alpha(N_t - Qx) - \mu_m(Q - q) = G(x, Q).$$

Then

$$\frac{\partial F}{\partial x} + \frac{\partial G}{\partial Q} = \mu_m \left(1 - \frac{q}{Q}\right) - D - \alpha x - \mu_m = -\frac{\mu_m q}{Q} - D - \alpha x < 0.$$

Then by the Bendixson's negative criterion theorem, there cannot be a closed orbit contained within Ω (defined in Lemma 1.2.1). Therefore, since Ω is simply connected, positively invariant by Lemma 1.2.1 and contains no orbits, then the Poincaré Bendixson Theorem implies that all solutions of the system (1.3) starting in Ω will converge to E_1. Therefore, E_1 is globally asymptotically stable. □

1.2.3 Comparison to Logistic Model

In 2004, Kuang *et al.* (2004a) mechanistically formulated a mathematically tractable plant-herbivore model in a closed phosphorus-limiting environment using Droop's equation. Using their model, they showed a mechanistic derivation of the logistic equation. Following their approach, since cell metabolic processes are much faster compared to the growth of the population, we can apply a quasi-steady state argument by letting $Q' = 0$:

$$\alpha(N_t - Qx) - \mu_m(Q - q) = 0$$

and so

$$Q = \frac{\alpha N_t + \mu_m q}{\alpha x + \mu_m}.$$

Then

$$\begin{aligned}
\frac{dx}{dt} &= \mu_m \left(1 - \frac{q}{Q}\right) x - Dx \\
&= \mu_m x \left(1 - \frac{x + \mu_m \alpha^{-1}}{N_t/q + \mu_m \alpha^{-1}}\right) - Dx \\
&= \frac{(\mu_m - D)x}{N_t/q + \mu_m \alpha^{-1}} \left(N_t/q + \mu_m \alpha^{-1} - \frac{x + \mu_m \alpha^{-1}}{(\mu_m - D)/\mu_m}\right) \\
&= \frac{(\mu_m - D)x}{N_t/q + \mu_m \alpha^{-1}} \left(\frac{\frac{N_t(\mu_m - D)}{q\mu_m} - \alpha^{-1} D - x}{(\mu_m - D)/\mu_m}\right) \\
&= \frac{x}{N_t/q + \mu_m \alpha^{-1}} \Big(N_t/q(\mu_m - D) - \alpha^{-1}\mu_m D - x\mu_m\Big) \\
&= \frac{\Big(N_t/q(\mu_m - D) - \alpha^{-1}\mu_m D\Big)x}{N_t/q + \mu_m \alpha^{-1}} \left(1 - \frac{x}{\frac{N_t}{q}\frac{(\mu_m - D)}{\mu_m} - \alpha^{-1} D}\right) \\
&= rx\left(1 - \frac{x}{K}\right),
\end{aligned}$$

where

$$r = \frac{(\mu_m - D)N_t/q - D\mu_m \alpha^{-1}}{N_t/q + \mu_m \alpha^{-1}} \text{ and } K = \frac{(\mu_m - D)N_t}{\mu_m q} - D\alpha^{-1},$$

or equivalently,

$$r = \frac{(\mu_m - D)N_t \alpha - D\mu_m q}{N_t \alpha + \mu_m q} \text{ and } K = \frac{(\mu_m - D)N_t \alpha - D\mu_m q}{\mu_m q \alpha}.$$

Since $r = \dfrac{K\mu_m}{N_t/q + \mu_m \alpha^{-1}}$, then the growth rate r and carrying capacity K are proportionally related. Note that r and K are both increasing functions of α, meaning that as the intake of nutrients increase, the growth rate and carrying capacity also increase (boundedly). Also, r and K are both decreasing functions of D, meaning as the death rate increases, the growth rate and carrying capacity decrease. Note that when there is no population death, $K = \frac{N_t}{q}$, which represents the total nutrient divided by the minimum cell quota needed for life; it is the maximum population possible given the amount of nutrient in the environment. This carrying capacity is

larger than the carrying capacity with a death rate, since now death is inhibiting the population from reaching its possible maximum.

1.3 Motivation and Goals

The Droop model, originally derived from observation, provides a simple mathematical expression to relate intracellular limiting nutrient concentration to growth rate. Although the Droop model has been an important modeling tool in ecology, it has only recently been applied to study cancer biology (e.g. (Nagy, 2007; Portz *et al.*, 2012; Saleem *et al.*, 2014)). Using Droop's model, Nagy (2007) applied ecological stoichiometry to cancer, an idea proposed by Elser *et al.* (2003). Ecological stoichiometry is the study of balance of energy and multiple chemical substances in ecological processes and interactions; it investigates the role of essential elements, such as carbon (C), nitrogen (N), and phosphorus (P), in ecological interactions (Sterner and Elser, 2002). An important hypothesis developed from ecological stoichiometry is the growth rate hypothesis, which states that "organismal C:N:P ratios are caused by differential allocations to RNA necessary to meet the protein synthesis demands of rapid rates of biomass growth and development" (Sterner and Elser, 2002). This means that organisms with high growth rates have high P:C ratios due to the increased allocation of P to RNA, and thus their growth will be constrained in P-limited environments. Since tumor cells often have high growth rates, it makes sense to apply this hypothesis to cancer biology. Elser *et al.* (2007) tested this hypothesis and concluded that the growth rate hypothesis might hold true for some cancers, but not for all. In order to further study the growth rate hypothesis in cancer, Nagy (2007) modified a previous tumor model to include phosphorus as a limiting nutrient using Droop's model. Saleem *et al.* (2014) also used Droop's model and applied stoichiometric principles to tumor growth by modeling the tumor-immune cell interactions in a potassium limited

environment. Portz *et al.* (2012) used Droop's equation in modeling prostate cancer treatment and interpreted the cell quota as the intracellular androgen concentration. Here we build on the work of Portz *et al.* and present several cancer models using Droop's cell quota model, specifically for prostate cancer (Chapter 2), chronic myeloid leukemia (Chapter 3), and ovarian cancer (Chapter 4).

Chapter 2

PROSTATE CANCER

2.1 Introduction

2.1.1 Prostate Cancer and Treatment

The probability of an American man developing prostate cancer in a lifetime is 1 in 6 (Siegel *et al.*, 2013). Although the incidence and death trends for prostate cancer are declining, there is still no curative treament for patients with distant metastases (Fong *et al.*, 2012). Androgen deprivation therapy (ADT) is one of the most common and effective therapies for patients with metastatic cancer (Nelson, 2012) and has recently been used to also treat non-metastatic disease (Crook *et al.*, 2012; Klotz and Toren, 2012). Although the initial response rate of ADT is above 90% (assessed by a decrease in the biomarker prostate specific antigen (PSA) levels (Amaral *et al.*, 2012)), most patients eventually develop castration-resistant prostate cancer (CRPC) (Nelson, 2012). CRPC is usually fatal, with a median survival time of 2.5 to 3 years (Nelson, 2012; Hussain *et al.*, 2013).

Androgens, specifically testosterone and 5α-dihydrotestosterone (DHT), are essential for maintenance of the prostate. Prostate secretory epithelial cells depend on androgens for proliferation and survival. The testes produce 90-95% of the androgens in the body with the adrenal gland producing the remainder (Fong *et al.*, 2012). Androgens regulate cellular proliferation and survival via activation of the androgen receptor (AR), a nuclear hormone receptor. Around 90% of serum testosterone that enters the prostate is enzymatically converted to DHT, which has a greater affinity for AR than that of testosterone. Ligand binding to AR initiates a cascade of events that

activate proliferation, survival, and PSA secretion pathways (Feldman and Feldman, 2001). Serum PSA is used as a biomarker for prostate cancer since PSA expression is maintained by cancerous cells. While its effectiveness as a diagnostic tool is controversial, PSA is useful for gauging the response of disease to ADT. ADT inhibits AR signaling by blocking androgen production. Therapy induces regression of both mass and PSA secretion by the prostate and cancer cells in particular.

ADT can be performed by surgical or chemical castration. Orchiectomy, the removal of the testes, is a relatively simple procedure that results in a decrease of testosterone levels. However, chemical castration is more common due to the psychological effects of the surgery (Sharifi *et al.*, 2005; Labrie, 2011). Current chemical castration options include luteinizing hormone release hormone (LHRH) agonists, gonadotropin releasing hormone (GnRH) antagonists, and anti-androgens. A combination of an anti-androgen and a LHRH agonist is called total androgen blockade (Feldman and Feldman, 2001; Fong *et al.*, 2012).

Intermittent androgen deprivation (IAD) therapy consists of alternating periods of on- and off-treatment and provides many benefits over continuous (CAD) therapy, including increased health-related quality of life, reduced therapy costs (LHRH agonists cost about $300 to $400 a month (Klotz and Toren, 2012)), and potentially delaying resistance to treatment, although the latter remains controversial (Gleave *et al.*, 2009; Klotz and Toren, 2012; Mitin *et al.*, 2012; Resnick, 2013). ADT causes numerous side effects such as erectile dysfunction, loss of libido, gynecomastia, osteoporosis, and anemia (Higano, 2003; Klotz and Toren, 2012). Some of these side effects can potentially lead to more serious conditions, such as diabetes, hypertension, and cardiovascular disease (Higano, 2003). Two recent studies by Crook *et al.* (2012) and Hussain *et al.* (2013) compared IAD to CAD therapy in patients with prostate cancer. Crook *et al.* concluded that IAD was not inferior to CAD in terms of survival, but

improvements in quality of life were observed in IAD patients (Crook *et al.*, 2012). Hussain *et al.* observed small improvements in quality of life for IAD patients, but their findings in terms of survival were statistically insignificant; they were not able to rule out a greater risk of death from IAD compared to CAD nor rule out significant inferiority of IAD (Hussain *et al.*, 2013). Crook *et al.* and Hussian *et al.* provide two examples of recent studies attempting to determine if IAD or CAD is more effective at delaying resistance to treatment. Although this topic remains controversial, (Gleave *et al.*, 2009; Klotz and Toren, 2012; Mitin *et al.*, 2012; Resnick, 2013) the European Association of Urology (EAU) recommends IAD as the standard of care for patients with metastatic or biochemically recurrent prostate cancer (Mitin *et al.*, 2012).

2.1.2 Recent Works

While IAD offers several benefits, there are still controversies in how the treatment should be applied, such as who should receive IAD therapy, when to start and stop therapy, and what thresholds should be used for starting and stopping treatment (Scholz *et al.*, 2011; Klotz and Toren, 2012). Mathematical models can be important tools for achieving improved therapy and might provide insights into some of these controversies for individual patients.

Jackson (2004a,b)

In 2004, Jackson used a system of partial differential equations to investigate the mechanisms for CRPC:

$$\underbrace{\frac{\partial p}{\partial t}}_{\text{Time ROC}} + \underbrace{\nabla \cdot (up)}_{\text{Collective motion}} = \underbrace{D_p \Delta p}_{\text{Random motion}} + \underbrace{\alpha_p \theta_p(a) p}_{a\text{-mediated proliferation}} - \underbrace{\delta_p \omega_p(a) p}_{a\text{-mediated apoptosis}} \tag{2.1a}$$

$$\underbrace{\frac{\partial q}{\partial t}}_{\text{Time ROC}} + \underbrace{\nabla \cdot (uq)}_{\text{Collective motion}} = \underbrace{D_q \Delta q}_{\text{Random motion}} + \underbrace{\alpha_q \theta_q(a) q}_{a\text{-mediated proliferation}} - \underbrace{\delta_q \omega_q(a) q}_{a\text{-mediated apoptosis}} \tag{2.1b}$$

The model assumes the tumor is radially symmetric and composed of two types of cells: androgen-dependent (AD), represented by p, and androgen-independent (AI), represented by q, with the latter contributing to the AI tumor relapse and resistance to therapy. The proliferation and death rates of both cell types, represented by $\theta_p(a), \theta_q(a), \delta_p(a), \delta_q(a)$, depend on androgen concentration a. During androgen deprivation, the AD proliferation rate decreases and the AD death rate increases while the AI proliferation rate remain constant and the AI death rate decreases. Parameters D_p, D_q represent the constant random motility coefficients and u represents the local cell velocity. In order to investigate the effects of ADT, Jackson follows the tumor radius $R(t)$:

$$\underbrace{\frac{dR}{dt}}_{\text{Time ROC of tumor radius}} = \underbrace{u(R(t),t).}_{\text{Tumor velocity at boundary}}$$

The model begins with a given cell density and radius, has zero local velocity at the tumor center, and no flux boundary conditions on the tumor center and outer boundary. Jackson assumes the androgen levels remain at a steady state until treatment begins and then decrease exponentially.

The behavior of this model agrees with experimental data, capturing the exponential growth pre-treatment, androgen-sensitivity following therapy, and eventual tumor regrowth. The results also predict that ADT can only be successful for a small range of parameters.

Ideta et al. *(2008)*

Ideta *et al.* presented the following ordinary differential equation model consisting of AI and AD cell populations in order to compare CAD and IAD with respect to

relapses:

$$\frac{dx_1(t)}{dt} = \{ \underbrace{\alpha_1 p_1\big(a(t)\big)}_{\text{proliferation rate}} - \underbrace{\beta_1 q_1\big(a(t)\big)}_{\text{apoptosis rate}} - \underbrace{m\big(a(t)\big)}_{\text{AD to AI mutation rate}} \}x_1(t) \tag{2.2a}$$

$$\frac{dx_x(t)}{dt} = \underbrace{m\big(a(t)\big)x_1(t)}_{\text{AD to AI mutation rate}} + \{\underbrace{\alpha_2 p_2\big(a(t)\big)}_{\text{proliferation rate}} - \underbrace{\beta_2 q_2\big(a(t)\big)}_{\text{apoptosis rate}} \}x_2(t) \tag{2.2b}$$

$x_1(t)$, $x_2(t)$ represent the size of the AD and AI populations, respectively. Similarly to Jackson, Ideta *et al.* also assumes that both the proliferation rate $\alpha_i p_i(a)$ and apoptosis rate $\beta_i q_i(a)$ for $i = 1, 2$ depend on androgen concentration $a(t)$, with a decrease in AD proliferation rate and increase in AD death rate during androgen deprivation. However Ideta *et al.* considers three possible net growth rates for AI cells. Their model also included mutations from AD to AI cells, where ma represents the rate at which these mutations occur. In order to model IAD therapy, Ideta *et al.* assume treatment is either present ($u = 1$) or absent ($u = 0$) and then they model the androgen with the following ODE:

$$\frac{da(t)}{dt} = \gamma(a(t) - a_0) - \gamma a_0 u(t).$$

When treatment is initiated, the androgen level decreases towards zero. When treatment is discontinued, the androgen level increases toward a steady state a_0. The parameter γ determines the speed by which the androgen concentration increases or decreases. Treatment switches from off to on when the PSA reaches an upper threshold r_1 and switches from on to off when the PSA reaches a lower threshold r_0. Both cell populations are assumed to contribute to the PSA concentration $y(t)$ at a constant rate:

$$y(t) = c_1 x_1 + c_2 x_2.$$

The numerical results demonstrated how the AI net growth rate influences whether or not a relapse can be avoided. Both numerical results and bifurcation analysis

showed that the parameters r_0 and r_1 greatly influence the time to relapse and relapse prevention. The results also show how the mutation rate m influences relapse prevention.

Hirata et al. *(2010, 2012)*

Hirata *et al.* considered three cell populations: AD (x_1), reversibly AI (x_2), and irreversibly AI (x_3) using the following model:

$$\frac{d}{dt}\begin{pmatrix} x_1(t) \\ x_2(t) \\ x_3(t) \end{pmatrix} = \begin{pmatrix} w^1_{1,1} & 0 & 0 \\ w^1_{2,1} & w^1_{2,2} & 0 \\ w^1_{3,1} & w^1_{3,2} & w^1_{3,3} \end{pmatrix} \begin{pmatrix} x_1(t) \\ x_2(t) \\ x_3(t) \end{pmatrix} \text{ for on-treatment periods, and} \tag{2.3a}$$

$$\frac{d}{dt}\begin{pmatrix} x_1(t) \\ x_2(t) \\ x_3(t) \end{pmatrix} = \begin{pmatrix} w^0_{1,1} & w^0_{1,2} & 0 \\ 0 & w^0_{2,2} & 0 \\ 0 & 0 & w^0_{3,3} \end{pmatrix} \begin{pmatrix} x_1(t) \\ x_2(t) \\ x_3(t) \end{pmatrix} \text{ for off-treatment periods.} \tag{2.3b}$$

The reversibly AI cells, possibly created by phenotypic plasticity, can revert back to AD cells, whereas the irreversibly AI cells cannot. Similarly to Ideta *et al.*, the irreversible changes can be due to mutations. The PSA levels P are modeled by the following:

$$P = x_1 + x_2 + x_3 \tag{2.4}$$

Hirata *et al.* (2010) fitted the model to clinical data and grouped patients into three categories: IAD prevents a relapse whereas CAD does not, IAD is more effective in delaying a relapse compared to CAD, and CAD is more effective in delaying a relapse compared to IAD. The first two and one-half cycles of treatment were used to find individualized parameters and then predict PSA responses to subsequent treatment. This approach was presented as a basis for future methods of individualized cancer treatment.

Portz et al. *(2012)*

Portz *et al.* developed a novel model of ADT by extending mathematical frameworks in ecology to the two-subpopulation models of ADT (Jackson, 2004b; Ideta *et al.*, 2008):

$$\frac{dX_1}{dt} = \underbrace{\mu_m\Big(1-\frac{q_1}{Q_1}\Big)X_1}_{\text{proliferation}} - \underbrace{d_1X_1}_{\text{death}} - \underbrace{\lambda_1(Q_1)X_1 + \lambda_2(Q_2)X_2}_{\text{switching}} \tag{2.5a}$$

$$\frac{dX_2}{dt} = \underbrace{\mu_m\Big(1-\frac{q_2}{Q_2}\Big)X_2}_{\text{proliferation}} - \underbrace{d_2X_2}_{\text{death}} - \underbrace{\lambda_2(Q_2)X_2 + \lambda_1(Q_1)X_1}_{\text{switching}} \tag{2.5b}$$

$$\frac{dQ_i}{dt} = \underbrace{v_m\frac{q_m-Q_i}{q_m-q_i}\frac{A}{A+v_h}}_{\text{uptake}} - \underbrace{\mu_m(Q_i-q_i)}_{\text{dilution}} - \underbrace{bQ_i}_{\text{degradation}} \tag{2.5c}$$

$$\frac{dP}{dt} = \underbrace{\sigma_0(X_1+X_2)}_{\text{baseline production}} + \underbrace{\sigma_1X_1\frac{Q_1^m}{Q_1^m+\rho_1^m} + \sigma_2X_2\frac{Q_2^m}{Q_2^m+\rho_2^m}}_{\text{androgen-dependent production}} - \underbrace{\varepsilon P}_{\text{clearance}} \tag{2.5d}$$

where

$$\underbrace{\lambda_1(Q) = c_1\frac{K_1^n}{Q^n+K_1^n}}_{\text{CS to CR}} \qquad \underbrace{\lambda_2(Q) = c_2\frac{Q^n}{Q^n+K_2^n}}_{\text{CR to CS}}$$

The cell quota model (Droop, 1968) is used for proliferation of both the AD (X_1) and AI (X_2) cell populations. Since AR signaling reflects the intracellular androgen-AR interactions, the cell quota (Q) is conceived as intracellular androgen concentrations. Two significant differences in this model from previous work (Ideta *et al.*, 2008) are how the AI cells are assumed be responsive to androgens and that PSA (P) production is androgen-dependent. The bidirectional mutation rates and cell-specific rates of PSA production are also functions of the cell quota. Cells have a constant death rate and also produce PSA at a constant, baseline rate. The model was validated with clinical data from Akakura *et al.* (1993) and its accuracy compared to that of the model by Ideta *et al.* (Ideta *et al.*, 2008). The androgen quota model exhibited significantly

greater accuracy for each patient data set. Portz *et al.*'s results supported the idea that ADT models should assume that AI cells maintain sensitivity to androgens, though to a lesser degree than AD cells. The model was also used to predict future hypothetical treatment cycles. However, unlike the method used by Hirata *et al.* (2010), predictive accuracy was not assessed using subsets of the data. While their conclusions provided information about the mechanisms of resistance, their patient specific predictions lack validity since they did not compare the predictions to 'future' data.

2.1.3 Methods and Findings

A mathematical model that accurately predicts the next cycle of treatment for an individual patient undergoing IAD therapy is an important tool that can potentially be used in a clinical setting. Here, we compare two models that are based on existing models to determine which is more accurate in predicting individual patients' PSA levels. For both models, parameters found for the first treatment cycle are then used to predict the observed response to the second cycle. We then compare this predicted second cycle to the data, when possible, to test the accuracy of the prediction. The process is then repeated in order to predict the third and fourth cycles, when possible. For each model, we also compare two different predictive methods; one method is based on previous cycles and the other depends on the PSA level. After comparing each model and method, our results suggest that a simpler model may be more beneficial for a predictive use and that further research is needed in this field prior to implementing mathematical models as a predictive method in a clinical setting.

2.2 Mathematical Models

2.2.1 Model 1: Extension of Model by Portz et al. *(2012)*

We propose the following prostate cancer model (Morken *et al.*, 2014), which is an extension of the model by Portz *et al.* with death rates dependent on cell androgen quotas:

$$\frac{dX_1}{dt} = \underbrace{\mu_m\Big(1-\frac{q_1}{Q_1}\Big)X_1}_{\text{proliferation}} - \underbrace{D_1(Q_1)X_1}_{\text{death}} - \underbrace{\lambda_1(Q_1)X_1 + \lambda_2(Q_2)X_2}_{\text{switching}} \tag{2.6a}$$

$$\frac{dX_2}{dt} = \underbrace{\mu_m\Big(1-\frac{q_2}{Q_2}\Big)X_2}_{\text{proliferation}} - \underbrace{D_2(Q_2)X_2}_{\text{death}} - \underbrace{\lambda_2(Q_2)X_2 + \lambda_1(Q_1)X_1}_{\text{switching}} \tag{2.6b}$$

$$\frac{dQ_i}{dt} = \underbrace{v_m\frac{q_m-Q_i}{q_m-q_i}\frac{A}{A+v_h}}_{\text{uptake}} - \underbrace{\mu_m(Q_i-q_i)}_{\text{dilution}} - \underbrace{bQ_i}_{\text{degradation}} \tag{2.6c}$$

$$\frac{dP}{dt} = \underbrace{\sigma_0(X_1+X_2)}_{\text{baseline production}} + \underbrace{\sigma_1 X_1\frac{Q_1^m}{Q_1^m+\rho_1^m} + \sigma_2 X_2\frac{Q_2^m}{Q_2^m+\rho_2^m}}_{\text{androgen-dependent production}} - \underbrace{\varepsilon P}_{\text{clearance}} \tag{2.6d}$$

where

$$D_i(Q_i) = \underbrace{d_i\frac{R_i^\alpha}{Q_i^\alpha+R_i^\alpha}}_{\text{AD Apoptosis}} + \underbrace{\delta_i}_{\text{AI Death}}$$

and

$$\underbrace{\lambda_1(Q) = c_1\frac{K_1^n}{Q^n+K_1^n}}_{\text{CS to CR}} \qquad \underbrace{\lambda_2(Q) = c_2\frac{Q^n}{Q^n+K_2^n}}_{\text{CR to CS}}$$

Variables X_1 and X_2 represent the AD and AI cell populations, respectively. The terms 'androgen-dependent' and 'androgen-independent' have been used previously in both mathematical models as well as in biological literature (Isaacs, 1999; Feldman and Feldman, 2001; Jackson, 2004a; Ideta *et al.*, 2008; Hirata *et al.*, 2012). However, 'androgen-independent' cells are often not completely independent, but have a lower threshold for androgens. Thus, we refer to AD and AI cells as 'castration-sensitive'

(CS) and 'castration-resistant' (CR), respectively, as seen in recent literature (Scher *et al.*, 2004; Labrie, 2011; Fong *et al.*, 2012; Nelson, 2012). The proliferation rates are given by Droop's model, which is dependent upon some cell quota, or limiting nutrient. Here, the cell quota (Q) is interpreted as the quantity of intracellular androgen. The parameter μ_m represents the maximum proliferation rate and q_i is the minimum cell quota. Since CR cells are able to proliferate at lower levels of androgen, $q_2 < q_1$.

Portz *et al.* (2012) assume for simplicity the cell death rate is constant. Our extension incorporates an androgen-dependent death rate in addition to the constant death rate δ_i. The parameter d_i represents the maximum androgen-dependent death rate. The shape parameters R_i and α represent the half saturation level and Hill coefficient, respectively, which describe the cell death rate sensitivity to the cell quota level. Whereas Jackson (2004a,b) and Ideta *et al.* (2008) assume the AI death rate decreases as the androgen concentration decreases, we assume the death rate increases as the androgen concentration decreases, which is supported by biological results (Feldman and Feldman, 2001; Scher *et al.*, 2004).

The model also assumes androgen-dependent mutation rates, λ_i, to account for switching between the cell populations. The parameters c_1 and c_2 represent the maximum switching rates. The parameters K_i and n represent the half saturation level and Hill coefficient, respectively, which describe the cell switching sensitivity to the cell quota level. We interpret these switching rates as both accommodative and adaptive switching (Morken *et al.*, 2014).

As serum androgen A increases, androgen uptake rate increases but saturates. The asymptotic maximum uptake rate is regulated by the cell quota $Q(t)$, maximum cell quota q_m, minimum cell quota q_i, and maximum uptake rate v_m. The parameter v_h represents the uptake half saturation level. The term $\mu_m(Q_i - q_i)$ represents the amount of cell quota used by the cell for growth. Intracellular androgen degrades at

rate b.

Both cell populations contribute to the amount of PSA, P, at both a baseline rate σ_0 and an androgen-dependent rate. The parameters $\sigma_{1,2}$ represent the maximum androgen-dependent PSA productions by the two cell populations. The shape parameters ρ_i and m represent the half saturation level and Hill coefficient, respectively, which describe the PSA production rate sensitivity to the cell quota level. PSA is cleared from the blood at rate ε. For further details on the Portz *et al.* model formulation and explanation, see Section 2.1.2.

2.2.2 Model 2: Model by Hirata et al. *(2010, 2012)*

We compare the predictions produced using Model 1 to the predictions produced from the model by Hirata *et al.*, system (2.3). Whereas Model 1 captures the intermittent property using serum androgen levels as an input, Model 2 uses a binary on- or off-treatment input. Following Hirata *et al.*, the parameters were constrained so that the non-diagonal parameters are non-negative, $w^1_{3,3} \geq 0$, and the cell class can change its volume by at most 20% per day, namely $\left|\sum_{i\in\{1,2,3\}} w^m_{i,j}\right| < 0.2$, where $j \in \{1,2,3\}$ and $m \in \{0,1\}$. See (Hirata *et al.*, 2010, 2012) for further model details.

2.3 Data and Simulations

Akakura *et al.* (1993) studied seven patients undergoing intermittent androgen deprivation therapy. Four of the men (patients 1, 2, 3, 5) had stage C cancer, in which the cancer had spread outside the prostate, but not yet to other parts of the body; one man (patient 4) had stage D1 cancer, in which the cancer had only spread to local lymph nodes; two men (patients 6, 7) had stage D2 or widely disseminated metastatic cancer (National Cancer Institute, 2013). The data consisted of serum PSA and testosterone levels, obtained at monthly intervals. Patients received goserelin acetate

Para.	Meaning	Value	Reference
μ_m	Maximum proliferation rate	0.009 - 0.045 /day	(Berges *et al.*, 1995)
q_1	Minimum CS cell quota	0.19 - 0.29 nM	(Portz *et al.*, 2012)
q_2	Minimum CR cell quota	0.10 - 0.21 nM	(Portz *et al.*, 2012)
σ_1	CS PSA production rate	0.0001 - 0.28 ng/mL/cell/day	
σ_2	CR PSA production rate	0.06 - 0.36 ng/mL/cell/day	
σ_0	Baseline PSA production rate	0 - 0.031 ng/mL/cell/day	
d_1	Maximum CS CDR	0.0035 - 0.029 day^{-1}	*
d_2	Maximum CR CDR	0.0019 - 0.0059 day^{-1}	*
R_1	CS CDR half-saturation level	0.46 - 3.02 nM	*
R_2	CR CDR half-saturation level	0.96 - 6.17 nM	*
δ_1	CS androgen independent death rate	0.0006 - 0.0083 day^{-1}	*
δ_2	CR androgen independent death rate	0.011 - 0.042 day^{-1}	*
c_1	Maximum CS to CR mutation rate	0.00016 day^{-1}	(Portz *et al.* (2012) Ideta *et al.* (2008))
c_2	Maximum CR to CS mutation rate	0.00012 day^{-1}	(Portz *et al.*, 2012)
K_1	CS to CR mutation half-saturation level	0.8 nM	(Portz *et al.*, 2012)
K_2	CR to CS mutation half-saturation level	1.7 nM	(Portz *et al.*, 2012)
n	Selection function exponent	3	
q_m	Maximum cell quota	5 nM	(Portz *et al.*, 2012)
v_m	Maximum uptake rate	0.27 nM/day	(Portz *et al.*, 2012)
v_h	Uptake rate half-saturation level	4 nM	(Portz *et al.*, 2012)
b	Intracellular androgen degradradation rate	0.09 day^{-1}	(Portz *et al.*, 2012)
ρ_1	CS PSA production half-saturation level	1.3 nM	(Portz *et al.*, 2012)
ρ_2	CR PSA production half-saturation level	1.1 nM	(Portz *et al.*, 2012)
m	PSA production function exponent	3	(Portz *et al.*, 2012)
ε	PSA clearance rate	0.08 day^{-1}	(Portz *et al.*, 2012)
α	CDR function exponent	3	

Table 2.1: Model 1 Parameter Ranges. In the table, * indicates values such that total cell death rate (CDR) is within biological ranges (Berges *et al.*, 1995; Ideta *et al.*, 2008).

Para.	Meaning	Value
w_{11}^1	on-treat. AD growth rate	-.15 - -.015
w_{22}^1	on-treat. rAI growth rate	-0.015 - .0009
w_{33}^1	on-treat. irrAI growth rate	0.002-0.003
w_{21}^1	on-treat. AD to rAI influx rate	0.0006 - 0.002
w_{31}^1	on-treat. AD to irrAI influx rate	0.0003 - 0.001
w_{32}^1	on-treat. rAI to irrAI influx rate	0-0
w_{11}^0	off-treat. AD growth rate	.001 - .003
w_{22}^0	off-treat. rAI growth rate	.002 - .008
w_{33}^0	off-treat. irrAI growth rate	-.13 - -.0044
w_{12}^0	off-treat. rAI to AD influx rate	0.049 - 0.18

Table 2.2: Model 2 Parameter Ranges. In the table, rAI stands for reversible AI cells, irrAI stands for irreversible AI cells, and treat. stands for treatment. The value constraints follow Hirata *et al.* (2010, 2012).

(an LHRH agonist) and cyproterone acetate (an anti-androgen) until the PSA level reached a normal level and remained in this range for about four months, although the duration of remission varied greatly among the patients. The patients then stayed off therapy until PSA levels reached about 20 ng/mL. It should be noted that Akakura *et al.* state that the upper limit of 20 ng/mL was set arbitrarily and also seems to vary among the patients. For more information on the study, see (Akakura *et al.*, 1993).

Since we use the PSA data to verify the models, we are able to use the androgen data directly for Model 1. Following Portz *et al.* (2012), we interpolated the androgen data using piecewise cubic hermit splines and an exponential function between the last off-treatment $A(t_i)$ and first on-treatment $A(t_f)$ data points:

$$A(t) = A(t_f) + \big(A(t_i) - A(t_f)\big)e^{-(\gamma/l)(t-t_i)}, \tag{2.7}$$

where $l = 1$. This equation was also used for the predicted off-treatment PSA growth with $l = 100$ for Method 2 (Section 2.3.2).

After first fitting the free parameters by hand, we used the Nelder-Mead simplex algorithm (Lagarias *et al.*, 1998) to find the free parameters that minimized the mean square error (MSE) between the PSA data and model. The fixed parameter values as well as the free parameter ranges for Model 1 and Model 2 can be found in Table 2.1 and Table 2.2, respectively. In order to test the accuracy of the prediction, we first find the parameters using only 1.5 cycles of data. Using these parameters, we then run the model for another treatment cycle and compute the error between the future model and the remaining, or 'future', data. We repeat this process using 2.5 cycles of data and then 3.5 cycles of data when possible.

In order to make future PSA predictions, we must first generate future serum androgen levels. We propose two different methods, described below, for generating these future androgen levels and then apply these methods to the models. The models and methods are summarized in Table 2.3. To compare these methods and models, we compute both the MSE and mean relative error (MRE) (Table 2.6) as well as plot the results. The figures compare Model 1 and Model 2, each using both prediction methods, to clinical data for both the PSA levels (ng/mL) and the serum androgen levels (nM) where applicable. The right of the vertical dashed line represents the prediction with the 'future' data overlaid for comparison.

2.3.1 Prediction Method 1: Average Function

We implemented the method used by Portz *et al.* (2012) for generating future serum androgen levels, which consists of generating a rectangular function based on the average off- and on-treatment serum androgen values and off- and on-treatment durations. To apply this method to Model 2, we set the on- and off-treatment binary switch to occur after mean durations of on- and off-treatment.

	Model 1	Model 2
Method 1	Cell quota model with average function	Piecewise linear model with average function
Method 2	Cell quota model with threshold function	Piecewise linear model with threshold function

Table 2.3: Description of Methods and Models

2.3.2 Prediction Method 2: Threshold Function

During the clinical trial (Akakura *et al.*, 1993), the treatment resumed once the PSA levels reached the approximate threshold of 20 ng/mL. This implies that the future androgen levels should depend on the future PSA level. In this method, once the mean on-treatment duration ends, the androgen level increases using equation (2.7) until a PSA threshold is reached and then decays according to equation (2.7). Similarly, for Model 2, the treatment remained off until the PSA levels reached a threshold and then the model switched to the on-treatment equations.

2.4 Results

Portz *et al.* (2012) used all the provided data to predict the observed response to a hypothetical future cycle of treatment. However, in doing so, they were not able to test the accuracy of their predictions because they lacked the future data. We first use an extension of their model (Model 1) and their method (Method 1) and use the technique described above (parameterize with part of the data set and use the rest as the 'future' that the model is predicting) to determine the accuracy of the predictions. We then repeat the process using Method 2. Finally, we perform the same process on Model 2 (use methods 1 and 2 to make predictions) resulting in a total of 4 sets of predictions. The results are summarized in Table 2.4. A description of the patient-specific predictions are found in Table 2.5 and the patient-specific errors are

	Model 1	Model 2
Method 1	Not accurate	More accurate, incorrect timing or under
Method 2	More accurate, incorrect timing	More accurate, incorrect timing

Table 2.4: Method and Model Prediction Comparison Summary. Under refers to under-predicting the PSA levels.

Patient	Cycle	Description			
		Model 1		Model 2	
		Meth. 1	Meth. 2	Meth. 1	Meth. 2
1	1.5	under	shift	mostly accurate	mostly accurate
1	2.5	over	shift	shift	shift
2	1.5	under, shift	shift	under, shift	shift
3	1.5	over, shift	shift	shift	shift
4	1.5	under	under, shift	under	over, shift

Table 2.5: Testable Patient-Specific Prediction Summary. Under refers to under-predicts, over refers to over-predicts, and shift refers to a phase-shift. Cycle refers to the number of cycles of data used to make the prediction

found in Table 2.6. In the following subsections, we discuss the patient 1 predictions and the general results for each model and method.

2.4.1 Model 1, Method 1

The model is extremely accurate when fitting the data used to parameterize the model; however, the model is not always accurate when predicting the future cycle (Table 2.6). When using 1.5 cycles of data for patient 1 (Figure 2.1), the model under-predicts the PSA levels, only reaching about 6 ng/mL, when in reality the patient's levels reached about 13 ng/mL. In a clinical setting, the model would indicate that the patient could continue off-treatment when in reality the patient resumed

Patient	Cycle	Future MSE				Future MRE			
		Model 1		Model 2		Model 1		Model 2	
		Meth. 1	Meth. 2	Meth. 1	Meth. 2	Meth. 1	Meth. 2	Meth. 1	Meth. 2
1	1.5	20.26	34.50	17.02	17.05	.7190	2.076	.9650	.9665
1	2.5	111.7	42.23	22.41	22.62	2.433	1.278	.7278	.7519
2	1.5	27.80	47.83	22.67	50.628	.6249	.9888	.7510	1.0591
3	1.5	319.0	213.46	224.98	206.5	.5176	.2928	.4726	.4586
4	1.5	45.54	54.40	19.43	54.21	.5125	.5517	.3853	.7026

Table 2.6: Prediction Errors. Cycle refers to the number of cycles of data used to make the prediction

treatment. When assuming 2.5 cycles of data, the model over-predicts the PSA levels, reaching about 37 ng/mL, when in reality the patient reached levels around 20 ng/mL before resuming treatment. In this case, the model would recommend that the patient resume treatment much sooner that apparently necessary, shortening their off-treatment period, perhaps decreasing quality of life unnecessarily. With all 3.5 cycles of data, the model again suggests high PSA levels; however, we are not able to test the accuracy of the fourth cycle due to a limited amount of data. Similarly for patients 2-4 (Figures 2.2, 2.3, 2.4), the predictions are not very accurate in predicting the PSA levels (Tables 2.5, 2.6). Since the data for patients 5-7 (Figure 2.5) consisted of only 1.5 cycles of data, we were not able to test the accuracy of these predictions.

2.4.2 Model 1, Method 2

We repeated the process of predicting the outcomes of patients using Model 1 with Method 2. For patient 1 (Figure 2.1), assuming 1.5 cycles of data, Method 2 much more accurately predicts the maximum PSA level (about 13 ng/mL) compared to Method 1, although it takes more days to reach this maximum compared to the data. This 'shift' in the PSA levels explains the high error values (Table 2.6). Similarly,

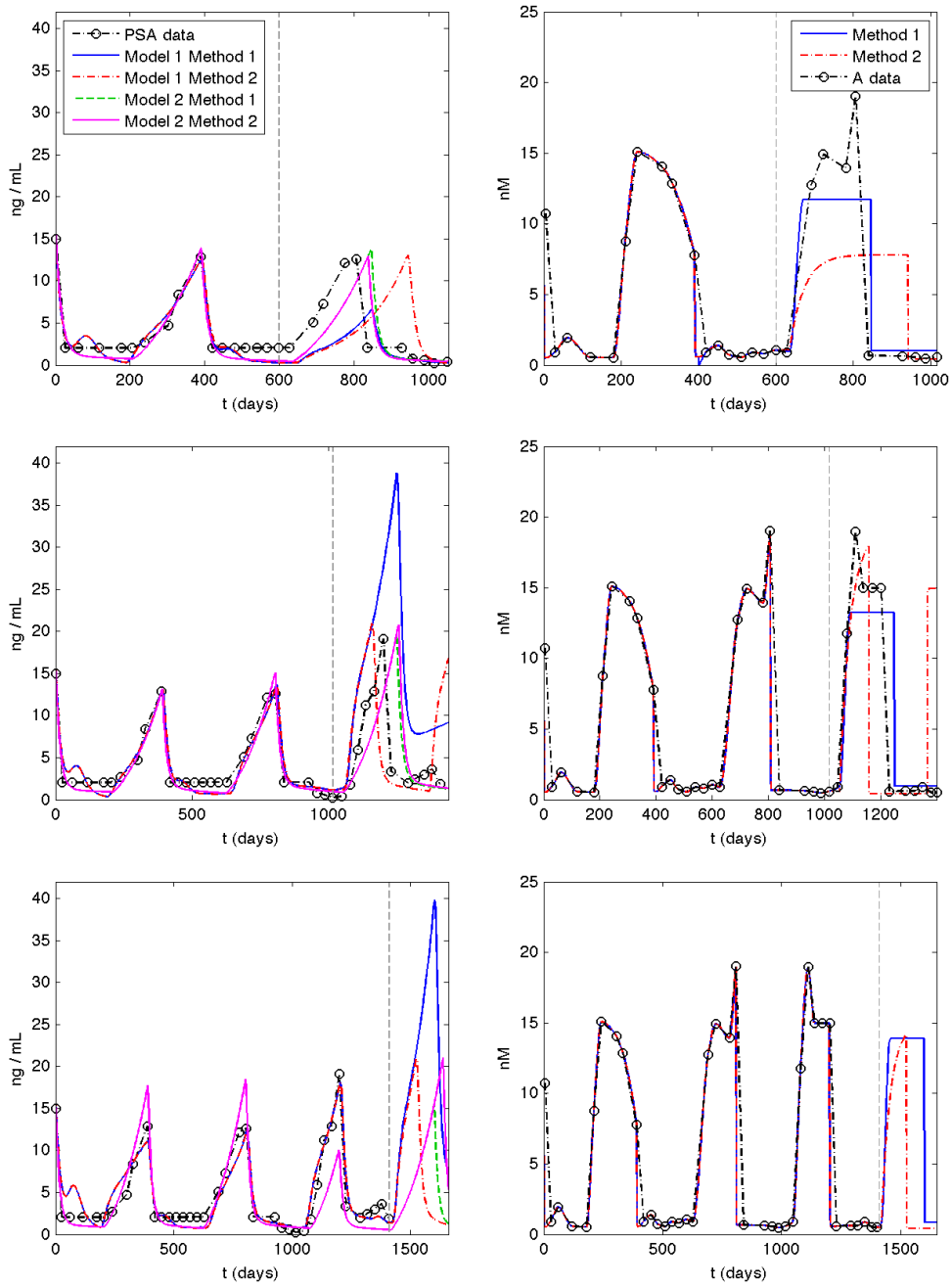

Figure 2.1: Patient 1 PSA levels (left) and serum androgen levels (right) using 1.5 cycles of data (top row), 2.5 cycles (second row), and all 3.5 cycles (third row). The right of the vertical dashed line represents the prediction with the 'future' data overlaid for comparison.

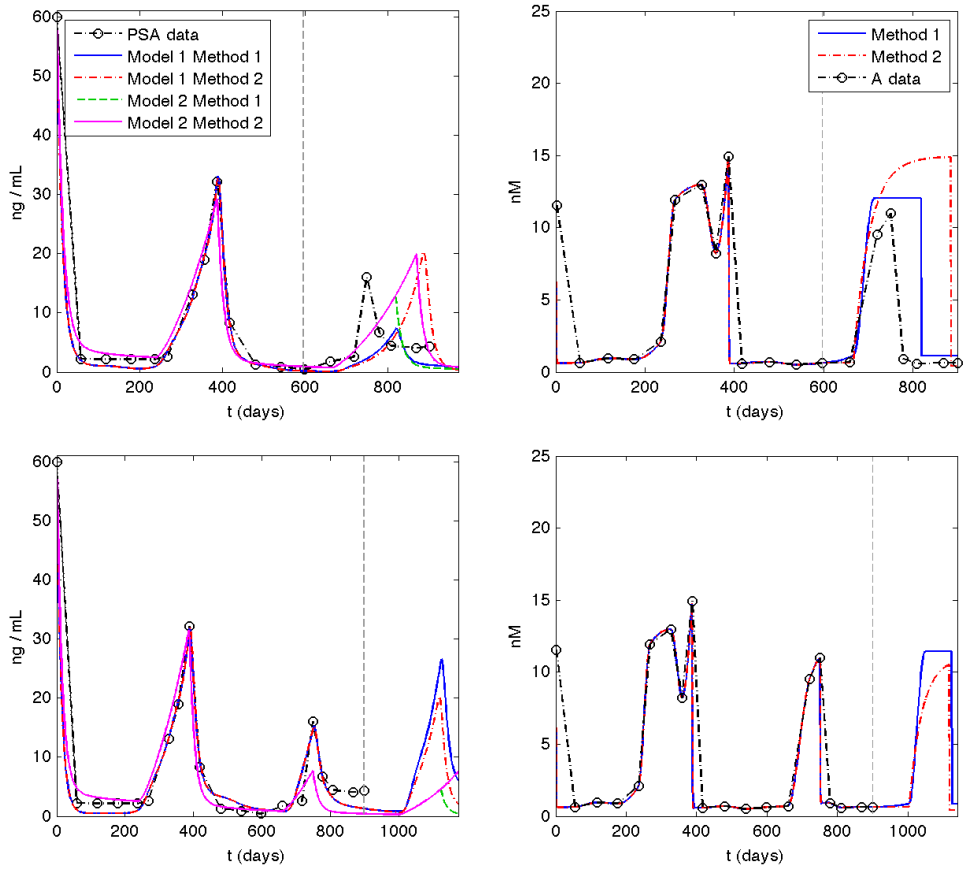

Figure 2.2: Patient 2 PSA levels (left) and serum androgen levels (right) using 1.5 cycles of data (top row) and all 2.5 cycles (second row). The right of the vertical dashed line represents the prediction with the 'future' data overlaid for comparison.

when using 2.5 cycles of data, the predicted PSA levels are 'shifted' compared to the data and thus incorrectly recommended an earlier start for the fourth cycle. However, the MSE and MRE values are smaller than with Method 1, suggesting a better overall fit. When using all 3.5 cycles of data, Method 2 predicts a maximum PSA level similar to that of the previous cycles, which is much smaller than the predicted PSA levels using Method 1. In general, Method 2 more accurately predicts the PSA peak, as expected, but the timing is often incorrect as seen by the 'shift' in PSA levels.

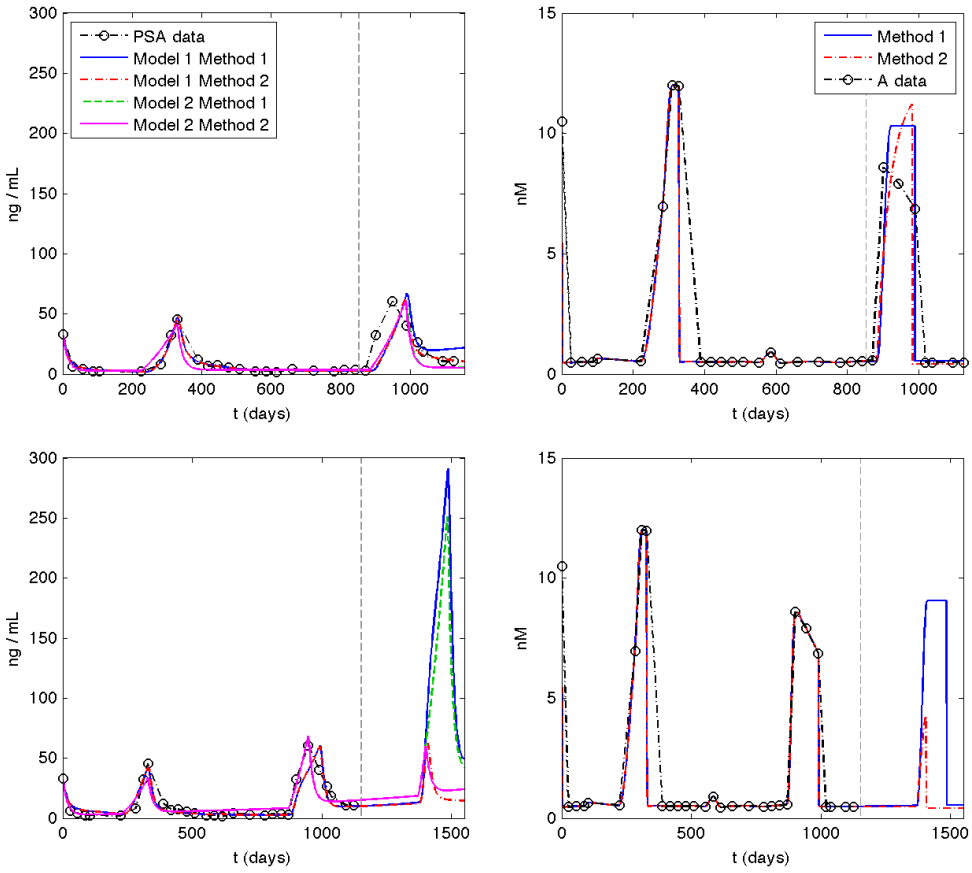

Figure 2.3: Patient 3 PSA levels (left) and serum androgen levels (right) using 1.5 cycles of data (top row) and all 2.5 cycles (second row). The right of the vertical dashed line represents the prediction with the 'future' data overlaid for comparison.

2.4.3 Model 2, Method 1

We repeated the process a third time using Model 2 with Method 1. For patient 1 using 1.5 cycles of data (Figure 2.1), the model accurately predicts the PSA level outcome with the smallest MSE value, although the PSA levels are shifted slightly (Table 2.6). Similarly, when assuming 2.5 cycles of data, the model produces the most accurate prediction, as measured by both MSE and MRE, even though there is a slight shift. In general, Model 2 using prediction Method 1 seems more accurate compared

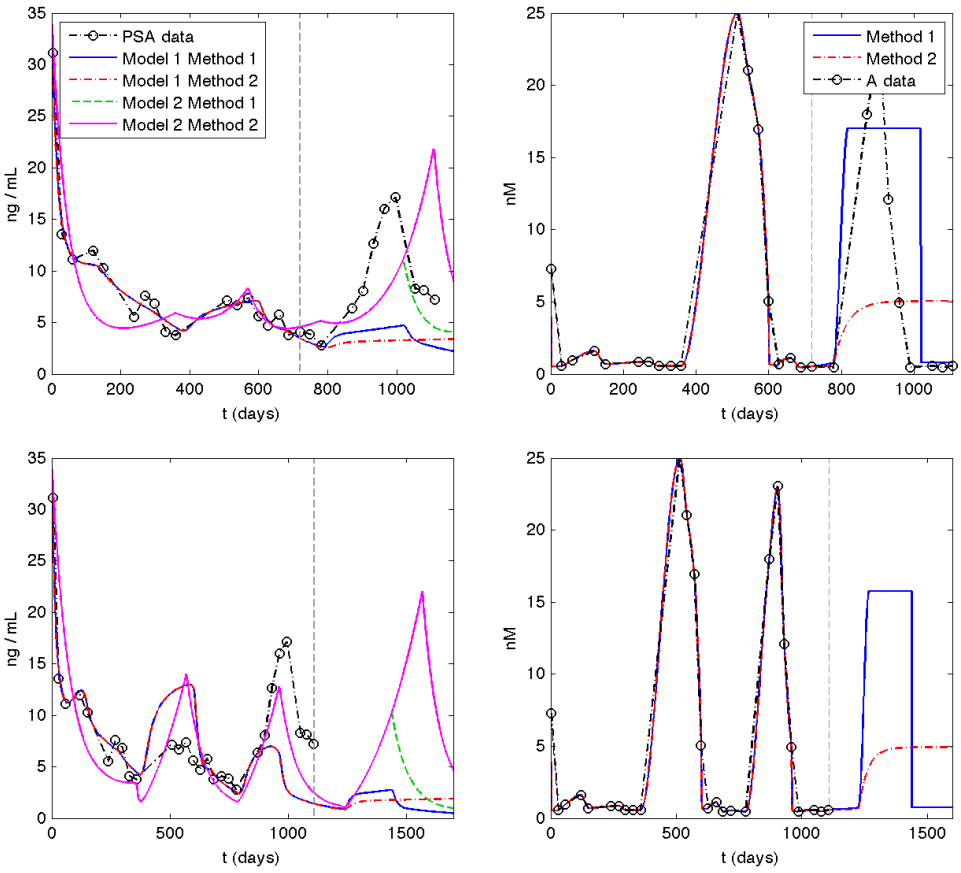

Figure 2.4: Patient 4 PSA levels (left) and serum androgen levels (right) using 1.5 cycles of data (top row) and all 2.5 cycles (second row). The right of the vertical dashed line represents the prediction with the 'future' data overlaid for comparison.

to Model 1; however, the reasons for the errors vary among patients between a 'shift' in PSA levels and under-predicting the PSA peak (Table 2.5).

2.4.4 Model 2, Method 2

Model 2 with Method 2 produced similar results to Model 2 with Method 1. During off-treatment, the PSA levels increase at the same rate for both methods; however, the timing for the switch to on-treatment is different, by design of the methods. For patient

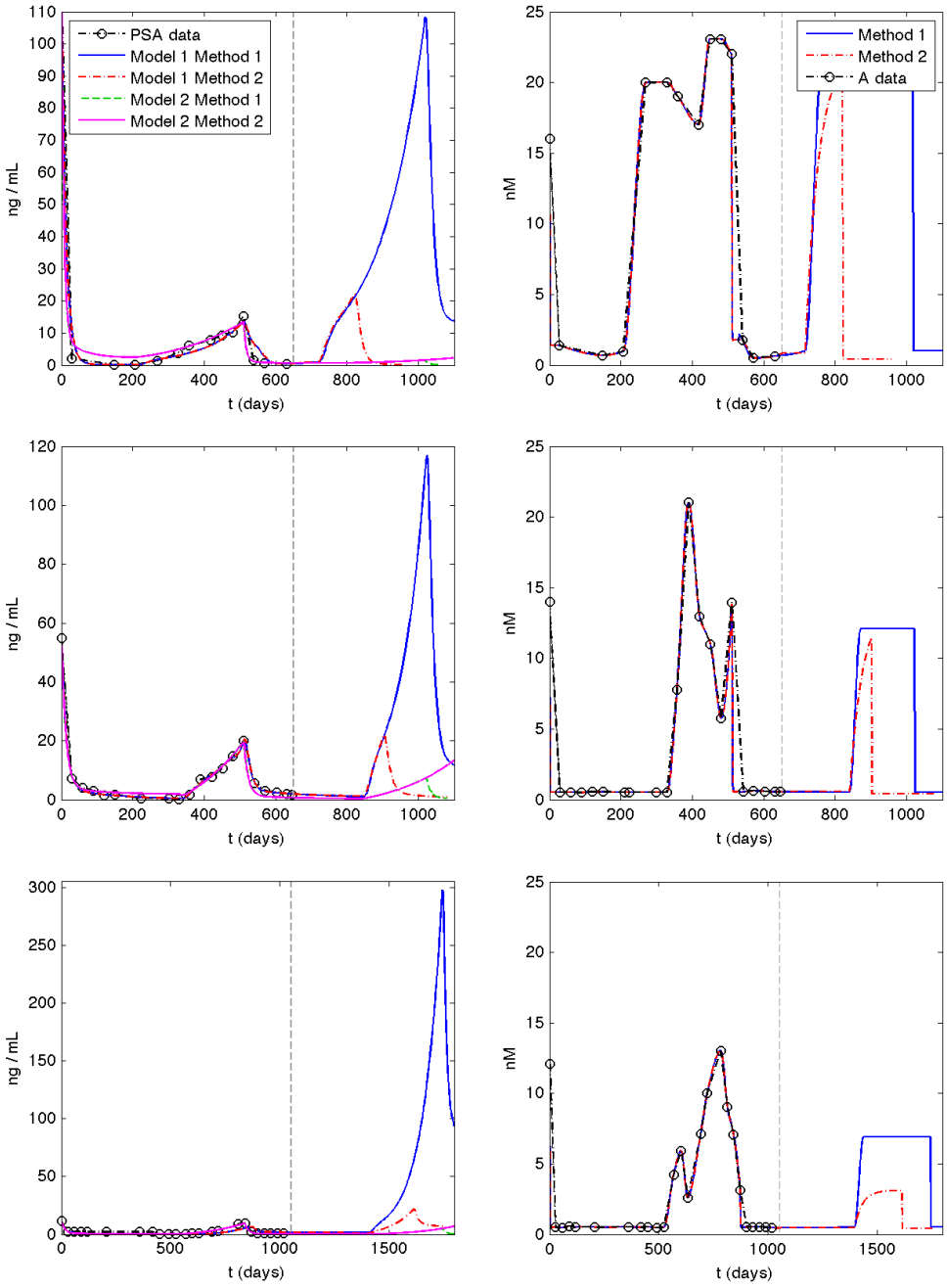

Figure 2.5: PSA levels (left) and serum androgen levels (right) for patient 5 (top row), patient 6 (second row), and patient 7 (third row) using all 1.5 cycles of data. The right of the vertical dashed line represents the prediction with the 'future' data overlaid for comparison.

1 (Figure 2.1) assuming both 1.5 and 2.5 cycles of data, Methods 1 and 2 produce very similar results. When using all 3.5 cycles, Method 2 switches to on-treatment later than Method 1, producing a larger maximum PSA value. When using 1.5 cycles, Model 2 produces a higher rate of increase in PSA levels than Model 1. However when assuming 2.5 and 3.5 cycles, Model 1 produces higher rate of increase in PSA levels. In general, as it did with Model 1, Method 2 here predicts the peak PSA values well, but the timing is often incorrect (Tables 2.4, 2.5).

2.5 Discussion

Here we extend the work of Portz *et al.* (2012) by first modifying their model to add biological realism and then testing the accuracy of the model's predictions. Similarly to Hirata *et al.* (2010, 2012), we use a portion of the data to find patient specific parameters that minimize the error between the data and the model, and then use these parameters to predict the next cycle of treatment. To determine the accuracy of our prediction, we calculate the MSE and MRE values to quantify how well the model predicted PSA dynamics for the portion of the data not used for parameterization (Table 2.6). We use this same process in order to compare the accuracy of the predictions produced by the two prostate cancer treatment models using the two different predictive methods. The model by Hirata *et al.* is a system of piecewise linear ordinary differential equations representing an AD and two AI cell populations. This model is simpler than the extended Portz *et al.* model; it contains fewer parameters and does not consider the serum androgen levels. While the first predictive method is based on previous treatment cycles, Method 2 more accurately follows the methods of the clinical study; the future serum androgen levels are dependent upon the PSA levels and thus prevent the PSA levels from becoming too high and biologically unreasonable. While Model 1, using the prediction method

proposed by Portz *et al.*, which we call "Method 1", is able to fit the data used for parameterization well, it is not very accurate in predicting the future cycle. In fact while using Model 1, both prediction methods are about equally (in)accurate. When comparing Model 1 to Model 2, Model 2 has smaller MSE values for all of the predicted cycles that were compared to 'future' data. Using Model 2, the prediction methods are again comparable, both in MSE and MRE values. Therefore, while neither model is extremely accurate, Model 2 is more accurate in predicting PSA values than Model 1 using the small sample of 7 patients. This implies that while a biologically-based model is important in understanding the biological mechanisms of the process, a simpler model is more accurate and may be more useful for predicting future outcomes of individual patients.

In a clinical setting, the goal is not only to accurately predict the future PSA levels, but to determine whether or not a patient can go off-treatment for another cycle, thus improving their health-related quality of life. Ideally once the patient resumes treatment, the PSA levels return back to normal and remain there while on-treatment. However, it is possible that the patient has developed resistance to treatment and the PSA levels remain higher than normal. Since doctors cannot know if a patient's tumor has become castration-resistant, the doctors must use their best judgment to determine if and when a patient should go off-treatment.

Our goal is to provide the doctors with a computational tool to help them make a more objective decision about a patient's treatment. We test our mathematical model to determine if it can predict whether or not a patient can go off-treatment. First we consider the predictions that could be compared with 'future' data, which we describe as testable, and we consider 'normal levels' to be the low PSA levels during the last on-treatment period. Model 1 using Method 1 was only able to correctly predict a return to normal levels for 3 out of the 5 testable predicted cycles. Model 1 using

Method 2 and Model 2 using Method 1 were able to predict this return to normal levels for all of the testable predicted cycles. With Method 2, Model 2 was only able to predict the return to normal levels for 4 of the 5 testable predicted cycles. However, for 4 of the 12 predicted cycles, the model had not yet predicted the full cycle in the given time, since the model predicted a very slow increase in PSA levels. Thus, Model 1 using Method 2 and Model 2 using Method 1 were able to correctly predict that the patient could go off-treatment for all the testable predicted cycles. Therefore Model 1 using Method 2 and Model 2 using Method 1 might be of some help in designing treatment protocols in a clinical setting.

We then consider the predictions which could not be compared to data since there was no more 'future' data, which we call non-testable. Here we consider a PSA level of 4 ng/mL to be normal (Hirata *et al.*, 2010). Model 1 using Method 1 predicted a return to normal levels in 1 of the 7 non-testable predicted cycles, Model 1 using Method 2 predicted this return for 5 of the 7, Model 2 using Method 1 predicted this for 6 of the 7, and Model 2 using Method 2 predicted this for 1 of the 7. Since we do not have data to compare these predictions to, we do not know if the levels return to normal or not, i.e. if the patient has developed resistance to the treatment or not. From the results above, Model 1 using Method 2 and Model 2 using Method 1 predict that a majority of the patients do not develop resistance in the time shown whereas Model 1, Method 1 and Model 2, Method 2 suggest that almost all the patients develop resistance in the time shown.

2.6 Future Research

One possible direction for furthering this research is to reduce the length of predicting time; you could predict a shorter time-span with the idea that you could update the prediction as more data is collected. Also, using only the most recent

1.5 cycles of data might produce a more accurate prediction. In order to test this hypothesis, a dataset with several cycles for a patient would be needed. Modeling the androgen levels, instead of using the serum levels as an input, might also be beneficial. Another interesting question to research would be determining the optimal time for switching between on- and off- treatment in individual patients. The goal would be to find the times for switching that allow for the longest off-treatment duration, in order to improve the patient's quality of life, while also decreasing the probability of a relapse.

In this research, the free parameters were determined using a method described in literature (Portz *et al.*, 2012). Additional biological insights might be gained by performing parameter sensitivity analysis on these parameters. While the Nelder-Mead simplex algorithm method finds a local minimum, it is not guaranteed to find a global minimum and is thus very dependent upon the initial guesses of the free parameters. Also, in the process parameterizing a model using a patient's data, we are disregarding the commonality of the parameters among all the patients. It would be interesting to explore the use of Bayesian inference to estimate the parameters using all the data, with the stochasticity being due to the measurement error when obtaining the serum PSA levels. Since the likelihood functions would be dependent upon solving the model, the Metropolis-Hastings algorithm, a Markov Chain Monte Carlo method, could be used for sampling from the target distribution. This could be extended to incorporate heterogeneity among patients by using hierarchal Bayesian methods and exploring whether the parameters depend on the stage of cancer, the number of cycles of IAS therapy, age, or other differences among the patients.

Chapter 3

CHRONIC MYELOID LEUKEMIA

3.1 Introduction

3.1.1 Chronic Myeloid Leukemia and Treatment

Chronic myeloid leukemia (CML) is a cancer of the tissue that produces white blood cells. It is a disorder of hematopoietic stem cells characterized by the increased growth of myeloid cells in the bone marrow and the excessive presence of these cells in the blood. CML can be molecularly diagnosed by detecting the presence of the Philadelphia (Ph) chromosome and the fusion oncogene *BCR-ABL*. This oncogene is the result of translocation of the *BCR*, or breakpoint cluster region, gene located on chromosome 22 and the *ABL*, or Ableson leukemia virus, gene located on chromosome 9 (Sawyers, 1999). This oncogene encodes the protein BCR-ABL, a constitutively active tyrosine kinase, which can result in deregulated cellular proliferation (Goldman and Melo, 2003). The progression of CML consists of three phases. The first phase, called the benign chronic phase, is typically asymptomatic and can last for several years untreated. The accelerated phase then follows and leads to the last phase, called blast crisis, which is characterized by an abnormally high number of stem cells and precursor cells in the blood or bone marrow (Abbott and Michor, 2006). CML can advance from the chronic phase to the fatal blast crisis phase in a timespan of 3 to 5 years (Sawyers, 1999).

For CML patients in which the *BCR-ABL* oncogene is detected, targeted molecular therapy can be used to inhibit the growth of stem cells. Imatinib, also known as STI-571 and Gleevec (Capdeville *et al.*, 2002), binds to the ATP binding site of BCR-ABL,

stopping cell-growth signals and decreasing cell proliferation (Frame, 2006). Previously, treatment options included other drugs, such as hydroxyurea or interferon alpha, and allogeneic bone marrow transplants. Imatinib, which is effective in all phases of CML progression, is now a widely used primary treatment option for BCR-ABL positive CML patients (Abbott and Michor, 2006).

Initial diagnosis of BCR-ABL-positive CML and subsequent treatment efficacy is typically measured using BCR-ABL transcript levels obtained using quantitative reverse transcription polymerase chain reaction (Roeder *et al.*, 2006). The amount of BCR-ABL transcript is then normalized using some control gene, usually BCR or ABL. Thus the data is presented as BCR-ABL/control gene percentages (BCR-ABL/ABL%) (Muller *et al.*, 2003; Roeder *et al.*, 2006).

Most CML patients with imatinib treatment exhibit a biphasic profile, which means that the patients exhibit an initial rapid decline followed by a gradual decline in BCR-ABL/ABL%. However, some patients exhibit a monophasic or triphasic profile. The BCR-ABL/ABL% for a monophasic profile gradually declines over time. Patients with a triphasic profile can exhibit a rapid BCR-ABL/ABL% decline followed by a relatively gradual BCR-ABL/ABL% decline, followed by a rapid BCR-ABL/ABL% increase (Stein *et al.*, 2011). The increase in the triphasic profile is most likely caused by mutations in the BCR-ABL gene that encode resistance to imatinib (Gorre *et al.*, 2001; Frame, 2006; Griswold *et al.*, 2006; Stein *et al.*, 2011), although gene amplification is also a possible cause for resistance (Gorre *et al.*, 2001). When treatment is stopped, the BCR-ABL/ABL% of some patients rapidly increases to levels at or beyond pre-treatment baseline (Michor *et al.*, 2005). There are different hypotheses as to the cause of this increase and mathematical modeling techniques have the potential to be helpful in elucidating the underlying mechanisms of therapy resistance.

3.1.2 *Recent Works*

Several groups have utilized mathematical modeling to study the effect of targeted treatment and imatinib on CML, including Roeder *et al.* (2006) and Michor *et al.* (2005); Michor (2007b).

Michor et al. *(2005); Michor (2007b)*

In 2005, Michor *et al.* (2005) proposed a mathematical model that describes the abundances of normal (x), imatinib dependent leukemic (y), and imatinib-resistant (z) cell populations in a CML patient. Each cell population comprises four cellular subpopulations: stem cells (i_0), progenitors (i_1), differentiated cells (i_2), and terminally differentiated cells (i_3), where $i = x, y, z$. The basic model is therefore described by the following ODEs:

$$\begin{array}{lll} \dot{x_0} = [\lambda(x_0) - d_0]x_0 & \dot{y_0} = [r_y(1-u) - d_0]y_0 & \dot{z_0} = (r_z - d_0)z_0 + r_y y_0 u \\ \dot{x_1} = a_x x_0 - d_1 x_1 & \dot{y_1} = a_y y_0 - d_1 y_1 & \dot{z_1} = a_z z_0 - d_1 z_1 \\ \dot{x_2} = b_x x_1 - d_2 x_2 & \dot{y_2} = b_y y_1 - d_2 y_2 & \dot{z_2} = b_z z_1 - d_2 z_2 \\ \dot{x_3} = c_x x_2 - d_3 x_3 & \dot{y_3} = c_y y_2 - d_3 y_3 & \dot{z_3} = c_z z_2 - d_3 z_3 \end{array} \tag{3.1}$$

The stem cells produce progenitor cells at a constant rate a, the progenitor cells produce differentiated cells at a constant rate b, and the progenitor cells produce terminally differentiated cells at a constant rate c. The parameters d_0, d_1, and d_2 represent the per capita death rates for stem cells, progenitors, differentiated cells, and terminally differentiated cells, respectively. Homeostasis of normal stem cells is given by a decreasing function λ, although this function was never provided. Leukemic and resistant stem cells divide at rate r_y and r_z, respectfully. They assume that imatinib mainly reduces the proliferation rate of the leukemic cells. The authors extended their model to include stochastic evolution of resistance. The parameter u represents the

rate of resistant cells produced per cell division.

Michor *et al.*'s model can exhibit a biphasic decline in BCR-ABL/BCR% as well as the rapid increase when treatment is stopped. The first phase of the biphasic decline represents the decrease in differentiated leukemic cells while the second phase represents the decline in leukemia progenitors. The authors concluded that leukemic stem cells are not completely depleted during imatinib therapy and thus imatinib therapy cannot eradicate the disease.

Glauche, Horn, and Roeder wrote a letter to the editor (Glauche *et al.*, 2007), discussing an inconsistency in the model by Michor *et al.* (2005). Data showed a continuing decrease of BCR-ABL transcripts after more than a year of imatinib treatment. The authors claim that the model by Michor *et al.* is not able to explain this behavior due to the continuing increase of malignant stem cells. Michor (2007b) responds to this letter by stating that the model was designed to reproduce the dynamics over only the first year of treatment and that the leukemic stem cells were not depleted during treatment so that the levels increased beyond pre-treatment baseline once therapy was stopped. Michor then presented a modified version of their model which takes into account density dependence of normal and leukemic stem cells:

$$\begin{aligned} \dot{x_0} &= [r_x\Phi - d_0]x_0 \quad & \dot{y_0} &= [r_y\phi - d_0]y_0 \\ \dot{x_1} &= a_x x_0 - d_1 x_1 \quad & \dot{y_1} &= a_y y_0 - d_1 y_1 \\ \dot{x_2} &= b_x x_1 - d_2 x_2 \quad & \dot{y_2} &= b_y y_1 - d_2 y_2 \\ \dot{x_3} &= c_x x_2 - d_3 x_3 \quad & \dot{y_3} &= c_y y_2 - d_3 y_3 \end{aligned} \tag{3.2}$$

where

$$\Phi = \frac{1}{1 + c_x(x_0 + y_0)}, \phi = \frac{1}{1 + c_y(x_0 + y_0)}.$$

The parameters c_x and c_y represent the crowding effect that is seen in the bone marrow microenvionrment. Michor shows that this model can reproduce the long-term imatinib behavior described by Glauche, Horn, and Roeder. Michor (2007a) also claims

that Roeder *et al.* (2006) are not able to explain the increase in BCR-ABL/BCR% levels beyond pre-treatment baseline.

Roeder et al. *(2006)*

While Michor *et al.* assumed imatinib had no effect on stem cells, Roeder *et al.* presents a single-cell based stochastic process model that assumes imatinib effects BCR-ABL positive stem cells, and shows the results are consistent with two independent datasets. In this model, the cells transition between two different growth environments (GE), a quiescent GE-A and a proliferative GE-Ω. There are three properties for each cell: GE membership m, position in the cell cycle c, and affinity for a cell to be in GE-A environment a. A cell in GE-A can transition to GE-Ω when $c = c_1$, the beginning of the S cell cycle phase. If the cell remains in GE-A, then $a(t)$ will increase by a factor of r. If the cell is in GE-Ω, it can only transition to GE-A in the G_1 cell cycle phase. If the cell remains in GE-Ω, then $a(t)$ decreases by a factor of $1/d$ and the cell cycle position is increased. Once a reaches $a_{\min}$, the cell becomes terminally differentiated. Once a cell cycle is completed, the cell cycle restarts and a new cell is generated, representing cell division. The transition probabilities depend on $a(t)$, $a_{\max}$, $a_{\min}$, and the total number of stem cells N_A, N_Ω. Without treatment, the malignant clone outcompetes the normal cell population. With treatment, each BCR-ABL positive cell has a probability of being affected by imatinib, which is assumed to decrease proliferation of Ph^+ cells by decreasing the transition from GE-A to GE-Ω. Proliferating Ph^+ cells are also killed with a given probability, representing imatinib's ability to induce apoptosis.

Roeder *et al.* demonstrated both a biphasic decline as well as the rapid increase in BCR-ABL/ABL% when treatment is stopped. The authors conclude that the first and steeper decline is due to the reduction in proliferating BCR-ABL positive cells,

while the second decline is due to the changes in the regulatory response of the system caused by the reduced stem cell population. Roeder *et al.* hypothesized a degradation of proliferating stem cells during treatment and concluded that imatinib treatment can eradicate the disease, assuming no mutations. When treatment is stopped, the relapse can be attributed to the proliferation of dormant stem cells that were not affected by the proliferation-specific degradation effect.

Stein et al. *(2011)*

Stein *et al.* compared different hypotheses of the models described above. Assuming a biphasic decline in BCR-ABL/ABL%, which was demonstrated by both models, there are two slopes: α, which corresponds to the initial rapid decrease and β, which corresponds to the long-term response. One hypothesis, supported by Roeder *et al.*, is the proliferating-quiescent hypothesis, where α is due to the proliferating stem cells and β is due to the quiescent stem cells. Another is the late-early progenitors hypothesis, supported by Michor *et al.*, where α is due to the late progenitor cells and β is due to the early progenitor cells. Stein *et al.* also considered a third hypothesis, the early stem cell hypothesis, which states that α is due to a decline of early progenitor cells and β is due to a decline of late progenitor cells. This hypothesis was supported by Bottino *et al.* (2009) in an abstract from the American Society of Clinical Oncology (ASCO) Annual Meetings Proceedings. Their mathematical model considers both normal and leukemic cells in four stages, with the stem cells being the only stage capable of self-renewal. Using clinical data, Stein *et al.* rejected the late-early progenitors hypothesis and concluded that β is due to late progenitor depletion. However, the factors contributing to the parameter α are still unknown.

3.1.3 Methods and Findings

These previous CML models described different cell environments and different cell populations, but not intracellular dynamics, which may provide insights into the intracellular origins of proliferation and resistance. Recently, Portz *et al.* (2012) presented a cell quota model that describes a treatment for patients with prostate cancer called intermittent androgen suppression, a hormone therapy (described in Section 2.1.2). Normal prostate cells as well as most prostate cancer cells depend on androgen signaling for survival and proliferation. Androgen suppression treatment lowers the androgen levels, which prevents the growth of cancer cells. The treatment can be initially successful; however, most patients experience a relapse. Portz *et al.* suggest that during the relapse, androgen-independent cells (AI), which can grow in low-androgen environments, replace androgen-dependent cells (AD). In one model, the growth rate of both the AD and AI populations are described by Droop's cell quota models, which introduce two new variables to represent the cell quotas for androgen. It is not always possible to determine the dependence of cancer cell phenotypes on intracellular factors. Portz *et al.* exemplified how mathematical modeling can yield insights into how intracellular dynamics may contribute to malignant cell growth.

Similar to prostate cancer, the proliferation of malignant cells in CML is dependent on the production of intracellular factors, namely the BCR-ABL protein. Therefore, it is natural to adapt the cell quota modeling approach of Portz *et al.* to CML. Additionally, the increases in BCR-ABL/ABL% that occur in some CML patients are comparable to the increases in androgen levels seen in prostate cancer patients following cessation of androgen therapy. Portz *et al.* showed that a cell quota model can accurately capture such increases in intracellular molecular factors that contribute to malignant proliferation (Portz *et al.*, 2012). Here, we compare two mathematical

models, a cell quota model similar to that of Portz *et al.* (2012) and a density dependent model based on a model described in Michor (2007a,b), for the treatment of CML. Our results show that additional insights into imatinib treatment for CML patients can be gained by accounting for the dynamics of BCR-ABL at the intracellular level.

3.2 Model 1: A Cell Quota Model

Our goal is to gain a more in-depth understanding of CML and imatinib treatment by developing a model that may produce plausible solutions that reasonably match clinical data. Our model is based on the model framework of Portz *et al.* (2012). The growth rate of the BCR-ABL-dependent and -independent populations are modeled using Droop's cell quota model, where $Q(t)$ represents the cell quota for BCR-ABL. The BCR-ABL-dependent, BCR-ABL-independent, and normal populations are modeled, respectively, by the following system of ODEs:

$$\frac{dx_1}{dt} = r_1\big(1 - \frac{q_1}{Q}\big)x_1 - d_0x_1 - m_{12}(Q)x_1 + m_{21}(Q)x_2, \tag{3.3a}$$

$$\frac{dx_2}{dt} = r_2\big(1 - \frac{q_2}{Q}\big)x_2 - d_0x_2 + m_{12}(Q)x_1 - m_{21}(Q)x_2, \tag{3.3b}$$

$$\frac{dx_3}{dt} = \Big(\frac{r_3}{1 + p_3(x_1 + x_2 + x_3)}\Big)x_3 - d_0x_3. \tag{3.3c}$$

The BCR-ABL dependent population is equivalent to non-resistant cells and the BCR-ABL independent population is equivalent to the resistant cells. It should be noted that the BCR-ABL independent population is assumed to not be completely independent, but have a lower threshold for BCR-ABL. We assume that the proliferation rates, $r_i(1 - \frac{q_i}{Q}), i = 1, 2$, of both BCR-ABL dependent and independent populations are BCR-ABL cell quota dependent while the proliferation rate, $\frac{r_3}{1+p_3(x_1+x_2+x_3)}$, for the normal population is density dependent. Notice that $r_i, i = 1, 2, 3$ are the corresponding maximum proliferation rates, and p_3 is the parameter that simulates the

crowding effect. The parameters $q_i, i = 1, 2$ are the minimum BCR-ABL cell quota for BCR-ABL dependent and independent cells. We assume $q_1 > q_2$ since BCR-ABL independent cells are more likely to proliferate than BCR-ABL dependent cells in low BCR-ABL environment. The term $r_i(1 - \frac{q_i}{Q}), i = 1, 2$ implies that at minimum BCR-ABL cell quota ($Q = q_i$), corresponding leukaemia cells do not proliferate, while the proliferation rate increases and approaches the maximum as the BCR-ABL cell quota increases. The death rate, d_0, is also assumed to be the same for all stem cells.

The mutation or switching rates between the BCR-ABL dependent and independent populations are given by the Hill equations

$$m_{12}(Q) = k_1 \frac{K_1^n}{Q^n + K_1^n},$$

$$m_{21}(Q) = k_2 \frac{Q^n}{Q^n + K_2^n}.$$

The maximum BCR-ABL dependent to independent mutation rate is given by k_1 and similarly, the maximum BCR-ABL independent to dependent mutation rate is given by k_2. K_1 and K_2 represent the half-saturation constants for their respective mutation functions.

We assume the cell quotas for both the BCR-ABL dependent and independent cells are the same and are modeled by

$$\frac{dQ}{dt} = v_m(q_{m1} - Q) - \mu_m(Q - q_1) - bQ. \tag{3.3d}$$

The maximum cell quota is q_{m1} and the minimum cell quota is q_1, with $q_1 > q_2$. We assume that the utilization of BCR-ABL for growth in both the dependent and independent population is $\mu_m(Q - q_1)$, and that $\mu_m(q_1 - q_2)$ represents utilization of BCR-ABL for some cellular process unique to the independent population, which we do not consider here. The parameter v_m represents the BCR-ABL protein production rate. We assume BCR-ABL degrades at a constant rate b.

Portz *et al.* (2012) assumed two cell quota variables, one for the dependent population and one for the independent population. However, the two cell quotas were very similar. Thus, for simplicity we assume that the cell quotas for both the dependent and independent cells are the same. It should be noted that this was not a biologic assumption but an assumption based on the results of Portz *et al.*. Future works includes considering two cell quota variables.

3.3 Basic Analysis of the Cell Quota Model

In the following we show that solutions of $(3.3a), (3.3b), (3.3c)$, and $(3.3d)$, with biologically appropriate initial values, stay positive. Specifically, we assume that $x_1(0) \geq 0$, $x_2(0) \geq 0$, $x_3(0) \geq 0$, $q_{m1} \geq Q(0) \geq q_1$, and all the parameters are positive. These assumptions are natural for our application.

Proposition 1. *Solutions of* $(3.3a), (3.3b), (3.3c)$, *and* $(3.3d)$ *stay in the region* $\{(x_1, x_2, x_3, Q) : x_1 \geq 0, x_2 \geq 0, 0 \leq x_3 \leq \max\{\frac{1}{d_0 p_3}(r_3 - d_0), x_3(0)\}, q_1 \frac{\mu_m}{\mu_m + b} \leq Q \leq q_{m1}\}$ *provided that* $x_1(0) \geq 0, x_2(0) \geq 0, x_3(0) \geq 0, q_{m1} \geq Q(0) \geq q_1$.

Proof. Observe that

$$Q' = v_m(q_{m1} - Q) - (\mu_m + b)\left(Q - q_1 \frac{\mu_m}{\mu_m + b}\right).$$

It is easy to see that $q_{m1} \geq Q(t) \geq q_1 \frac{\mu_m}{\mu_m + b}$ for $t > 0$ with initial condition $q_{m1} \geq Q(0) \geq q_1$. A straightforward application of standard comparison argument will establish the positivity of x_1, x_2 and x_3.

We consider now the boundedness of x_3.

$$\begin{aligned} x_3' &= \left(\frac{r_3}{1 + p_3(x_1 + x_2 + x_3)} - d_0\right) x_3 \leq \left(\frac{r_3}{1 + p_3 x_3} - d_0\right) x_3 \\ &= \frac{1}{1 + p_3 x_3}(r_3 - d_0 - d_0 p_3 x_3) x_3. \end{aligned}$$

From this, we see that $\lim_{t\to\infty} x_3(t) \leq \max\{\frac{1}{d_0 p_3}(r_3 - d_0), 0\}$, and $x_3(t) \leq \max\{\frac{1}{d_0 p_3}(r_3 - d_0), x_3(0)\}$ for $t \geq 0$. □

We are now in a position to consider the uniform boundedness of x_1 and x_2:

$$x_1' + x_2' = r_1(1 - \frac{q_1}{Q})x_1 + r_2(1 - \frac{q_2}{Q})x_2 - d_0(x_1 + x_2).$$

Since $Q(t) \leq q_{m1}$, we have

$$x_1' + x_2' \leq M(x_1 + x_2) - d_0(x_1 + x_2) = (M - d_0)(x_1 + x_2),$$

where $M = \max\{r_1(1 - \frac{q_1}{q_{m1}}), r_2(1 - \frac{q_2}{q_{m1}})\}$. We see that $x_1 + x_2 \leq x_1(0) + x_2(0)$ if $M - d_0 \leq 0$. Biologically, $M - d_0 \leq 0$ amounts to saying that even at the maximum intracellular BCR-ABL concentration q_{m1}, the populations x_1 and x_2 grow at a rate less than their death rate d_0, which trivializes this modeling task. A much more natural mechanism that shall ensure the boundedness of solutions is the density dependent death rate. In more plausible CML models with more desirable long term dynamics, one can add an additional term such as $d_1 x_1^2$ to (3.3a) and $d_1 x_2^2$ to (3.3b).

In the following, we assume that

$$\Big(r_1\Big(1 - \frac{q_1}{Q_1}\Big) - d_0 - m_{12}(Q_1)\Big)\Big(r_2\Big(1 - \frac{q_2}{Q_1}\Big) - d_0 - m_{21}(Q_1)\Big) \neq m_{12}(Q_1)m_{21}(Q_1),$$

where

$$Q_1 = \frac{v_m q_{m1} + \mu_m q_1}{v_m + \mu_m + b}.$$

The following proposition provides some basic local stability results for the Cell Quota Model.

Proposition 2. *System* $(3.3a), (3.3b), (3.3c)$ *and* $(3.3d)$ *has no positive periodic solutions. It has two possible boundary equilibria:* $E_0 = (0, 0, 0, Q_1)$, $E_1 = (0, 0, \frac{r_3 - d_0}{p_3 d_0}, Q_1)$ *and no interior equilibrium.*

1. *Assume that* $r_1(1-\frac{q_1}{Q_1})+r_2(1-\frac{q_2}{Q_1})-2d_0-m_{12}(Q_1)-m_{21}(Q_1)<0$ *and* $\Big(r_1(1-\frac{q_1}{Q_1})-d_0-m_{12}(Q_1)\Big)\Big(r_2(1-\frac{q_2}{Q_1})-d_0-m_{21}(Q_1)\Big)$ $-m_{12}(Q_1)m_{21}(Q_1)>0$.

   (a) *If* $r_3<d_0$, *then* E_0 *is the unique equilibrium and it is (locally) stable.*

   (b) *If* $r_3>d_0$, *then we have equilibria* E_0 *and* E_1, *while* E_0 *is unstable and* E_1 *is (locally) stable.*

2. *If* $r_1(1-\frac{q_1}{Q_1})+r_2(1-\frac{q_2}{Q_1})-2d_0-m_{12}(Q_1)-m_{21}(Q_1)>0$ *or* $\Big(r_1(1-\frac{q_1}{Q_1})-d_0-m_{12}(Q_1)\Big)\Big(r_2(1-\frac{q_2}{Q_1})-d_0-m_{21}(Q_1)\Big)$ $-m_{12}(Q_1)m_{21}(Q_1)<0$, *then both* E_0 *and* E_1 *are unstable.*

Proof. Observe that

$$Q'=-(v_m+\mu_m+b)Q+v_mq_{m1}+\mu_mq_1.$$

It is easy to see that $\lim_{t\to\infty}Q(t)=Q_1$. Then we can look at the limiting case of (3.3a) and (3.3b):

$$\frac{dx_1}{dt}=r_1\big(1-\frac{q_1}{Q_1}\big)x_1-d_0x_1-m_{12}(Q_1)x_1+m_{21}(Q_1)x_2,$$
$$\frac{dx_2}{dt}=r_2\big(1-\frac{q_2}{Q_1}\big)x_2-d_0x_2+m_{12}(Q_1)x_1-m_{21}(Q_1)x_2.$$

Since there is no positive steady state for the limiting case, then by the positivity of the solutions and the fact that a periodic orbit must enclose at least one equilibrium, there are no periodic solutions for the limiting case. Thus, (x_1,x_2) is either unbounded or approaches the steady state (0,0), which makes x_3 approach a steady state by (3.3c). Hence there are no nontrivial periodic solutions for (3.3a), (3.3b), (3.3c), and (3.3d).

We now only need to consider the stability of (x_1,x_2,x_3). Routine local stability analysis shows that the eigenvalues of the Jacobian, λ_1, λ_2, and λ_3, satisfy

$$\lambda_1+\lambda_2=r_1(1-\frac{q_1}{Q_1})+r_2(1-\frac{q_2}{Q_1})-2d_0-m_{12}(Q_1)-m_{21}(Q_1),$$

$$\lambda_1\lambda_2 = \left(r_1(1-\frac{q_1}{Q_1}) - d_0 - m_{12}(Q_1)\right)\left(r_2(1-\frac{q_2}{Q_1}) - d_0 - m_{21}(Q_1)\right) - m_{12}(Q_1)m_{21}(Q_1),$$

and

$$\lambda_3 = -\frac{r_3 p_3 x_3}{(1+p_3(x_1+x_2+x_3))^2} + \frac{r_3}{1+p_3(x_1+x_2+x_3)} - d_0.$$

It is thus straightforward to conclude the linear stability for the three different cases. □

Proposition 2 implies that there is no oscillatory behavior of the BCR-ABL/ABL% (see (3.6)), which suggests that the oscillatory nature of some individual patients' data may be caused by stochastic factors not considered here or that the model is incorrect. Also notice that E_1 corresponds to 0% in BCR-ABL/ABL(%), while BCR-ABL/ABL(%) does not apply to E_0.

3.4 Model 2: A Simple Density Dependent Model

The second model, based on a model by Michor (2007a,b), describes the change in abundances of normal stem cells x and leukemia stem cells y, respectively:

$$x' = [r_x\Phi - d_0]x \text{ where } \Phi = \frac{1}{[1+c_x(x+y)]} \tag{3.4}$$

$$y' = [r_y\phi - d_0]y \text{ where } \phi = \frac{1}{[1+c_y(x+y)]} \tag{3.5}$$

$r_x\Phi, r_y\phi$ represent the density dependent cell division rates, and c_x, c_y are parameters that simulate the crowding effect that is seen in the bone marrow microenvironment. The normal and leukemia stem cells divide at rates at most r_x, r_y, respectively, per day. The death rate of both normal and leukemia stem cells is represented by d_0. This model assumes that cells can reproduce both symmetrically and asymmetrically; therefore, stem cell populations are capable of expansion.

3.5 Basic Analysis of the Density Dependent Model

Our first proposition presents the positivity and boundedness results for the Density Dependent Model.

Proposition 3. *Solutions of* (3.4) *and* (3.5) *stay in* $\{(x,y) : 0 \le x \le \max\{\frac{1}{d_0 c_x}(r_x - d_0), x(0)\}, 0 \le y \le \max\{\frac{1}{d_0 c_y}(r_y - d_0), y(0)\}\}$ *provided that* $x(0) \ge 0, y(0) \ge 0$.

Proof. We first establish the positivity of the solutions. If the contrary were true, then there is a first time $t_1 > 0$ such that $x(t_1) = 0$ or $y(t_1) = 0$. Assume first that $x(t_1) = 0$. Then for $t \in [0, t_1]$, we see that $x'(t) \ge -d_0 x(t)$ and hence $x(t_1) \ge x(0)e^{-d_0 t_1} > 0$, a contradiction. A similar contradiction can be obtained by assuming that $y(t_1) = 0$, proving the positivity of the solutions.

Next we establish the boundedness of solutions. Observe that

$$x' = \left[\frac{r_x}{1 + c_x(x+y)} - d_0\right] x \le \left(\frac{r_x}{1 + c_x x} - d_0\right) x$$
$$y' = \left[\frac{r_y}{1 + c_y(x+y)} - d_0\right] y \le \left(\frac{r_y}{1 + c_y y} - d_0\right) y.$$

By a comparison argument, we can conclude that x is bounded by $\max\{\frac{1}{d_0 c_x}(r_x - d_0), x(0)\}$ and y is bounded by $\max\{\frac{1}{d_0 c_y}(r_y - d_0), y(0)\}$. □

The next proposition presents stability results for the Density Dependent Model.

Proposition 4. *There are three possible boundary equilibria:* $E_0 = (0,0)$, $E_1 = (0, \frac{1}{d_0 c_y}(r_y - d_0))$ *(when* $r_y > d_0$*),* $E_2 = (\frac{1}{d_0 c_x}(r_x - d_0), 0)$ *(when* $r_x > d_0$*), and no interior equilibrium. There are no periodic solutions of* (3.4) *and* (3.5).

1. *If* $r_x < d_0$ *and* $r_y < d_0$*, then* E_0 *is the unique equilibrium and* E_0 *is (globally) stable.*

2. *If* $r_x > d_0$ *and* $r_y < d_0$*, we have equilibria* E_0 *and* E_2*, while* E_0 *is unstable and* E_2 *is (globally) stable.*

3. *If $r_x < d_0$ and $r_y > d_0$, we have equilibria E_0 and E_1, while E_0 is unstable and E_1 is (globally) stable.*

4. *If $r_x > d_0$ and $r_y > d_0$, we have all three equilibria: E_0, E_1, and E_2. E_0 is unstable.*

   (a) *If $\frac{1}{c_x}(r_x - d_0) < \frac{1}{c_y}(r_y - d_0)$, then E_1 is (globally) stable and E_2 is unstable;*

   (b) *If $\frac{1}{c_x}(r_x - d_0) > \frac{1}{c_y}(r_y - d_0)$, then E_1 is unstable and E_2 is (globally) stable.*

Proof. All the equilibria can be easily calculated. Since there is no interior equilibrium and the solutions are bounded, then by the fact that a periodic orbit must enclose at least one equilibrium, there are no periodic solutions of (3.4) and (3.5).

Routine local stability analysis leads to the conclusion that stability of the equilibria depends on eigenvalues

$$\lambda_1 = r_x - d_0, \lambda_2 = r_y - d_0 \text{ for } E_0;$$
$$\lambda_1 = \frac{c_y(r_x - d_0) - c_x(r_y - d_0)}{c_y + \frac{1}{d_0}c_x(r_y - d_0)}, \lambda_2 = -\frac{d_0}{r_y}(r_y - d_0) \text{ for } E_1;$$

and

$$\lambda_1 = -\frac{d_0}{r_x}(r_x - d_0), \lambda_2 = \frac{c_x(r_y - d_0) - c_y(r_x - d_0)}{c_x + \frac{1}{d_0}c_y(r_x - d_0)} \text{ for } E_2.$$

Then it is straightforward to establish the linear stability for the four different cases. Since we have eliminated the existence of periodic solutions, local stability implies global stability for cases (1), (2), and (3). □

Proposition 4 implies that there is no oscillatory behavior of the BCR-ABL/ABL%, again suggests that the oscillatory nature of some individual patients' data may be caused by stochastic factors not considered here or that the model is incorrect. Also notice that E_1 corresponds to 100% in BCR-ABL/ABL(%) and E_2 corresponds to 0% in BCR-ABL/ABL(%), while BCR-ABL/ABL(%) does not apply to E_0.

3.6 Data

We used data from a previous study (Muller *et al.*, 2003; Roeder *et al.*, 2006) that consists of samples from 139 German patients who had been recently diagnosed BCR-ABL positive, chronic phase CML and were recruited and enrolled in the International Randomized Study of Interferon and STI571 (IRIS study) between June 2000 and January 2001. Out of these patients, 69 were treated with imatinib and 70 were treated with interferon (IFN)/Ara-C. Our analysis only considers the 69 patients treated with imatinib. These patients received 400mg orally daily. The blood samples were collected monthly for the first 3 months, and then once every 3 months thereafter. The data consists of BCR-ABL/ABL% from months ranging from 0 to 66 from each patient. For more information, see (Muller *et al.*, 2003).

To compare the clinical data to the Cell Quota Model (Model 1), we used the following formula to approximate the percentages:

$$\frac{0.5x_1 + 0.5x_2}{0.5x_1 + 0.5x_2 + x_3} \times 100\%. \tag{3.6}$$

To compare the clinical data to the Density Dependent Model (Model 2), we used the following to approximate the percentages:

$$\frac{0.5y}{0.5y + x} \times 100\%. \tag{3.7}$$

In using these approximations, we assume that a BCR-ABL positive cell also contains a non mutated chromosome 9 and 22 and thus the BCR-ABL/ABL% values cannot be over 100. Therefore we did not analyze any patients with BCR-ABL/ABL values over 100% and only analyzed data from the remaining 51 patients. Since the data ranges from 0 to 66 months and after month 3, the samples were collected every 3 months, ideally each patient should have 25 data points. Out of these 51 patients, 11 patients had fewer than 10 data points. Since we are comparing the two models to the

Model	Average	Median	Range (Max-Min)
Model 1	2.030	0.9939	18.13 (18.14-0.0137)
Model 2	2.181	1.080	17.06 (17.06-0.0047)
Model 1-Model 2	-0.1514	-0.0897	2.887 (1.185-(-1.702))

Table 3.1: Error Statistics Comparing the Cell Quota Model (Model 1) to the Density Dependent Model (Model 2).

data, we only considered the 40 patients with more than 10 data points. We assume that, for each patient, the initial BCR-ABL/ABL% value consists of 99% BCR-ABL dependent cells and 1% BCR-ABL independent cells.

3.7 A Comparison of the Two Models

To compare the two models we ran simulations with MATLAB using the clinical data of the 40 patients from the earlier study (Muller *et al.*, 2003). We used the MATLAB built-in function fminsearch, which uses the Nelder-Mead simlex algorithm (Lagarias *et al.*, 1998), to find the optimum parameters for each model for each patient. We calculated the error using the following equation:

$$\text{error}^{\,2} = \frac{\sum_i (y_i - \hat{y}_i)^2}{N} \tag{3.8}$$

where N represents the total number of data points, y_i represents the actual value, and $\hat{y}_i$ represents the estimated value from the models.

After comparing the errors for each patient from each of the models, 26 out of 40 patients had a smaller error associated with the Cell Quota Model compared to the Density Dependent Model. Table 3.1 contains statistical information about the errors of the two models. The median error for the Cell Quota Model was 0.9939 whereas the median error for the Density Dependent Model was 1.080. The average

Parameter	Meaning
r_1	Maximum proliferation rate of BCR-ABL D population
r_2	Maximum proliferation rate of BCR-ABL I population
r_3	Maximum proliferation rate of Normal population
p_3	Parameter that simulates the crowding effect
n	Hill coefficient
q_1	Minimum BCR-ABL D cell quota
q_2	Minimum BCR-ABL I cell quota
k_1	Maximum BCR-ABL D to BCR-ABL I mutation rate
k_2	Maximum BCR-ABL I to BCR-ABL D mutation rate
K_1	BCR-ABL D to BCR-ABL I mutation half-saturation level
K_2	BCR-ABL I to BCR-ABL D mutation half-saturation level
q_{m1}	Maximum BCR-ABL cell quota
v_m	Cell quota production rate
b	Cell quota degradation rate
μ_m	Rate at which BCR-ABL is used within the cell for growth

Table 3.2: Cell Quota Model (Model 1) Parameter Meanings. BCR-ABL D refers to BCR-ABL dependent and BCR-ABL I refers to BCR-ABL independent.

error for the Cell Quota Model was 2.030 whereas the average error for the Density Dependent Model was 2.181. When comparing the difference between the errors for each model for each patient, only 4 out of the 40 patients had a difference in error that was greater than 1. Figure 3.1 shows the data fitting for three patients whose error was smaller with the Cell Quota Model compared to the Density Dependent Model. Figure 3.2 shows the data fitting for three patients whose error was smaller with the Density Dependent Model compared to the Cell Quota Model. Figure 3.3 shows the data fitting for three patients where the two models were similar in terms of error.

3.7.1 Parameters

Tables 3.2 and 3.4 contain the parameter meanings for the Cell Quota Model and the Density Dependent Model, respectively. Tables 3.3 and 3.5 contain statistical information about the parameters for the 40 patients for the Cell Quota Model and the Density Dependent Model, respectively. We used the fminsearch function in MATLAB to find optimal model parameters with respect to the error defined in (3.8). The initial guesses for the parameters of the models were initially fit by hand to provide good qualitative agreement with the clinical CML data. Note that both models use the stem cell death rate, $d_0 = 0.003$/day (Michor *et al.*, 2005). We can see that, although Model 2 has fewer parameters, the range of the values is extremely large and biologically unrealistic. The maximum value for r_3 in the Cell Quota Model is about 0.015 per day, whereas the maximum dividing rate for normal stem cells in the Density Dependent Model is 6.518×10^9 per day. The average value for r_3 in the Cell Quota Model is 0.0061 per day whereas the average value for r_x in the Density Dependent Model is about 2.341×10^8 per day. Previous literature (Foo *et al.*, 2009) have used the value of 0.005 per day to represent the growth rate of normal stem cells, which is much closer to the maximum and average values for the Cell Quota Model. Although

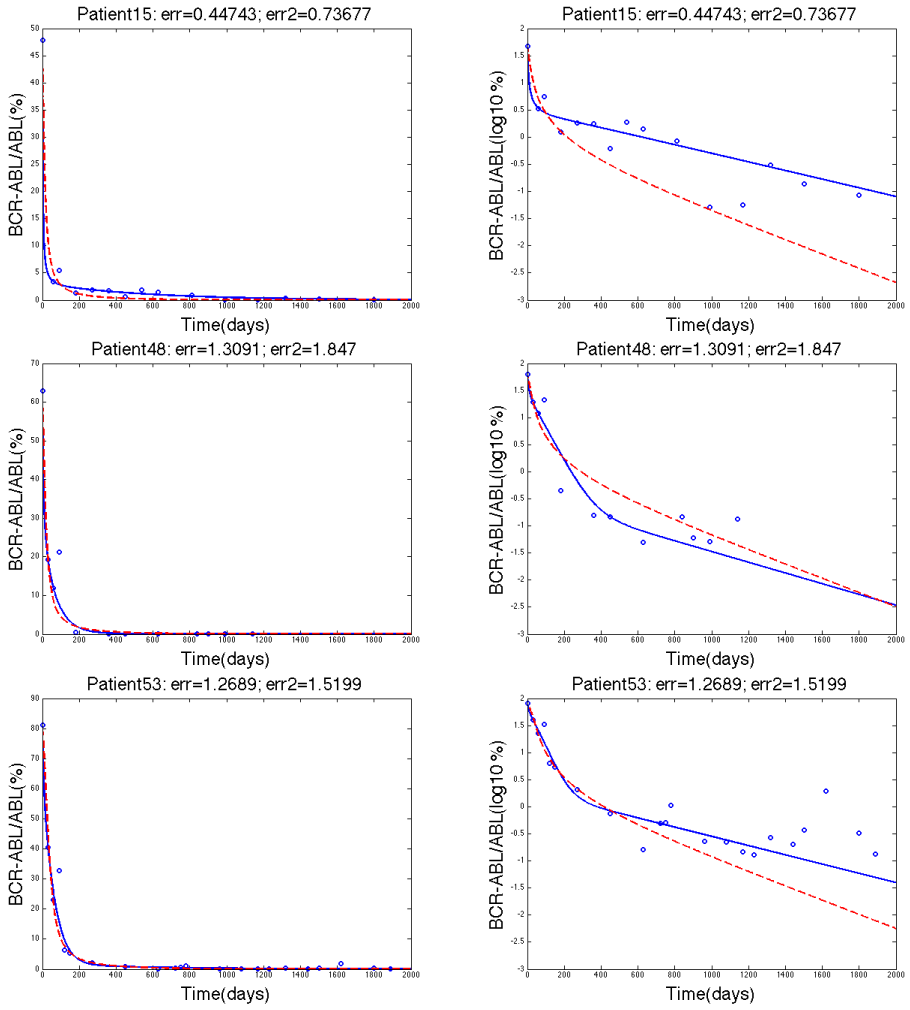

Figure 3.1: The three rows show the data fitting for patients 15, 48, and 53 respectively where the blue solid line represents the Cell Quota Model (Model 1), the dashed red line represents the Density Dependent Model (Model 2), and the blue circles represent the clinical data. The left column and the right column both show the same data fitting. The left column has a y-axis of BCR-ABL/ABL(%) whereas the right column have y-axis as $\log_{10}$(BCR-ABL/ABL(%)) values.

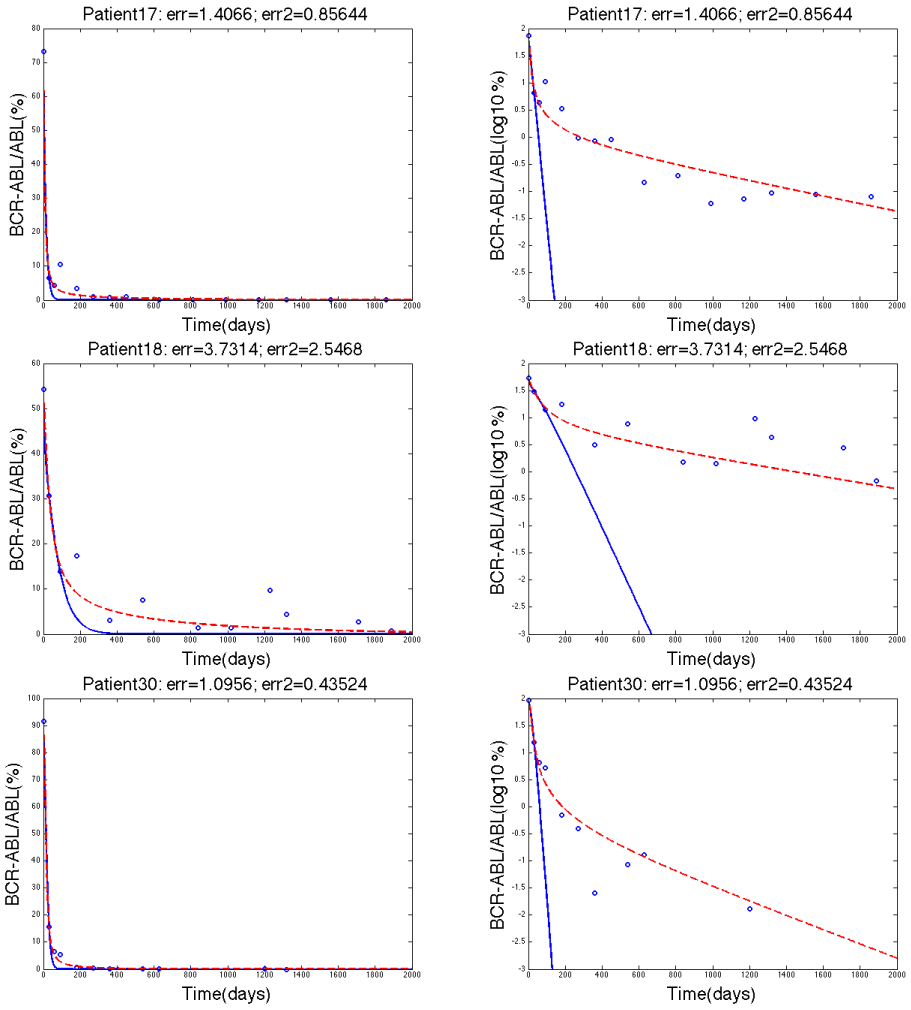

Figure 3.2: The three rows show the data fitting for patients 17, 18, and 30 respectively where the blue solid line represents the Cell Quota Model (Model 1), the dashed red line represents the Density Dependent Model (Model 2), and the blue circles represent the clinical data. The left column and the right column both show the same data fitting. The left column has a y-axis of BCR-ABL/ABL(%) whereas the right column have y-axis as $\log_{10}$(BCR-ABL/ABL(%)) values.

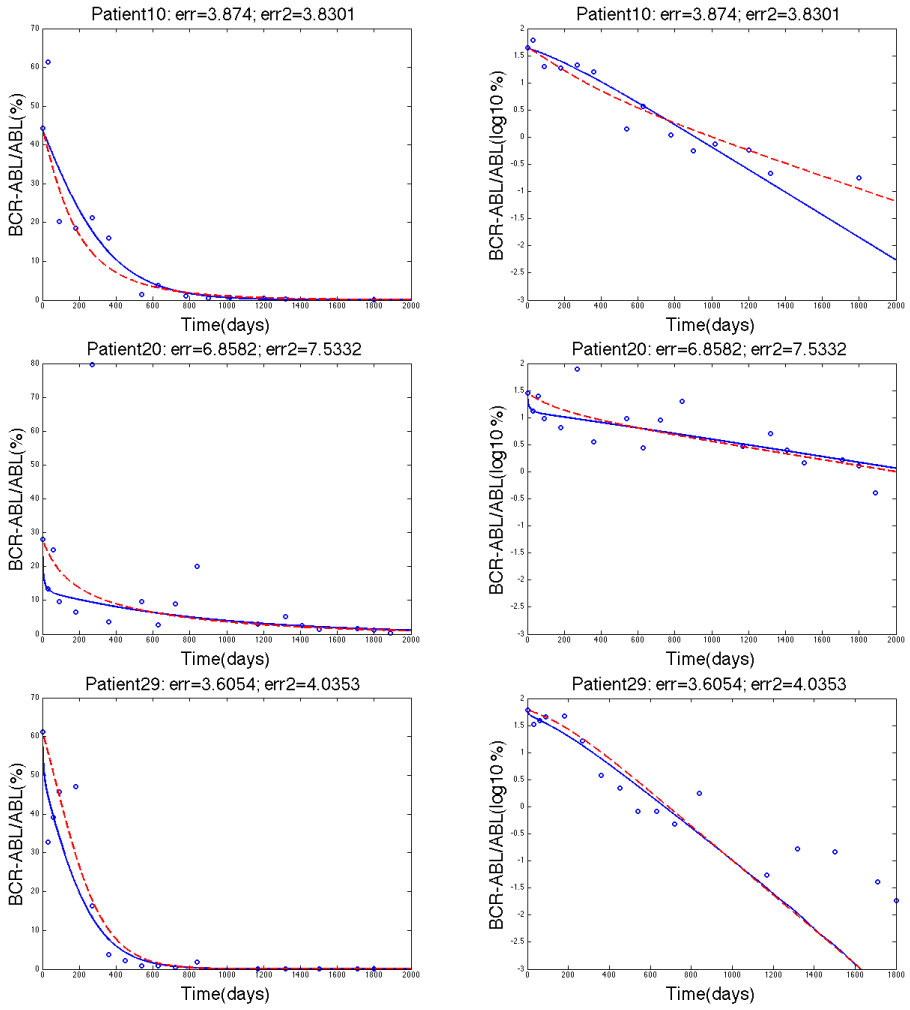

Figure 3.3: The three rows show the data fitting for patients 10, 20, and 29 respectively where the blue solid line represents the Cell Quota Model (Model 1), the dashed red line represents the Density Dependent Model (Model 2), and the blue circles represent the clinical data. The left column and the right column both show the same data fitting. The left column has a y-axis of BCR-ABL/ABL(%) whereas the right column have y-axis as $\log_{10}$(BCR-ABL/ABL(%)) values.

the averages and ranges are very different for the normal stem cell division rate for the two models, the median values are close. The median value for r_3 in the Cell Quota Model is about 0.005 while the median value for r_x in the Density Dependent Model is about 0.048. Both the median value of r_x in the Density Dependent Model and the median value for r_3 in the Cell Quota Model are similar to the values found in literature.

In the Cell Quota Model, the growth rate of the nonresistant leukemic stem cells has a maximum value of about 0.021 per day, which is somewhat close to the value of 0.008 per day used by Michor *et al.* (2005). However, the maximum value of r_y in the Density Dependent Model is about 4.392×10^7 per day, which is biologically unrealistic. For the Cell Quota Model, the median and average values for r_1 are 0.0036 and 0.0054 respectively, while the median and average values for r_y in the Density Dependent Model are 0.011 and 1.738×10^6 respectively. Although the Density Dependent Model seems to be a much simpler model and fit the data similarly to the Cell Quota Model, we can see that the parameter ranges are biologically unrealistic, suggesting the Cell Quota Model to be biologically more plausible.

3.7.2 Resistance

Some patients exhibit a triphasic profile where there is an increase in BCR-ABL/ABL% values after the decline. This increase is most likely due to resistance to imatinib. Although both models were able to show resistance for at least one patient, the resistance described by the Cell Quota Model seems more biologically relevant. The BCR-ABL dependent population in the Cell Quota Model represents the non-resistant cells while the BCR-ABL independent population represents the resistant cells. The Cell Quota Model suggests that a relapse occurs when the BCR-ABL dependent population is replaced by the BCR-ABL independent population. Abbott

Parameter	Average	Median	Range (Max-Min)
r_1	0.0054	0.0036	0.021 (0.021-2.713E-11)
r_2	0.0225	0.0235	0.042 (0.042-2.587E-4)
r_3	0.0061	0.0053	0.015 (0.015-4.919E-8)
p_3	1.208E-6	9.454E-7	3.559E-6 (3.563E-6-4.145E-9)
n	2.363	2.050	6.138 (6.238-0.099)
q_1	0.2854	0.3210	1.011 (1.011-1.722E-8)
q_2	0.2149	0.2302	0.674 (0.675-2.704E-4)
k_1	0.0001	0.0001	0.001 (0.001-3.973E-5)
k_2	0.0001	0.0001	2.091E-04 (2.132E-4-4.132E-6)
K_1	0.0730	0.0753	0.151 (0.162-0.011)
K_2	1.6722	1.772	4.025 (4.300-0.275)
q_{m1}	5.0489	4.993	14.42 (14.42-0.005)
v_m	6.5600E-4	2.879E-4	0.0101 (0.0101-1.3886E-11)
b	0.1469	0.1143	0.470 (0.474-0.004)
μ_m	0.0125	0.0127	0.061 (0.061-2.058E-8)

Table 3.3: Cell Quota Model (Model 1) Parameter Statistics

Parameter	Meaning
r_y	Maximum dividing rate of leukemic stem cells
r_x	Maximum dividing rate of normal stem cells
c_y	Parameter that simulates the crowding effect
c_x	Parameter that simulates the crowding effect

Table 3.4: Density Dependent Model (Model 2) Parameter Meanings

Parameter	Average	Median	Range (Max-Min)
r_y	1.738E+6	0.0109	4.392E+7 (4.392E+7-5.202E-9)
r_x	2.341E+8	0.0480	6.518E+9 (6.518E+9-0.002)
c_y	1.387E+10	217.6	3.352E+11(3.352E+11-0.075)
c_x	1.466E+9	0.1282	2.319E+10 (2.319E+10-3.499E-8)

Table 3.5: Density Dependent Model (Model 2) Parameter Statistics

and Michor (2006) describe a slightly more complex model, which also describes resistance; however, the model was not available nor completely described in the paper, so we were not able to compare the Cell Quota Model to their model with resistance.

Models that describe treatment resistance are important biologically since resistance is a common problem in cancer treatments. A model by Foo *et al.* predicted that, for every 100 patients treated with only imatinib, 89 will eventually develop resistance (Foo *et al.*, 2009). Models can provide insights into when a patient might stop responding to treatment based on their previous data. For chronic phase patients who start imatinib treatment early, only 12% develop resistance within the first two years of treatment (Michor *et al.*, 2005). This implies that resistance is probably not an immediate occurrence.

We searched for signatures of resistance using the parameters estimated from patient data. Although the clinical study at hand lasted only about 5.5 years, we ran the simulations for a longer time span to compare the ability of the Cell Quota Model and the Density Dependent Model to predict long-term resistance. The simulation for patient 1 in the Density Dependent Model showed an increase in BCR-ABL/ABL% around day 1000 (Figure 3.4), caused by the CML population outgrowing the normal cell population. However, patient 1 had the largest error out of all of the other patients

for both models. The error for patient 1 from the Cell Quota Model was 18.14 and the error from the Density Dependent Model was 17.06. The next largest error out of all the patients for the Cell Quota Model was 6.858 and for the Density Dependent Model was 7.533, which are relatively small errors (errors for patient 20). Thus, neither model accurately describes the patient 1 data, so it seems irrelevant that the Density Dependent Model describes resistance for patient 1. Figure 3.4 also contains graphs where resistance was predicted by the Cell Quota Model by an increase in BCR-ABL/ABL%, an increase in the proportion of CML cells, and a decrease in the proportion of normal cells. The errors for these patients were relatively smaller than the errors for patient 1.

3.8 Discussion

The two models compared in this paper both describe the treatment of chronic myeloid leukemia but do so in different ways. The Density Dependent Model describes the competition of leukemic and normal stem cells. In the Cell Quota Model, normal stem cells are in competition with leukemic cells and the growth of leukemic cells depends on the concentration of BCR-ABL. The Cell Quota Model also incorporates more biological detail than the Density Dependent Model by describing the intracellular dynamics of BCR-ABL and allowing for phenotypic switching between BCR-ABL dependent and independent leukemic cell populations. We compared these two models using clinical data and simulations in order to gain insights into whether these additional biological details are correct and relevant. We found that although the Density Dependent Model is a much simpler model, it still describes the data well for some patients. However, the parameter ranges for the Density Dependent Model are extremely large and biologically unrealistic. In contrast, the Cell Quota Model fits the clinical data better for more patients (26/40) and the estimated parameter

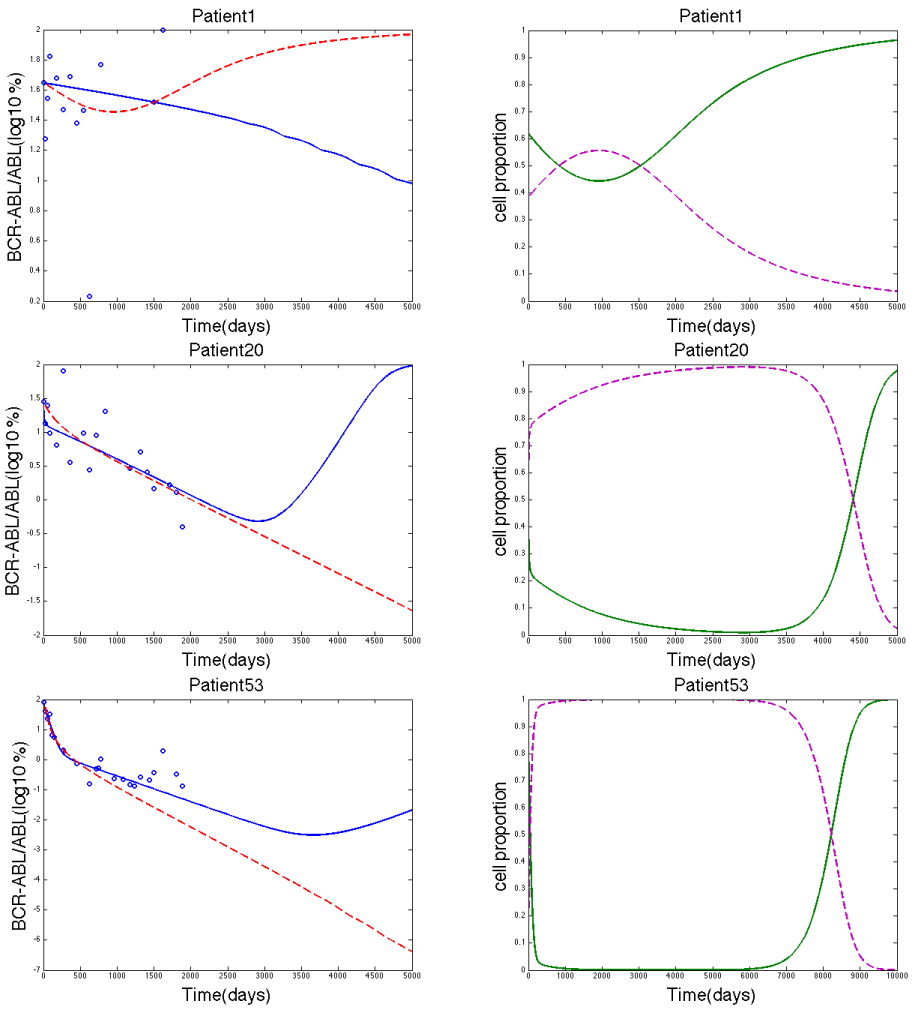

Figure 3.4: The three rows show simulations for patients 1, 20, and 53 respectively. The left column shows the data fitting for each patient with the y-axis as $\log_{10}$(BCR-ABL/ABL(%)) values, where the blue solid line represents the Cell Quota Model (Model 1), the dashed red line represents the Density Dependent Model (Model 2), and the blue circles represent the clinical data. The right column shows the proportion of the cell populations, where the green solid line represents the leukemic cells and the dashed purple line represents the normal cells. The model that showed resistance in the left column was used in the simulation for the right column. Model 1 was used for the simulation of the proportion of cells for patients 20 and 53 and Model 2 was used for the simulation of the proportion of cells for patient 1.

ranges were more realistic, as discussed in Section 3.7. This result suggests that the Cell Quota Model is a better hypothesis than the Density Dependent Model, but it still needs independent verification from independent data before we can argue that it accurately captures biological realism.

A novel mechanism encoded in the Cell Quota Model is the BCR-ABL dependent switching between BCR-ABL dependent and independent populations. We speculate that these transitions could have an epigenetic basis. This is in contrast to previous CML models that have only considered transitions due to genetic mutations (Abbott and Michor, 2006) or switching between a proliferative and non-proliferative state (Roeder *et al.*, 2006; Komarova and Wodarz, 2007). Indeed, recent studies have elucidated important epigenetic changes that may cause resistance to the imatinib drug. For example, imatinib therapy could cause drug resistance by affecting epigenetic alterations in cells that down-regulates tumor suppressor genes (Nishioka *et al.*, 2011). Such alterations could lead to a reduced dependence of leukemic cells on BCR-ABL to express a malignant phenotype, i.e. a BCR-ABL independent cell population. Another study showed that aberrant changes in DNA methylation could be an epigenetic marker associated with imatinib resistance (Jelinek *et al.*, 2011). Our computational work here highlights the importance of further experimental work to ascertain the rate at which epigenetic transitions occur in CML, how this rate is related to imatinib dosage, and how it affects imatinib resistance.

3.9 Future Research

The results we have discussed for the Cell Quota Model, although promising, are mainly computational and in need of further exploration. A thorough mathematical analysis of the Cell Quota Model can provide additional insights into how the intracellular regulation of BCR-ABL levels dictates the long-term transition of

CML cells to an imatinib resistant phenotype, i.e. BCR-ABL independent. In future computational work, we can further evaluate the accuracy of the Cell Quota Model to predict resistance by using patient data that exhibits long-term (i.e. > 2 years) resistance to imatinib. For example, the simulations for the Cell Quota Model where resistance occurs suggest that a more optimal patient data set for evaluating the accuracy of this model is on the time scale of 5-10 years post-treatment initiation. Another direction could investigate more methods for estimating parameters using the same data, since these results were determined using only one method for determining the parameters, as well as performing parameter sensitivity analysis.

Kareva *et al.* (2010) analyze the balance between immature and mature myeloid cells and how this balance affects tumors. They claim that if there is a small enough population of cancer cells, then there is a small region of initial conditions where the immune system alone may cure the cancer and the patient will not need treatment. Future work could look into incorporating the mature and immature myeloid cell populations into the normal cell population in the Cell Quota Model as well as combining intermittent imatinib therapy with the immune system's defense. The work can also be expanded in the future by using more biologically relevant function forms of $p(x)$ and mortality, considering two cell quota variables, and also comparing the Cell Quota Model to the model by Roeder *et al.* (2006).

Chapter 4

OVARIAN CANCER

4.1 Introduction

Ovarian cancer, also known as the 'silent killer' (Goff *et al.*, 2000; Bast Jr *et al.*, 2009), causes more deaths than any other gynecological malignancies and is the 5th leading cause of death from non-skin cancers among women (Gómez-Raposo *et al.*, 2009; Siegel *et al.*, 2014). The American Cancer Society estimates 21,290 new cases of ovarian cancer and 14,180 deaths due to ovarian cancer in the United States in 2015 (Siegel *et al.*, 2015). Only about 20% of ovarian cancers are detected at an early stage (Bast Jr *et al.*, 2009), in part due to the lack of an effective screening strategy and in part since the indications are often symptomatic of other diseases; symptoms include abdominal discomfort or fullness, bloating, and dyspepsia (Aravantinos and Pectasides, 2014). Ovarian cancer is characterized by intraperitoneal (IP) tumors and ascitic fluid (Mesiano *et al.*, 1998; Hu *et al.*, 2000).

While cytoreductive surgery and chemotherapy are common treatments for ovarian cancer, more than 70% of advanced-stage patients will develop drug resistance and the disease recurs within 5 years (Bast Jr *et al.*, 2009; Aravantinos and Pectasides, 2014). Thus molecular targeted therapy has been recently researched, particularly anti-angiogenesis therapy (Aravantinos and Pectasides, 2014), an idea proposed by Folkman more than 40 years ago (Folkman, 1971). Angiogenesis, the development of new blood vessels from pre-existing vessels, is essential for tumor growth and expansion by providing the necessary oxygen and nutrient support to the tumor (Folkman, 1990; Mesiano *et al.*, 1998; Folkman, 2002). Angiogenesis is regulated by

pro-angiogenic and anti-angiogenic factors. When these factors become unbalanced in favor of angiogenesis, the tumor acquires angiogeneic properties, known as the 'angiogenic switch' (Folkman, 2002). One of these pro-angiogenic factors, vascular endothelial growth factor (VEGF), is expressed in most malignant tumors and is one of the most important tumor angiogenesis factors (Sitochy *et al.*, 2012), although its role in tumor angiogenesis is still not understood completely (Waldner and Neurath, 2012). Although VEGF is involved in cyclic growth of ovarian follicles and corpus luteum development and maintenance (Geva and Jaffe, 2000), it is expressed higher in women with ovarian cancers compared to those with benign tumors (Gómez-Raposo *et al.*, 2009).

Several studies have investigated the relationship between VEGF and tumor growth. In 1998, Mesiano *et al.* (1998) analyzed the role of VEGF in tumor growth, progression and ascites formation in ovarian cancer in tumors induced in immunodeficient mice using the human ovarian carcinoma cell line SKOV-3. The authors concluded that tumor-derived VEGF is necessary for the formation of ascites, but may not be obligatory for IP growth. In 2000, Hu *et al.* (2000) researched the effects of a PI3-K inhibitor, LY294002, on tumor progression and ascites formation in the same mouse model of IP ovarian carcinoma using the OVCAR-3 ovarian cancer cell line. The authors concluded that LY294002 significantly inhibited growth and ascites formation. While this study did not investigate VEGF directly, the authors believe LY294002 may have blocked the signal transduction pathway of VEGF. The monoclonal anti-VEGF antibody bevacizumab became approved by the FDA in 2004 for first-line treatment of metastatic colorectal cancer (Waldner and Neurath, 2012). In 2013, Ye and Chen (2013) analyzed the efficacy and safety of bevacizumab in ovarian cancer treatment using four, phase III randomized controlled trials. They concluded that combining bevacizumab to chemotherapy provided improvement in objective response

rate and progression-free survival for both first-line and recurrent disease treatment, but provided no benefits to overall survival. These results were confirmed by a 2014 systematic review of bevacizumab combined with chemotherapy for ovarian cancer treatment (Aravantinos and Pectasides, 2014). This result is typical of treatments targeting angiogenesis in humans. Although many anticipated great benefits of anti-VEGF/VEGF receptor therapy, studies across several cancers have shown only modest results (Sitochy *et al.*, 2012). One possible explanation for this is that tumors adapt to anti-VEGF treatment by using secondary angiogenic pathways, such as the platelet derived growth factor (PDGF) pathway, the fibroblast growth factor (FGF) pathway, and the angiopoietin family (Ang) pathway (Burger, 2011; Davidson and Secord, 2014). Agents such as pazopanib, ninedanib, and trebananib, which target these other pathways, are currently being studied (Burger, 2011; Coleman *et al.*, 2013; Davidson and Secord, 2014).

One approach to modeling angiogenesis and tumor growth is to apply ecological modeling techniques to cancer modeling. Healthy and cancerous cells live in an ecological system where they interact with each other, competing for resources, nutrition, and space (Nagy, 2004, 2005; Merlo *et al.*, 2006; Pienta *et al.*, 2008; Nagy and Armbruster, 2012; Basanta and Anderson, 2013; Bickel *et al.*, 2014; Korolev *et al.*, 2014). Kuang *et al.* (2004b), applied the theory of ecological stoichiometry to a model of tumor angiogenesis. This theory considers the balance of multiple chemical substances, or sometimes energy and materials, in ecological interactions and processes (Sterner and Elser, 2002). One of the main hypothesis from this theory is the growth rate hypothesis, which, "proposes that ecologically significant variations in the relative requirements of an organism for C, N and P are determined by its mass-specific growth rate because of the heavy demand for P-rich ribosomal RNA under rapid growth" (Sterner and Elser, 2002; Kuang *et al.*, 2004b); organisms with high growth rates have

high P:C ratios due to the increased allocation of P to RNA. Since tumor cells often have high growth rates, it makes sense to apply this hypothesis to cancer biology. Elser *et al.* (2007) tested this and determined that the growth rate hypothesis might hold true for some cancers, but not for all cancers. Kuang *et al.* (2004b) propose a model which considers healthy cells, tumor cells, and tumor microvessels, or mature vascular endothelial cells (VECs) in the tumor. The growth rate of these cells are possibly limited by the nutrient phosphorus, depending on the concentration of extracellular phosphorus. The growth of the cancerous cells can also be limited by a lack of blood vessels, which carry important nutrients and supplies. The authors assume a time delay τ, which represents the time it takes for the tumor vessels to form. This idea of representing the micro vessel formation process using a time delay has also been used in previous mathematical models of tumor-induced angiogenesis (Agur *et al.*, 2004; Jain *et al.*, 2008).

We present a first approximation mathematical model of tumor growth and tumor-induced angiogenesis in the simplest context, using a minimum number of parameters. We apply the idea of nutrient limited induced angiogenesis from Kuang *et al.* (2004b) through the use of Droop's cell quota model (Droop, 1968). We also express the processes of microvessel formation through the use of a time delay. We consider the tumor growth both on and off anti-VEGF treatment using the same parameter set. We present our mathematical model in Section 4.2 and then present the analysis of the model in Sections 4.3 and 4.4. Section 4.5 contains simulations and comparisons of the model to clinical data from Mesiano *et al.* (1998).

4.2 Tumor Model

We present a simple vascularized tumor growth model where tumor growth is governed by the Droop equation (Droop, 1968). Let y represent the vascularized

tumor volume and Q represent the intracellular concentration of necessary nutrients provided by angiogenesis, or the cell quota of some limiting nutrient from angiogenesis. Our model takes the following form:

$$y' = \underbrace{\mu_m \left(1 - \frac{q}{Q}\right) y}_{\text{growth}} - \underbrace{dy}_{\text{death}} , \tag{4.1a}$$

$$Q' = \underbrace{\alpha \frac{y(t-\tau)}{y(t)}}_{\text{nutrient uptake}} - \underbrace{\mu_m (Q - q)}_{\text{dilution}} . \tag{4.1b}$$

The growth of the tumor is given by the Droop equation, where μ_m represents the maximum tumor growth rate and q represents the minimum cell quota, or minimum concentration of limiting nutrient needed to sustain the cell. The tumor death rate is assumed to be constant, represented by d. Similarly to Kuang *et al.* (2004b), we assume that it takes τ time for the vascular endothelial cells to respond to the angiogenic signal and mature to fully functional vessels. While a mechanistic model would need to track the blood vessels, we simplify by assuming that the nutrient uptake rate is proportional to the nutrient concentration in the interstitial fluid, which in turn is proportional to the blood vessel density τ time units in the past. The delay arises because the tumor is assumed to grow into regions that are unvascularized, and it takes τ units of time for them to vascularize. Once a region is vascularized, it remains static. VEGF is assumed to be the primary signal generating new blood vessel growth and is secreted primarily where new tumor tissue is forming, since these are the regions that are hypoxic. Parameter α represents both uptake rate of the nutrients in the interstitial fluid and resulting nutrient concentration per tumor unit. Term $\mu_m(Q - q)$ represents the dilution of the nutrient as the tumor grows. We assume that when the cells die they release the nutrient, which remains in the nearby environment (Kuang *et al.*, 2004b). See Table 4.1 for a list of the variable and parameter meanings,

units, and values.

We now consider the model when an anti-VEGF treatment is applied. During treatment, the blood vessel growth will be impaired due to the inhibition of VEGF, but existing vasculature is likely not to be affected by the treatment. In that case nutrient delivery no longer depends upon the tumor volume τ days ago, but remains constant due to the static vasculature. We assume that blood vessel sprouts that began forming within τ time units before the onset of treatment will not be fully formed and patent. Let t_0 represent the time of treatment onset and $\bar{y} = y(t_0 - \tau)$. Then nutrient delivery is dependent upon $\bar{y}$, and the delay differential equation model becomes an ordinary differential equation model:

$$y' = \underbrace{\mu_m \left(1 - \frac{q}{Q}\right) y}_{\text{growth}} - \underbrace{dy}_{\text{death}} \tag{4.2a}$$

$$Q' = \underbrace{\alpha p \frac{\bar{y}}{y(t)}}_{\text{nutrient uptake}} - \underbrace{\mu_m (Q - q)}_{\text{dilution}}. \tag{4.2b}$$

When comparing the model to clinical data from Mesiano *et al.* (1998), the parameter α was too large during treatment. Therefore, the α during treatment cannot be the same as during off-treatment. Thus, we introduced a discount parameter p to account for this biological observation. Since the nutrient uptake term is capturing the processes of angiogenic signaling, angiogenesis itself, and uptake of nutrients, the parameter p could represent an additional inhibition, above the treatment effect originally modeled, in any of these processes. One possible explanation could be the characteristic blood-filled cysts that form in untreated ovarian malignancies that are often depleted once treatment is ongoing (Mesiano *et al.*, 1998). If this explanation is correct, then blood within these cysts must provide nutrients to the tumor.

Par	Meaning	Unit	Value	Ref
y	tumor volume	mm^3	-	(Mesiano *et al.*, 1998)
Q	cell quota (cell nutrient density)	mol/vol	-	
q	minimum cell quota	mol/vol	0.0021-0.0099	
μ_m	maximum growth rate	day^{-1}	0.47-1.58	(Panetta, 1997)
d	death rate	day^{-1}	0.28-1.43	(Panetta, 1997)
α	nutrient uptake coefficient	mol/vol/day	0.0084-0.70	
p	reduction in nutrient uptake rate	-	0.17-0.47	
τ	time delay	day	10	(Leunig *et al.*, 1992)

Table 4.1: Tumor Model Parameter Ranges. In the table, Par stands for Parameter, vol stands for volume unit, and Ref stands for Reference.

4.3 Basic Analysis for the System (4.1)

The following section provides a mathematically basic but practically adequate analysis of system (4.1), verifying the positivity of the solution in order to be biologically meaningful, providing a simple condition ensuring the tumor cell population tends to 0, and discussing a condition for approximating the solution.

Theorem 4.3.1. *Solutions system* (4.1) *with the initial conditions* $Q_M > Q(t) > q$ *and* $y(t) > 0$ *for* $t \in [-\tau, 0]$ *will remain in this region for all* $t > 0$*, where* $Q_M = \max\left\{Q(s), q + \frac{\alpha}{\mu_m}e^{d\tau}, s \in [0, \tau]\right\}$*. If* $\mu_m \leq d$*, then* $\lim_{t\to\infty} y(t) = 0$.

Proof. We first establish the positivity of the solutions. Assume by contradiction, there exists time $t_1 \in [0, \tau]$ such that a trajectory with initial conditions $Q(t) > q$ and $y(t) > 0$ for $t \in [-\tau, 0]$ crosses a boundary $Q = q$ or $y = 0$ for the first time.

Case 1. Assume the trajectory crosses the boundary $Q(t_1) = q$ first. Then for

$t \in [0, t_1]$, $y(t) > 0$ and

$$\begin{aligned} Q'(t) &= \frac{\alpha y(t-\tau)}{y(t)} - \mu_m(Q(t) - q) \\ &\geq -\mu_m(Q(t) - q). \end{aligned}$$

Then

$$Q'(t) + \mu_m Q(t) \geq \mu_m q$$

and so

$$Q(t) \geq q + (Q(0) - q)e^{-\mu_m t} > q.$$

Thus $Q(t_1) > q$, which contradicts $Q(t_1) = q$. Therefore a trajectory cannot cross this boundary first.

Case 2. Assume the trajectory crosses the boundary $y(t_1) = 0$ first or the trajectory crosses both $y(t_1) = 0$ and $Q(t_1) = q$ at the same time. Then for $t \in [0, t_1]$, $Q(t) \geq q$ and

$$y'(t) = \left(\mu_m \left(1 - \frac{q}{Q(t)}\right) - d\right) y(t) \geq -dy(t).$$

Then $y(t) \geq y_0 e^{-dt} > 0$. Therefore $y(t_1) > 0$, which contradicts $y(t_1) = 0$. Therefore a trajectory cannot cross the boundary $y = 0$ first nor both boundaries at the same time.

Now we will show Q is bounded above. Since $y' \geq -dy$, then $y(t) \geq y(t-\tau)e^{-d\tau}$ and so $\dfrac{y(t-\tau)}{y(t)} \leq e^{d\tau}$. Then for $t > \tau$,

$$Q' \leq \alpha e^{d\tau} - \mu_m(Q - q),$$

which implies

$$Q(t) \leq q + \frac{\alpha}{\mu_m} e^{d\tau} + \left(Q(\tau) - q - \frac{\alpha}{\mu_m} e^{d\tau}\right) e^{-\mu_m t}.$$

Then

$$\limsup_{t \to \infty} Q(t) \leq q + \frac{\alpha}{\mu_m} e^{d\tau}$$

and

$$Q(t) \leq \max\left\{Q(s), q + \frac{\alpha}{\mu_m}e^{d\tau}, s \in [0,\tau]\right\} = Q_M.$$

Assume now $\mu_m \leq d$, we see that

$$y' \leq -\frac{\mu_m q}{Q}y \leq -\frac{\mu_m q}{Q_M}y$$

and so

$$y'(t) \leq y(0)e^{-\frac{\mu_m q}{Q_M}t}.$$

Therefore as $t \to \infty, y(t) \to 0$.

□

In the following, we assume that $\mu_m > d$.

The full system described in (4.1) is nonlinear with a time delay and so there is no standard approach for handling the system in order to study the dynamics of the solution. Biologically we can assume that the uptake of nutrients is on a faster time scale than the population dynamics. Thus we apply a quasi-steady state argument by allowing $Q' = 0$. Then

$$Q'(t) = 0 = \frac{\alpha y(t-\tau)}{y(t)} - \mu_m(Q^*(t) - q)$$

and so

$$Q^*(t) = \frac{\alpha y(t-\tau)}{\mu_m y(t)} + q.$$

Then

$$\begin{aligned} y'(t) &= \mu_m\left(1 - \frac{q}{Q^*(t)}\right)y(t) - dy(t) \\ &= \mu_m\left(1 - \frac{q\mu_m y(t)}{\alpha y(t-\tau) + q\mu_m y(t)}\right)y(t) - dy(t) \\ &= \left(\frac{\mu_m \alpha y(t-\tau)}{\alpha y(t-\tau) + q\mu_m y(t)} - d\right)y(t) \\ &= f\left(y(t), y(t-\tau)\right). \end{aligned} \tag{4.3}$$

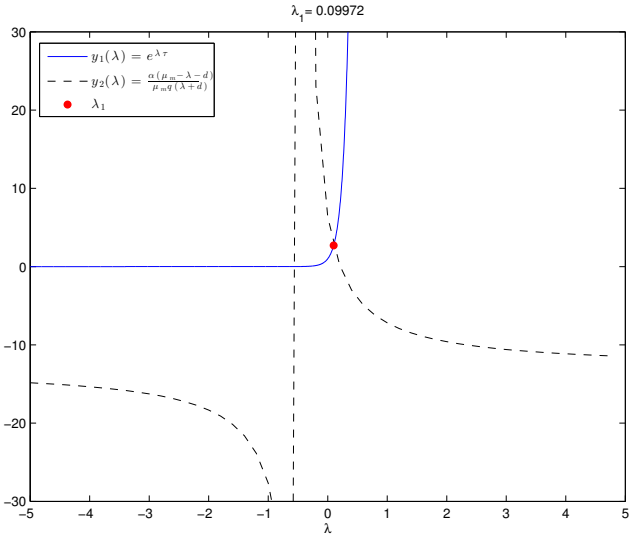

Figure 4.1: Plot of (4.4) with $\mu_m = .64, d = .43, q = .006, \alpha = .05, \tau = 10$

Motivated by the off-treatment tumor growth data in (Mesiano *et al.*, 1998) (see Section 4.5), we look for the existence of a dominating exponential solution. Let $y(t) = y_0 e^{\lambda t}$. Then

$$e^{\lambda\tau} = \frac{\alpha(\mu_m - \lambda - d)}{\mu_m q(\lambda + d)}. \tag{4.4}$$

Note that $e^{\lambda\tau}$ is a monotone increasing function of lambda and $\frac{\alpha(\mu_m-\lambda-d)}{\mu_m q(\lambda+d)}$ is a monotone decreasing function of lambda (see Figure 4.1). Observe that if $\alpha(\mu_m - d) > \mu_m qd$, we see that there exists a unique real eigenvalue, $0 < \lambda_1 < \mu_m - d$, that satisfies (4.4). Then a solution to the system is

$$(y_1(t), Q^*) = \left(y_0 e^{\lambda_1 t}, \frac{\alpha e^{-\lambda_1\tau} + \mu_m q}{\mu_m} \right). \tag{4.5}$$

However, there are also infinitely many complex solutions to the equation (4.4). The following theorem provides a sufficient condition that ensures λ_1 as the dominant eigenvalue, i.e. when the solution can be approximated by (4.5). Also, note that since $y_1(t) = y_0 e^{\lambda_1 t}$ is a solution to the system, we know that $y(t)$ is not bounded above.

Theorem 4.3.2. *If* $\alpha(\mu_m - d) > \mu_m qd$ *and* $\alpha < \mu_m q e^{\lambda_1\tau}$, *then* $\lambda_1 \geq \sup\{Re(\lambda) :$

λ *is any solution of* (4.4)$\}$.

Proof. Consider the characteristic equation defined in (4.4) and let λ_1 be the unique positive real eigenvalue that satisfies the characteristic equation. Then

$$\left\|e^{\lambda_1 \tau}\right\| = \left\|\frac{\alpha(\mu_m - \lambda_1 - d)}{\mu_m q(\lambda_1 + d)}\right\|$$

implies

$$e^{2\lambda_1 \tau} = \frac{\left(\alpha(\mu_m - \lambda_1 - d)\right)^2}{\left(\mu_m q(\lambda_1 + d)\right)^2}.$$

We assume, by contradiction, that there exists a $\lambda = a + ib$ such that $a > \lambda_1$. Then

$$\left\|e^{(a+ib)\tau}\right\| = \left\|\frac{\alpha(\mu_m - a - d) + i(-\alpha b)}{\mu_m q(a + d) + i(\mu_m q b)}\right\|$$

implies

$$e^{2a\tau} = \frac{\left(\alpha(\mu_m - a - d)\right)^2 + (\alpha b)^2}{\left(\mu_m q(a + d)\right)^2 + \left(\mu_m q b\right)^2} = \frac{A + C}{B + D}, \tag{4.6}$$

where $A = \left(\alpha(\mu_m - a - d)\right)^2$, $B = \left(\mu_m q(a + d)\right)^2$, $C = (\alpha b)^2$, and $D = (\mu_m q b)^2$.

Since $a > \lambda_1$ and $0 < \lambda_1 < \mu_m - d$, we have

$$e^{2a\tau} > e^{2\lambda_1 \tau} = \frac{\left(\alpha(\mu_m - \lambda_1 - d)\right)^2}{\left(\mu_m q(\lambda_1 + d)\right)^2} > \frac{\left(\alpha(\mu_m - a - d)\right)^2}{\left(\mu_m q(a + d)\right)^2} = \frac{A}{B}. \tag{4.7}$$

Let $E = e^{2\lambda_1 \tau}$ and $F = 1$. Then by (4.7), $\dfrac{A}{B} < \dfrac{E}{F}$.

Since $\dfrac{\alpha}{\mu_m q} < e^{\lambda_1 \tau}$, then $\dfrac{(\alpha b)^2}{(\mu_m q b)^2} < e^{2\lambda_1 \tau}$ and so $\dfrac{C}{D} < \dfrac{E}{F}$.

Note that if $\dfrac{A}{B} < \dfrac{E}{F}$ and $\dfrac{C}{D} < \dfrac{E}{F}$, then $\dfrac{A + C}{B + D} < \dfrac{E}{F}$.

Then by (4.6), $e^{2a\tau} = \dfrac{A + C}{B + D} < \dfrac{E}{F} = e^{2\lambda_1 \tau}$. However, by (4.7), $e^{2a\tau} > e^{2\lambda_1 \tau}$. Thus we have reached a contradiction. Therefore $\lambda_1 \geq \sup\{\mathrm{Re}(\lambda) : \lambda \text{ is any solution of (4.4)}\}$.

□

4.4 Global Analysis for the System (4.2)

The following section provides a global analysis of the model in system (4.2), verifying the boundedness and invariance of the solution and discussing the stability

and global stability of the positive equilibrium solution.

Theorem 4.4.1. *The solutions of the system* (4.2) *are bounded away from zero.*

Proof. First we will show y is bounded away from 0.

We will show by contradiction that $y > L$, where L is chosen to be sufficiently small. Let $t_L = \min\{t > 0 : y(t) = L\}$, i.e., let t_L be the first time $y(t)$ reaches L. We now choose M such that $L < M < y_0$. Let $t_M = \max\{t < t_L : y(t) = M\}$, i.e., let t_M be the last time $y(t)$ reaches M before it reaches L. Then $0 < t_M < t_L$ and $y(t) < M$ for $t \in (t_M, t_L]$. See Figure 4.2 for a sketch.

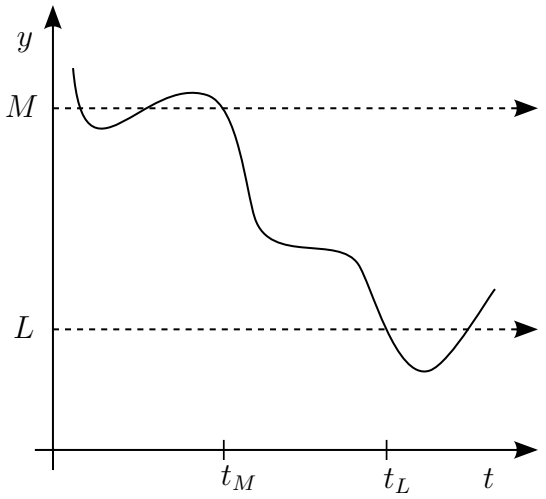

Figure 4.2: Sketch of Proof

We first choose M such that

$$M < \min\left\{y_0, \frac{\alpha p \bar{y}(\mu_m - d)}{q\mu_m^2}\right\}$$

which implies that

$$\frac{\alpha p \bar{y}}{M\mu_m} > \frac{q\mu_m}{\mu_m - d}.$$

We now choose L such that

$$\left|\left(M - \frac{\alpha p \bar{y}}{M\mu_m} - q\right) e^{\frac{-\mu_m}{d}\ln\left(\frac{M}{L}\right)}\right| < q,$$

or equivalently

$$L < M\left(\frac{q}{\left|M - \frac{\alpha p\bar{y}}{M\mu_m} - q\right|}\right)^{\frac{d}{\mu_m}}.$$

Since t_L is the first time $y(t)$ reaches L and $L < y_0$, then

$$y'(t_L) = \left(\mu_m\left(1 - \frac{q}{Q(t_L)}\right) - d\right)y(t_L) \leq 0$$

and so

$$\mu_m\left(1 - \frac{q}{Q(t_L)}\right) \leq d$$

or equivalently

$$Q(t_L) \leq \frac{q\mu_m}{\mu_m - d}. \tag{4.8}$$

Since $y < M$ for $t \in (t_M, t_L]$, then for all $t \in (t_M, t_L]$,

$$Q' = \frac{p\alpha\bar{y}}{y} - \mu_m(Q - q) > \frac{\alpha p\bar{y}}{M} - \mu_m(Q - q)$$

and so

$$Q(t) > \frac{\alpha p\bar{y}}{M\mu_m} + q + \left(M - \frac{\alpha p\bar{y}}{M\mu_m} - q\right)e^{\mu_m(t_M - t)}.$$

Then for $t = t_L$,

$$Q(t_L) > \frac{\alpha p\bar{y}}{M\mu_m} + q + \left(M - \frac{\alpha p\bar{y}}{M\mu_m} - q\right)e^{-\mu_m(t_L - t_M)}.$$

If $\left(M - \frac{\alpha p\bar{y}}{M\mu_m} - q\right) \geq 0$, then

$$\begin{aligned} Q(t_L) &> \frac{\alpha p\bar{y}}{M\mu_m} + q + \left(M - \frac{\alpha p\bar{y}}{M\mu_m} - q\right)e^{-\mu_m(t_L - t_M)} \\ &\geq \frac{\alpha p\bar{y}}{M\mu_m} + q \\ &> \frac{q\mu_m}{\mu_m - d}, \end{aligned}$$

a contradiction to equation (4.8).

We now consider the case when $\left(M - \frac{\alpha p \bar{y}}{M\mu_m} - q\right) \leq 0$. Since $y' \geq -dy$ for all $t > 0$, then $y(t_L) \geq y(t_M)e^{-d(t_L - t_M)}$ or equivalently

$$t_L - t_M \geq \frac{1}{d} \ln\left(\frac{M}{L}\right).$$

Then

$$e^{-\mu_m(t_L - t_M)} \leq e^{\frac{-\mu_m}{d} \ln\left(\frac{M}{L}\right)}$$

and so

$$\left(M - \frac{\alpha p \bar{y}}{M\mu_m} - q\right) e^{-\mu_m(t_L - t_M)} \geq \left(M - \frac{\alpha p \bar{y}}{M\mu_m} - q\right) e^{\frac{-\mu_m}{d} \ln\left(\frac{M}{L}\right)} > -q.$$

Then

$$\begin{aligned} Q(t_L) &> \frac{\alpha p \bar{y}}{M\mu_m} + q + \left(M - \frac{\alpha p \bar{y}}{M\mu_m} - q\right) e^{-\mu_m(t_L - t_M)} \\ &> \frac{\alpha p \bar{y}}{M\mu_m} \\ &> \frac{q\mu_m}{\mu_m - d}. \end{aligned}$$

However, this again contradicts (4.8) and therefore $y > L$.

Now we will show Q is bounded below by q. For $t > 0$,

$$\begin{aligned} Q' &= \frac{\alpha p \bar{y}}{y} - \mu_m(Q - q) \\ &\geq -\mu_m(Q - q). \end{aligned}$$

Then

$$Q' + \mu_m Q \geq \mu_m q$$

and so

$$Q(t) \geq q + (Q_0 - q)e^{-\mu_m t} > q.$$

Therefore $Q(t) > q$ for all $t > 0$.

Therefore the solutions of the system (4.2) are bounded away from zero. □

Theorem 4.4.2. *The solutions to the system* (4.2) *are bounded from above.*

Proof. Let $z = yQ$ and $z_0 = y_0Q_0$. Then

$$z' = \alpha p\bar{y} - dz$$

which implies

$$z(t) = \frac{\alpha p\bar{y}}{d} + \left(z_0 - \frac{\alpha p\bar{y}}{d}\right)e^{-dt}.$$

Then

$$\limsup_{t\to\infty} z(t) \leq \frac{\alpha p\bar{y}}{d}$$

and

$$z(t) \leq \max\left\{z_0, \frac{\alpha p\bar{y}}{d}\right\} = \bar{M}. \tag{4.9}$$

Thus $y(t)Q(t) \leq \bar{M}$.

Since $Q > q$ by Theorem 4.4.1, then $y(t) \leq \frac{\bar{M}}{Q(t)} < \frac{\bar{M}}{q}$. Therefore y is bounded.

Since $y > L$ by Theorem 4.4.1, then $Q(t) \leq \frac{\bar{M}}{y(t)} < \frac{\bar{M}}{L}$. Thus Q is bounded above. Therefore the solutions of the system (4.2) are bounded. □

The only steady state of the system is $E_1 = (y^*, Q^*) = \left(\frac{\alpha p\bar{y}(\mu_m - d)}{\mu_m qd}, \frac{q\mu_m}{\mu_m - d}\right)$. See Figure 4.3 for the phase plane. In order for the steady state to be positive, we assume $\mu_m - d > 0$. The following theorem discusses the global stability of this positive equilibrium point.

Theorem 4.4.3. *The equilibrium point E_1 is globally asymptotically stable.*

Proof. We will first show that E_1 is locally asymptotically stable. Using the Jacobian, we see

$$J(E_1) = \begin{bmatrix} 0 & \frac{\alpha p\bar{y}(\mu_m - d)}{(q\mu_m)^2 d} \\ \frac{-(\mu_m qd)^2}{\alpha p\bar{y}(\mu_m - d)^2} & -\mu_m \end{bmatrix}.$$

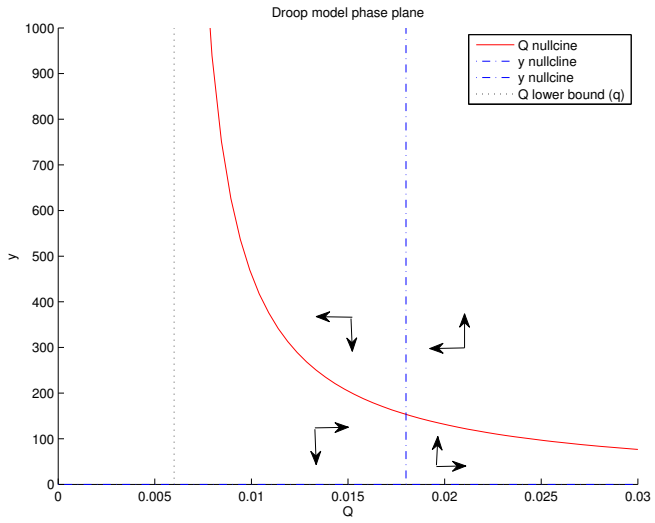

Figure 4.3: Phase Plane with Steady State Value $(y^*, Q^*) = \left(\frac{\alpha p \bar{y}(\mu_m - d)}{\mu_m q d}, \frac{q\mu_m}{\mu_m - d}\right)$

Then $\text{Tr}(E_1) = -\mu_m < 0$ and $\text{Det}(E_1) = \dfrac{d}{\mu_m - d} > 0$. Thus E_1 is a stable equilibrium point. Now we must show there are no periodic orbits. Let $\bar{M}$ be defined as in (4.9) and

$$\Omega = \left\{ 0 < y < \frac{\bar{M}}{q}, q < Q < \frac{\bar{M}}{L} \right\}.$$

Consider the system

$$y' = \mu_m \left(1 - \frac{q}{Q}\right) y - dy = F(y, Q) \tag{4.10}$$

$$Q' = \alpha p \frac{\bar{y}}{y(t)} - \mu_m (Q - q) = G(y, Q). \tag{4.11}$$

Then

$$\frac{dF}{dy} + \frac{dG}{dQ} = \mu_m \left(1 - \frac{q}{Q}\right) - d - \mu_m = \frac{-\mu_m q}{Q} - d < 0.$$

Then by the Bendixon's negative criterion theorem, there cannot be a closed orbit contained within Ω. Therefore, since Ω is simply connected and positively invariant and contains no orbits, by the Poincaré-Bendixson Theorem, all solutions of the system (4.2) starting in Ω will converge to E_1. Thus, E_1 is globally asymptotically stable. $\square$

4.5 Data and Simulation Results

We compare our model to clinical data from Mesiano *et al.* (1998). The authors first studied subcutaneous (SC) tumors induced in immunodeficient mice using the human ovarian carcinoma cell line SKOV-3, in order to monitor the tumor growth directly. The data we compare to simulated values using our model consists of the SC tumor volume (mm^3) over time (days). Since ovarian cancer is not a subcutaneous cancer, the authors also studied IP tumors. However, these tumors could not be monitored directly due to the spread within the abdomen and the results were only obtained from postmortem examination. Thus we do not have data for the IP tumor volume over time to compare to our model.

We performed simulations in MATLAB. After first fitting parameters by hand, we used the function fminsearchbnd, a bounded version of the built-in function fminsearch that uses the Nelder-Mead simplex algorithm (Lagarias *et al.*, 1998), to find values for the free parameters that minimize mean square error (MSE) between the laboratory data and model-generated data within a pre-determined bounded region. The delay differential equation (4.1) simulations begin on the third data point in order to avoid modeling the transitional dynamics. Since the first three data points are fairly constant, we assume a constant y history of the average of the first three data points. We also assume a constant $Q = Q_0$ history, which was considered a parameter and found using fminsearchbnd. The initial conditions for the ordinary differential equation (4.2) simulations were assumed to be the value of the third data point for y and $Q = Q_0$.

Figures 4.4-4.8 show the simulation results compared to the data as well as the corresponding dynamics on the phase plane. In Figures 4.4-4.6, we are able to use the same parameter values to model both the on-treatment and off-treatment tumor volumes. To confirm computationally that the solution defined in equation (4.5) is

in fact a solution to the off-treatment model, we ran the simulation with the history equivalent to equation (4.5) (Figure 4.5). We can see that the off-treatment solution is the same as $y_0 e^{\lambda_1 t}$ and the Q value is equivalent to Q^*. As expected, the ratio between the off-treatment solution and $y_0 e^{\lambda_1 t}$ was equal to one at each time step. We then considered a constant $Q = Q_0$ history with the y history remaining the exponential solution (Figure 4.6). The Q solution approached Q^* and the ratio between the off-treatment solution and $y_0 e^{\lambda_1 t}$ approached a constant value. This suggests that even when perturbing the initial condition, the solution still has the same exponential form.

Figures 4.7 and 4.8 show solutions where the model reverses from off-treatment to on-treatment and from on-treatment to off-treatment, respectively. When reversing from off-treatment to on-treatment, the initial conditions of the ordinary differential equations are last values of the off-treatment solution. When reversing from on-treatment to off-treatment, we approximate the on-treatment solution for the last τ days with a function and use this function as the history for the delay differential equations. These approximations are plotted in Figure 4.8.

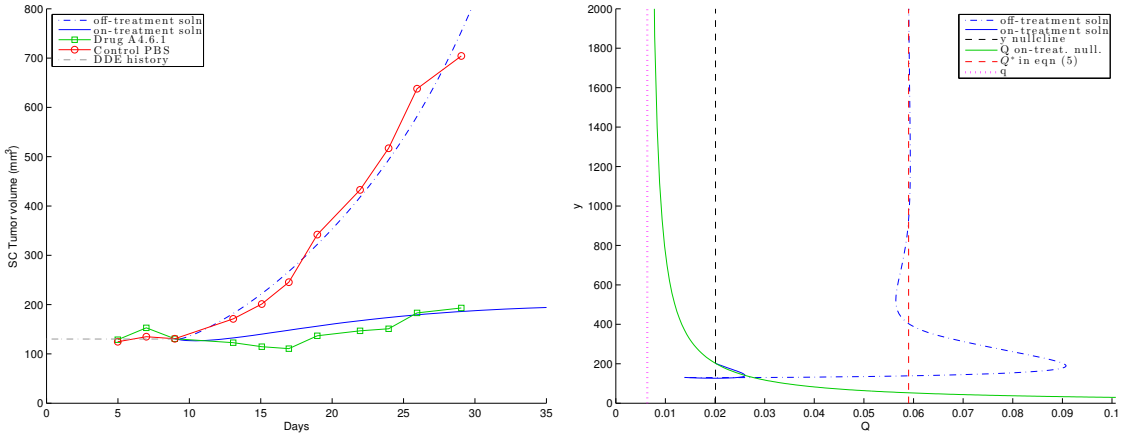

Figure 4.4: y vs. t (left) and phase plane (right) simulation of (4.1) and (4.2) with $\mu_m = 0.47, d = 0.28, q = 0.0064, a = 0.050, p = 0.17, Q_0 = 0.014$

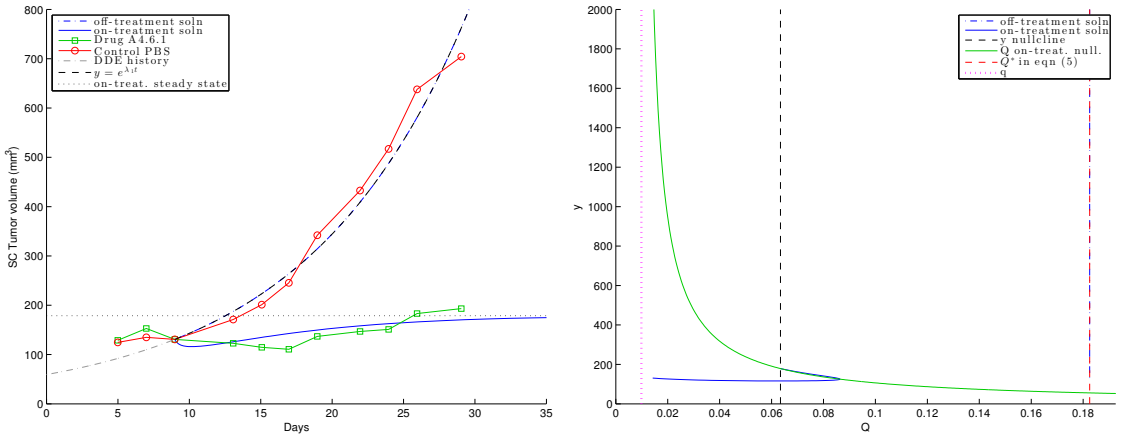

Figure 4.5: y vs. t (left) and phase plane (right) simulation of (4.1) and (4.2) with $\mu_m = 0.87, d = 0.73, q = 0.0099, a = 0.36, p = 0.18, Q_0 = 0.014$

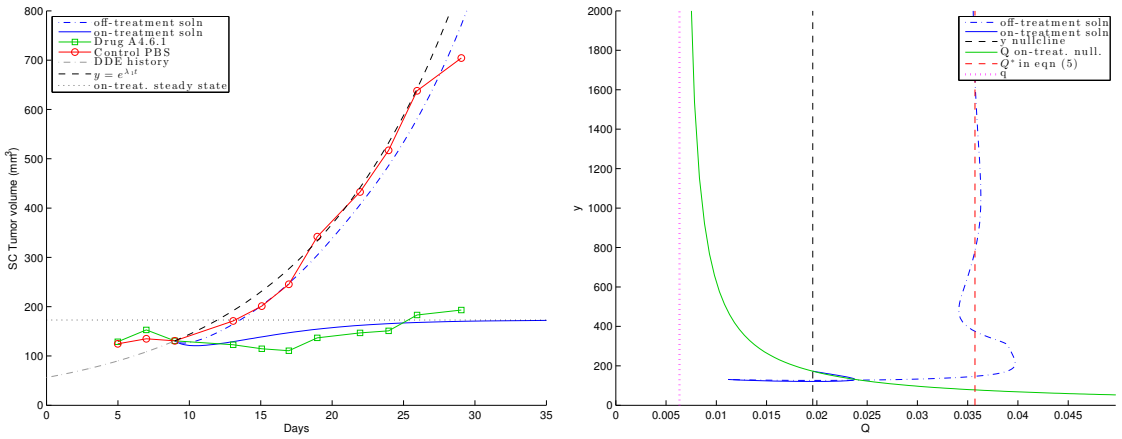

Figure 4.6: y vs. t (left) and phase plane (right) simulation of (4.1) and (4.2) with $\mu_m = 0.64, d = 0.43, q = 0.0063, a = 0.048, p = 0.23, Q_0 = 0.011$

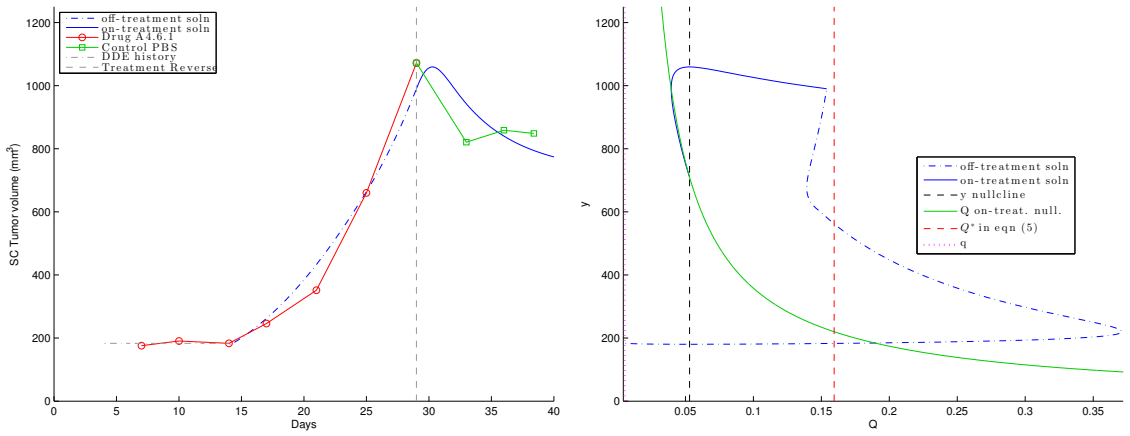

Figure 4.7: y vs. t (left) and phase plane (right) simulation of (4.1) and (4.2) with $\mu_m = 1.58, d = 1.43, q = 0.0053, a = 0.70, p = 0.23, Q_0 = 0.0060$

4.6 Discussion

We present a simple yet biologically meaningful model that considers ovarian tumor growth and tumor induced angiogenesis, subject to both on and off anti-VEGF treatment. The growth of the tumor is governed by the intracellular limiting nutrient concentration, or cell quota. We present analysis of the off-treatment model, and verify positivity of the solutions so that the solutions are biologically meaningful. Motivated by the data, we also discuss approximating the solution with an exponential solution. We analyze the on-treatment model, proving positivity of solutions and the existence of a globally stable equilibrium point.

We can see that the steady states makes sense biologically. When the nutrient uptake decreases then the on-treatment tumor volume steady state $y^* = \frac{\alpha p \bar{y}(\mu_m - d)}{\mu_m q d}$ also decreases. Similarly, the off-treatment solution $y_1(t) = y_0 e^{\lambda_1 t}$ grows at a slower rate since λ_1, the real solution of the characteristic equation $e^{\lambda\tau} = \frac{\alpha(\mu_m - \lambda - d)}{\mu_m q(\lambda + d)}$, also decreases. As the minimum intracellular nutrient concentration q increases or the death rate d increases, y^* and λ_1 decrease. To consider the maximum growth rate

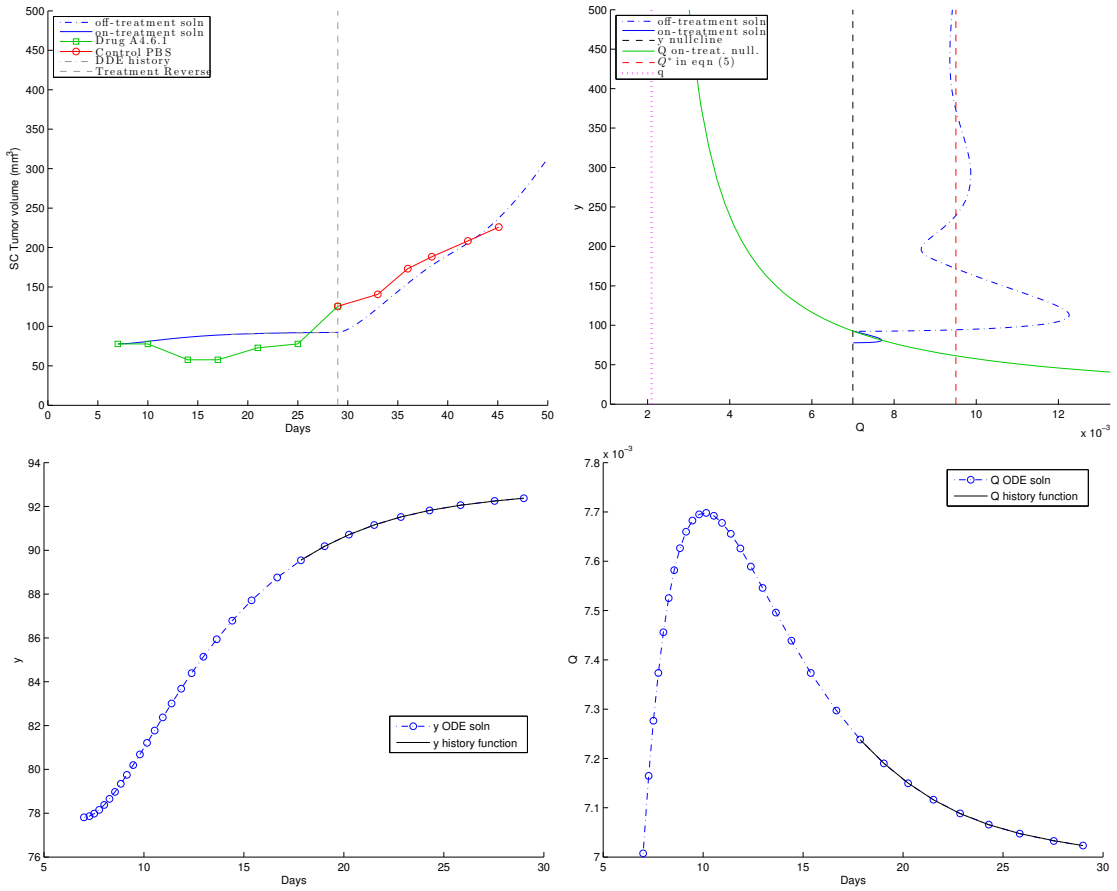

Figure 4.8: First row: y vs. t (left) and phase plane (right) simulation of (4.1) and (4.2) with $\mu_m = 0.67, d = 0.47, q = 0.0021, a = 0.0084, p = 0.47, Q_0 = 0.0070$. Second row: corresponding plot of y (left) and Q (right) history functions that approximate the on-treatment ODE solution in the top left figure.

μ_m, we can rewrite the on-treatment tumor volume steady state as $y^* = \frac{\alpha p\bar{y}(1-\frac{d}{\mu_m})}{qd}$ and the right hand side of the characteristic equation as $\frac{\alpha(1-\frac{1}{\mu_m}(\lambda+d))}{q(\lambda+d)}$. Then it is easy to see that as μ_m increases, y^* and λ_1 also increase. However, if we consider a proportional relationship between the death rate and maximum growth rate by letting $d = k\mu_m$ where $k < 1$, then $y^* = \frac{\alpha p\bar{y}(1-k)}{qk\mu_m}$. Assuming this relationship between μ_m and d, then we can see that y^* is inversely proportional to μ_m. This suggests that while on-treatment and assuming a proportional relationship between μ_m and d, a faster growing ovarian tumor may have a smaller equilibrium size.

We then compare the simulation results to both on and off treatment biological data. The tumor-derived VEGF activity was inhibited using the function-blocking monoclonal antibody A4.6.1, the murine-equivalent of bevacizumab (Avastin) (Gerber and Ferrara, 2005), which blocks VEGF receptors VEGFR-1(*flt-1*) and VEGFR-2 (*KDR/flk-1*). The authors concluded that the antibody significantly inhibited the growth of the SC tumors, by significantly inhibiting tumor vascularization, though tumor growth resumed once treatment stopped. From postmortem examination of the IP tumors, the authors observed partially inhibited tumor growth in the treatment group compared to the controls for a variety of treatment regimes. Tumor burden in treated IP mice varied from minimal to high. Therefore, Mesiano *et al.* suggested that IP metastasis might contain both angiogenesis-independent (thin layer tumor growth) and angiogenesis-dependent (large solid tumors) components. The simulations fit both the on-treatment and off-treatment data using the same parameters as well as reversing from off- to on-treatment and vice versa, which supports using Droop's model and applying ecological ideas to cancer biology.

4.7 Future Work

Here, we assume that the limiting nutrient is delivered to the tumor via the blood vessels, although we do not specify the limiting nutrient. However, a future direction would be to consider a specific limiting nutrient supplied through the blood vessels, such as oxygen, phosphorus, nitrogen, or glucose. When considering a specific nutrient, parameter ranges can be more tightly specified, because it is likely that at least some data regarding uptake of the specific nutrient and minimum cell quota can be obtained. Nagy (2007) suggested a "best guess" minimum intracellular phosphorus concentration parameter value of approximately 0.01. Since our simulations suggested a minimum cell quota less than about 0.0099, perhaps phosphorus is the limiting nutrient provided by angiogenesis. We hope that these results will motivate biologists to consider a limiting nutrient when collecting data in the future.

Another possible direction for future work could consider an alternative ODE model and compare the results to the model presented here. Following Kuang *et al.* (2004b), we use a time delay to represent the time it takes for the tumor vessels to form. However, an alternative ODE model could use a mechanistic modeling approach and track the vessel growth directly.

The work presented here considers only anti-angiogenic therapy in mice. However, until an anti-angiogenic agent that does not harm normal vessels is developed, humans receive a combination of chemotherapy with anti-angiogenic therapy (Jain, 2005). The benefit of this combination is that the cancerous cells are being attacked both directly and indirectly; the chemotherapy kills the cells directly while the anti-angiogenic therapy inhibits the cancerous cells from receiving nutrients. However, chemotherapy is delivered through the vasculature. Applying chemotherapy along with anti-angiogenic therapy could hinder the delivery of the chemotherapy. Jain (2005) hypothesizes that

the anti-angiogenic agents "normalize" the abnormal tumor vasculature, balancing the anti- and pro-angiogenic factors and allowing for more efficient drug delivery. Furthermore, by continuing to apply anti-angiogenic therapy, the tumor vasculature may continue to reduce, thus starving the tumor of blood supply. This presents the problem of determining the best time to deliver chemotherapy along with anti-angiogenic therapy (Jain, 2005; Burger, 2011).

Although the model we present is quite simple, there still remain open questions in analyzing the system. We were able to show positivity of the solutions for the off-treatment model as well as proving the dominance of λ_1 given a condition. In the simulations presented, that given condition does not hold, yet the solutions seem to take the form $y_0 e^{\lambda_1 t}$. This suggests that Theorem 4.3.2 can be improved. We end this paper with the following intriguing mathematical question:

Is it always true that $\lambda_1 \geq \sup\{\mathrm{Re}(\lambda) : \lambda \text{ is any solution of (4.4)}\}$?

Abbott, L. and F. Michor, "Mathematical models of targeted cancer therapy", British Journal of Cancer **95**, 9, 1136 – 1141 (2006).

Agur, Z., L. Arakelyan, P. Daugulis and Y. Ginosar, "Hopf point analysis for angiogenesis models", Discrete and Continuous Dynamical Systems-Series B **4**, 1, 29–38 (2004).

Akakura, K., N. Bruchovsky, S. L. Goldenberg, P. S. Rennie, A. R. Buckley and L. D. Sullivan, "Effects of intermittent androgen suppression on androgen-dependent tumors", Cancer **71**, 9, 2782–90 (1993).

Amaral, T. M. S., D. Macedo, I. Fernandes and L. Costa, "Castration-resistant prostate cancer: Mechanisms, targets, and treatment", Prostate Cancer **2012**, 327253 (2012).

Aravantinos, G. and D. Pectasides, "Bevacizumab in combination with chemotherapy for the treatment of advanced ovarian cancer: a systematic review", Journal of Ovarian Research **7**, 57, 1–13 (2014).

Basanta, D. and A. R. A. Anderson, "Exploiting ecological principles to better understand cancer progression and treatment", Interface Focus **3**, 20130020 (2013).

Bast Jr, R. C., B. Hennessy and G. B. Mills, "The biology of ovarian cancer: new opportunities for translation", Nature Reveiws Cancer **9**, 415–528 (2009).

Berges, R. R., J. Vukanovic, J. I. Epstein, M. CarMichel, L. Cisek, D. E. Johnson, R. W. Veltri, P. C. Walsh and J. T. Isaacs, "Implication of cell kinetic changes during the progression of human prostatic cancer", Clinical Cancer Research **1**, 5, 473–480 (1995).

Bickel, S. T., J. D. Juliano and J. D. Nagy, "Evolution of proliferation and the angiogenic switch in tumors with high clonal diversity", PLoS ONE **9**, 4, e91992 (2014).

Bottino, D., Y. Chia, A. Stein, A. Georgieva, J. Yu, J. Kahn, G. Helmlinger and T. Kalebic, "Inference of imatinib (IM) effects on leukemic stem cell (SC) compartment via mathematical modeling of IRIS treatment response data", Journal of Clinical Oncology, 2009 ASCO Annual Meeting Proceedings (Post-Meeting Edition) **27**, 15S, 7056 (2009).

Brandford, S., Z. Rudzki, A. Grigg, J. Seymour, K. Taylor, R. Herrmann, C. Arthur, J. Szer and K. Lynch, "The incidence of BCR-ABL kinase mutations in chronic myeloid leukemia patients is as high in the second year of imatinib therapy as the first but survival after mutation detection is significantly longer for patients with mutations detected in the second year of therapy", BLOOD **102**, 11, 414A (2003).

Burger, R. A., "Overview of anti-angiogenic agents in development for ovarian cancer", Gynecologic Oncology **121**, 230–238 (2011).

Capdeville, R., E. Buchdunger, J. Zimmermann and A. Matter, "Glivec (sti571, imatinib), a rationally developed, targeted anticancer drug", Nature Reviews Drug Discovery **1**, 493 – 502 (2002).

Coleman, R. L., B. J. Monk, A. K. Sood and T. J. Herzog, "Latest research and clinical treatment of advanced-stage epithelial ovarian cancer", Nature Reviews Clinical Oncology **10**, 211–224 (2013).

Crook, J. M., C. J. O'Callaghan, G. Duncan, D. P. Dearnaley, C. S. Higano, E. M. Horwitz, E. Frymire, S. Malone, J. Chin, A. Nabid, P. Warde, T. Corbett, S. Angyalfi, S. L. Goldenberg, M. K. Gospodarowicz, F. Saad, J. P. Logue, E. Hall, P. F. Schellhammer, K. Ding and L. Klotz, "Intermittent androgen suppression for rising PSA level after radiotherapy", New England Journal of Medicine **367**, 10, 895–903 (2012).

Davidson, B. A. and A. A. Secord, "Profile of pazopanib and its potential in the treatment of epithelial ovarian cancer", International Journal of Women's Health **6**, 289–300 (2014).

Droop, M., "Vitamin B12 and marine ecology, IV: the kinetics of uptake, growth and inhibition in monochrysis lutheri", Journal of the Marine Biological Association of the United Kingdom **48**, 3, 689–733 (1968).

Droop, M., "Some thoughts on nutrient limitation in algae", Journal of Phycology **9**, 264–272 (1973).

Elser, J. J., M. M. Kyle, M. S. Smith and J. D. Nagy, "Biological stoichiometry in human cancer", PLoS ONE **10**, e1028, 1–7 (2007).

Elser, J. J., J. D. Nagy and Y. Kuang, "Biological stoichiometry: An ecological perspective on tumor dynamics", BioScience **53**, 11, 1112–1120 (2003).

Feldman, B. J. and D. Feldman, "The development of androgen-independent prostate cancer", Nature Reveiws Cancer **1**, 1, 34–45 (2001).

Folkman, J., "Tumor angiogenesis: Therapeutic implications", The New England Journal of Medicine **118**, 1182–1186 (1971).

Folkman, J., "What is the evidence that tumors are angiogenesis dependent?", Journal of the National Cancer Institute **82**, 1, 4–6 (1990).

Folkman, J., "Role of angiogenesis in tumor growth and metastasis", Seminars in Oncology **29**, 6, 15–18 (2002).

Fong, M. K., R. Hare and A. Jarkowski, "A new era for castrate resistant prostate cancer: A treatment review and update", Journal of Oncology Pharmacy Practice **18**, 3, 343–354 (2012).

Foo, J., M. W. Drummond, B. Clarkson, T. Holyoake and F. Michor, "Eradication of chronic myeloid leukemia stem cells: A novel mathematical model predicts no therapeutic benefit of adding G-CSF to imatinib", PLoS Computational Biology **5**, 9, 1–11 (2009).

Frame, D., "Chronic myeloid leukemia: Standard treatment options", American Journal of Health-System Pharmacy **63**, S10 – S14 (2006).

Gerber, H.-P. and N. Ferrara, "Pharmacology and pharmacodynamics of bevacizumab as monotherapy or in combination with cytotoxic therapy in preclinical studies", Cancer Research **65**, 3, 671–680 (2005).

Geva, E. and R. B. Jaffe, "Role of vascular endothelial growth factor in ovarian physiology and pathology", Fertility and Sterility **74**, 3, 429–438 (2000).

Glauche, I., M. Horn and I. Roder, "Leukaemia stem cells: hit or miss?", British Journal of Cancer **96**, 677–678 (2007).

Gleave, M., L. Klotz and S. S. Taneja, "The continued debate: intermittent vs. continuous hormonal ablation for metastatic prostate cancer", in "Urologic Oncology: Seminars and Original Investigations", vol. 27, pp. 81–86 (Elsevier, 2009).

Goff, B. A., L. Mandel, H. G. Muntz and C. H. Melancon, "Ovarian carinoma diagnosis", Cancer **89**, 10, 2068–2075 (2000).

Goldman, J. M. and J. V. Melo, "Chronic myeloid leukemia-advances in biology and new approaches to treatment", The New England Journal of Medicine **349**, 15, 1451–15464 (2003).

Gómez-Raposo, C., M. Mendiola, J. Barriuso, E. Casado, D. Hardisson and A. Redondo, "Angiogenesis and ovarian cancer", Clinical and Translational Oncology **11**, 564–571 (2009).

Gorre, M. E., M. Mohammed, K. Ellwood, N. Hsu, R. Paquette, P. N. Rao and C. L. Sawyers, "Clinical resistance to STI-571 cancer therapy caused by BCR-ABL gene mutation or amplification", Science **293**, 876 – 880 (2001).

Griswold, I. J., M. MacPartline, T. Bumm, V. L. Goss, T. O'Hare, K. A. Lee, A. S. Corbin, E. P. Stoffregen, C. Smith, K. Johnson, E. M. Moseson, L. J. Wood, R. D. Polakiewicz, B. J. Druker and M. W. Deininger, "Kinase domain mutants of bcr-abl exhibit altered transformation potency, kinase activity, and substrate utilization, irrespective of sensitivity to imatinib", Molecular and Cellular Biology **26**, 16, 6082 – 6093 (2006).

Hanahan, D. and R. A. Weinberg, "The hallmarks of cancer", Cell **100**, 57–70 (2000).

Higano, C. S., "Side effects of androgen depreivation therapy: Monitoring and minimizing toxicity", Urology **61**, 2A, 32–38 (2003).

Hirata, Y., K. Akakura, C. S. Higano, N. Bruchovsky and K. Aihara, "Quantitative mathematical modeling of PSA dynamics of prostate cancer patients treated with intermittent androgen suppression", Journal of molecular cell biology **4**, 3, 127–132 (2012).

Hirata, Y., N. Bruchovsky and K. Aihara, "Development of a mathematical model that predicts the outcome of hormone therapy for prostate cancer", Journal of Theoretical Biology **264**, 517–527 (2010).

Howlander, N., A. Noone, M. Krapcho, J. Garshell, D. Miller, S. Altekruse, C. Kosary, M. Yu, J. Ruhl, Z. Tatalovich, A. Mariotto, D. Lewis, H. Chen, E. Feuer and K. Cronin, "Seer cancer statistics review, 1975-2011", National Cancer Institute (2011).

Hu, L., C. Zaloudek, G. B. Mills, J. Gray and R. B. Jaffe, "*In Vivo* and *in Vitro* ovarian carcinoma growth inhibition by a phosphatidylinositol 3-kinase inhibitor (LY294002)", Clinical Cancer Research **6**, 880–886 (2000).

Hussain, M., C. M. Tangen, D. L. Berry, C. S. Higano, E. D. Crawford, G. Liu, G. Wilding, S. Prescott, S. Kanaga Sundaram, E. J. Small, N. A. Dawson, B. J. Donnelly, P. M. Venner, U. N. Vaishampayan, P. F. Schellhammer, D. I. Quinn, D. Raghavan, B. Ely, C. M. Moinpour, N. J. Vogelzang and I. M. Thompson, "Intermittent versus continuous androgen deprivation in prostate cancer", New England Journal of Medicine **368**, 14, 1314–1325 (2013).

Ideta, A. M., G. Tanaka, T. Takeuchi and K. Aihara, "A mathematical model of intermittent androgen suppression for prostate cancer", Journal of Nonlinear Science **18**, 593–614 (2008).

Isaacs, J. T., "The biology of hormone refracory prostate cancer: Why does it develop?", Urologic Clinics of North America **26**, 2, 263–273 (1999).

Jackson, T., "A mathematical model of prostate tumor growth and androgen-independent relapse", Discrete and Continuous Dynamical Systems-Series B **4**, 1, 187–201 (2004a).

Jackson, T. L., "A mathematical investigation of the multiple pathways to recurrent prostate cancer: comparison with experimental data", Neoplasia **6**, 6, 697–704 (2004b).

Jain, H. V., J. E. Nör and T. L. Jackson, "Modeling the VEGF-Bcl-2-CXCL8 pathway in intratumoral angiogenesis", Bulletin of Mathematical Biology **70**, 89–117 (2008).

Jain, R. K., "Normalization of tumor vasculature: An emerging concept in antiangiogenic therapy", Science **307**, 58–62 (2005).

Jelinek, J., G. V., M. Estecio, K. Kondo, R. He, W. Chung, Y. Lu, N. Zhang, S. Liang, H. Kantarjian, J. Cortes and J.-P. Issa, "Aberrant DNA methylation is associated with disease progression, resistance to imatinib and shortened survival in chronic myelogenous leukemia", PLoS ONE **6**, 7, e22110 (2011).

Kareva, I., "What can ecology teach us about cancer?", Translational Oncology **4**, 5, 266–270 (2011).

Kareva, I., F. Berezovskaya and C. Castillo-Chavez, "Myeloid cells in tumour-immune interactions", Journal of Biological Dynamics **4**, 4, 315–327 (2010).

Klotz, L. and P. Toren, "Androgen deprivation therapy in advanced prostate cancer: is intermittent therapy the new standard of care?", Current Oncology **19**, 3, S13–21 (2012).

Komarova, N. and D. Wodarz, "Effect of cellular quiescence on the success of targeted CML therapy", PLoS ONE **2**, 10, e990 (2007).

Korolev, K. S., J. B. Xavier and J. Gore, "Turning ecology and evolution against cancer", Nature Reveiws Cancer **14**, 371–380 (2014).

Kuang, Y., J. Huisman and J. J. Elser, "Stoichiometric plant-herbivore models and their interpretation", Mathematical Biosciences and Engineering **1**, 2, 215–222 (2004a).

Kuang, Y., J. D. Nagy and J. J. Elser, "Biological stoichiometry of tumor dynamics: Mathematical models and analysis", Discrete and Continuous Dynamical Systems-Series B **4**, 1, 221–240 (2004b).

Labrie, F., "Blockade of testicular and adrenal androgens in prostate cancer treatment", Nature Reviews Urology **8**, 73–80 (2011).

Lagarias, J. C., J. A. Reeds, M. H. Wright and P. E. Wright, "Convergence properties of the nelder-mead simplex method in low dimensions", SIAM Journal on Optimization **9**, 1, 112–147 (1998).

Leadbeater, B. S., "The 'droop equation' - michael droop and the legacy of the 'cell-quota model' of phytoplankton growth", Protist **157**, 345–358 (2006).

Leunig, M., F. Yuan, M. D. Menger, Y. Boucher, A. E. Goetz, K. Messmer and R. K. Jain, "Angiogenesis, microvascular architecture, microhemodynamics, and interstitial fluid pressure during early growth of human adenocarcinoma LS174T in SCID mice", Cancer Research **52**, 6553–6560 (1992).

Merlo, L. M. F., J. W. Pepper, B. J. Reid and C. C. Maley, "Cancer as an evolutionary and ecological process", Nature Reveiws Cancer **6**, 924–935 (2006).

Mesiano, S., N. Ferrara and R. B. Jaffe, "Role of vascular endothelial growth factor in ovarian cancer: Inhibition of ascites formation by immunoneutralization", American Journal of Pathology **153**, 4, 1249–1256 (1998).

Michor, F., "Quantitative approaches to analyzing imatinib-treated chronic myeloid leukemia", TRENDS in Pharmacological Sciences **28**, 5, 197 – 199 (2007a).

Michor, F., "Reply: The long-term response to imatinib treatment of CML", Biritish Journal of Cancer **96**, 697 – 680 (2007b).

Michor, F., T. P. Hughes, Y. Iwasa, S. Branford, N. P. Shah, C. L. Sawyers and M. A. Nowak, "Dynamics of chronic myeloid leukemia", Nature **435**, 1267–1270 (2005).

Mitin, T., J. A. Efstathiou and W. U. Shipley, "Urological cancer: The benefits of intermittent androgen-deprivation therapy", Nature Reviews Clinical Oncology **9**, 12, 672–673 (2012).

Morken, J., A. Packer, R. Everett, J. Nagy and Y. Kuang, "Predicting mechanisms of treatment resistance to intermittent androgen deprivation in prostate cancer patients by cell-death rate analysis", Cancer Research **74**, 14, 3673–3683 (2014).

Muller, M., N. Gattermann, T. Lahaye, M. Deininger, A. Berndt, S. Fruehauf, A. Neubauer, T. Fischer, D. Hossfeld, F. Schneller, S. Krause, C. Nerl, H. Sayer, O. Ottmann, C. Waller, W. Aulitzky, P. le Coutre, M. Freund, K. Merx, P. Paschka, H. Konig, S. Kreil, U. Berger, H. Gschaidmeier, R. Hehlmann and A. Hochhaus, "Dynamics of BCR-ABL mRNA expression in first-line therapy of chronic myelogenous leukemia patients with imatinib or interferon α/ara-C", Leukemia **17**, 2392–2400 (2003).

Nagy, J. D., "Competition and natural selection in a mathematical model of cancer", Bulletin of Mathematical Biology **66**, 663–687 (2004).

Nagy, J. D., "The ecology and evolutionary biology of cancer: A review of mathematical models of necrosis and tumor cell diversity", Mathematical Biosciences and Engineering **2**, 2, 381–418 (2005).

Nagy, J. D., "Hypertumors in cancer can be caused by tumor phosphorus demand", Proceedings in Applied Mathematics and Mechanics **7**, 1121703–1121704 (2007).

Nagy, J. D. and D. Armbruster, "Evolution of uncontrolled proliferation and the angiogenic switch in cancer", Mathematical Biosciences and Engineering **9**, 4, 843–876 (2012).

National Cancer Institute, N. I. H., "Nci dictionary of cancer terms", URL `http://www.cancer.gov/dictionary` ((accessed online dictionary) 2013).

Nelson, P. S., "Molecular states underlying androgen receptor activation: a framework for therapeutics targeting androgen signaling in prostate cancer", Journal of Clinical Oncology **30**, 6, 644–646 (2012).

Nishioka, C., T. Ikezoe, K. Udaka and A. Yokoyama, "Imatinib causes epigenetic alterations of *PTEN* gene via upregulation of DNA methyltransferases and polycomb group proteins", Blood Cancer Journal **1**, 12, e48 (2011).

Panetta, J. C., "A mathematical model of breast and ovarian cancer treated with paclitaxel", Mathematical Biosciences **146**, 89–113 (1997).

Pienta, K. J., N. McGregor, R. Axelrod and D. E. Axelrod, "Ecological therapy for cancer: Defining tumors using an ecosystem paradigm suggests new opportunities for novel cancer treatments", Translational Oncology **1**, 4, 158–164 (2008).

Portz, T., Y. Kuang and J. D. Nagy, "A clincial data validated mathematical model of prostate cancer growth under intermittent androgen suppression therapy", AIP Advances **2**, 011002, 1–14 (2012).

Resnick, M. J., "Urological cancer: Walking the tightrope of survival and quality of life with ADT", Nature Reviews Clinical Oncology (2013).

Roeder, I., M. Horn, I. Glauche, A. Hochhaus, M. C. Mueller and M. Loeffler, "Dynamic modeling of imatinib-treated chronic myeloid leukemia: functional insights and clinical implications", Nature Medicine **12**, 10, 1181 – 1184 (2006).

Saleem, M., T. Agrawal and A. Anees, "A study of tumor growth based on stoichiometric principles: a continuous model and its discrete analogue", Journal of Biological Dynamics **8**, 1, 117–134 (2014).

Sawyers, C. L., "Chronic myeloid leukemia", The New England Journal of Medicine **340**, 17, 1330 – 1340 (1999).

Scher, H. I., G. Buchanan, W. Gerald, L. M. Butler and W. D. Tilley, "Targeting the androgen receptor: improving outcomes for castration- resistant prostate cancer", Endocrine-Related Cancer **11**, 459–476 (2004).

Scholz, M. C., R. Y. Lam, S. B. Strum, D. J. LaBarba, L. K. Becker, P. Chang, N. Farhoumand and R. I. Jennrich, "Primary intermittent androgen deprivation as initial therapy for men with newly diagnosed prostate cancer", Clinical Genitourinary Cancer **9**, 2, 89–94 (2011).

Sharifi, N., J. L. Gulley and W. L. Dahut, "Androgen deprivation therapy for prostate cancer", JAMA: the journal of the American Medical Association **294**, 2, 238–244 (2005).

Siegel, R., C. DeSantis, K. Virgo, K. Stein, A. Mariotto, T. Smith, D. Cooper, T. Gansler, C. Lerro, S. Fedewa, C. Lin, C. Leach, R. S. Cannady, H. Cho, S. Scoppa, M. Hachey, R. Kirch, A. Jemal and E. Ward, "Cancer treatment and suvivorship statistics, 2012", CA: A Cancer Journal for Clinicians **62**, 220–241 (2012).

Siegel, R., J. Ma, Z. Zou and A. Jemal, "Cancer statistics, 2014", CA: A Cancer Journal for Clinicians **64**, 1, 9–29 (2014).

Siegel, R., K. D. Miller and A. Jemal, "Cancer statistics, 2015", CA: A Cancer Journal for Clinicians **65**, 1, 5–29 (2015).

Siegel, R., D. Naishadham and A. Jemal, "Cancer statistics, 2013", CA: A Cancer Journal for Clinicians **63**, 1, 11–30 (2013).

Sitochy, B., J. A. Nagy and H. F. Dvorak, "Anti-VEGF/VEGFR therapy for cancer: Reassessing the target", Cancer Research **72**, 8, 1909–1914 (2012).

Stein, A. M., D. Bottino, V. Modur, S. Branford, J. Kaeda, J. M. Goldman, T. P. Hughes, J. P. Radich and A. Hochhaus, "Bcr-abl transcript dynamics support the hypothesis that leukemic stem cells are reduced during imatinib treatment", Clinical Cancer Research **17**, 6812–6821 (2011).

Sterner, R. W. and J. J. Elser, *Ecological Stoichiometry The Biology of Elements from Molecules to the Biosphere* (Princeton University Press, 2002).

Waldner, M. J. and M. F. Neurath, "Targeting the VEGF signaling pathway in cancer therapy", Expert Opinion on Therapeutic Targets **16**, 1, 5–13 (2012).

Ye, Q. and H.-L. Chen, "Bevacizumab in the treatment of ovarian cancer: a meta-analysis from four phase III randomized controlled trials", Archives of Gynecology and Obstetrics **288**, 3, 655–666 (2013).